IRON FISCHER-TROPSCH CATALYSIS

by

Kandis Sudsakorn

B.S. in Chemical Engineering, Mahidol University, Thailand, 1995

M.S. in Chemical Engineering, West Virginia University, USA, 1999

Submitted to the Graduate Faculty of

the School of Engineering in partial fulfillment of

of the requirements for the degree of

Doctor of Philosophy

University of Pittsburgh

2002

UNIVERSITY OF PITTSBURGH

SCHOOL OF ENGINEERING

This dissertation was presented

by

Kandis Sudsakorn

It was defended on

May 10, 2002

and approved by

Dr. Irving Wender, Professor, Department of Chemical and Petroleum Engineering

Dr. Robert M. Enick, Professor, Department of Chemical and Petroleum Engineering

Dr. Joseph J. McCarthy, Professor, Department of Chemical and Petroleum Engineering

Dr. Jayant Rajgopal, Professor, Department of Industrial Engineering

Dissertation Director: Dr. James G. Goodwin, Jr., Professor, Department of Chemical and Petroleum Engineering

IRON FISCHER-TROPSCH CATALYSIS

Kandis Sudsakorn, PhD

University of Pittsburgh, 2002

Signature _____
Dr. James G. Goodwin, Jr.

Application of Fe catalysts on a commercial scale using slurry bubble column reactors (SBCR) has been held back due to their poor attrition resistances. Recently, high attrition resistant catalysts have been successfully prepared using spray drying. Their improved physical strength was found to depend greatly on particle density, which was determined by type and concentration of SiO_2 added to the catalysts. However, only Fe catalysts containing binder or binder + precipitated SiO_2 were studied.

To improve our understanding of the role of SiO_2 on attrition properties of Fe catalysts, in general, attrition of spray-dried Fe catalysts prepared with only precipitated SiO_2 was investigated. The amount of precipitated SiO_2 that optimized catalyst performance (attrition resistance and activity) during an SBCR operation was suggested to be ca. 11 wt%. The strong relationship between catalyst attrition and particle density was consistent with the previous findings.

Unlike high attrition resistant catalysts, whose physical and chemical attrition properties remained essentially unchanged after pretreatment, the physical strength of poor attrition-

resistant catalysts was able to be improved significantly by pretreatment (CO or H_2). This improvement was surprisingly decreased by the addition of water vapor during pretreatment. The presence of water vapor was found to prevent sintering of Fe pore structure but to provide no significant additional interaction between Fe and SiO_2. The conventional CO-pretreatment was suggested as the best activation for Fe catalysts, since it results in high attrition resistance and reasonably high surface area.

Different activation pretreatments (H_2, CO, or syngas) result in different Fe phases, and the relationship of these phases with catalyst activity during FTS has been debated among researchers up to the present day. Steady-state isotopic transient kinetic analysis (SSITKA) was used to study at the site level the activity of differently activated Fe during CO hydrogenation. It was found that the H_2-pretreated sample exhibited the highest concentration of surface reaction intermediates (N_M) while those of CO- and syngas-pretreated ones were similar. The intrinsic site activity (k_M) of differently pretreated catalyst samples was essentially identical. These results suggested that the active sites were on the surface of carburized Fe.

DESCRIPTORS

Fischer-Tropsch synthesis
Attrition resistance
Attrition improvement
Slurry bubble column reactor
SSITKA
Surface reaction intermediates
Methanation
Spray-dried Fe catalysts
Jet cup attrition test
Pretreatment effect
Intrinsic site activity
Carburization
Activation
Deactivation

ACKNOWLEDGEMENTS

This work could not have been finished without the help from many people. Above all, I would like to express my sincere gratitude to my Ph.D. research advisor, Dr. James G. Goodwin, Jr., who had provided me invaluable guidance throughout the whole course of this research. His understanding and generosity helped eliminate any non-technical difficulties and created such a nice working environment.

I would like to thank Dr. K. Jothimurugesan at Conoco, Inc. and Dr. Adeyinka A. Adeyiga and Ms. Miamee at Hampton University for catalyst preparation. The participation of Dr. Irving Wender, Dr. Robert M. Enick, Dr. Joseph McCarthy, and Dr. Jayant Rajgopal as members of the thesis committee is gratefully acknowledged.

My thanks also go to people at Clemson University: Dr. David A. Bruce in the Chemical Engineering Department for allowing me to use his research facilities, Dr. Mariusz Krawiec in the Chemistry Department for helping me with X-ray diffraction, and Mr. William T. Kay, Ms. Joan S. Hudson, and Ms. Jennifer Wyffels for their help on scanning electron microscopy. Special thanks go to Mr. William Coburn for helping me build the methanation system and for many laborious tasks during the lab set up.

I would like to thank the Royal Thai Government for financial support and the opportunity to pursue my Ph.D. My thanks also go to my colleagues and friends for their help in so many ways and the great time we shared.

I wish to express my deep appreciation to my family in Thailand and in New York, USA, and my girlfriend, Piyachat Jarutirasarn, for their love and support that helped me overcome the difficulties through all these years.

TABLE OF CONTENTS

LIST OF TABLES

LIST OF FIGURES

Figure No. Page

NOMENCLATURE

$F^I(t)$	normalized inert tracer transient response
$F^P(t)$	normalized step-decay transient response
$F^{*P}(t)$	normalized step-input transient response
N	number of particles
N_p	concentration of surface reaction intermediates
P	unlabeled product
*P	labeled product
$r^p(t)$	rate of the unlabeled product
$r^{*p}(t)$	rate of the labeled product
r_{SS}	steady-state rate
t_P	surface residence time
W_b	weight of particles remaining at the bottom of the jet cup
W_f	weight of fines generated
W_r	weight of total particles recovered
x_{VM}	volume moment
x	size of particle

1.0 INTRODUCTION

Fischer-Tropsch synthesis provides an efficient means to produce environmental-friendly, clean transportation fuels of superior quality [1]. Iron-based catalysts have not only high F-T activity but also high water-gas-shift activity that provides supplemental H_2, permitting the use of H_2 deficit syngas, such as that derived from coal gasification. However, one of the major drawbacks in the application of iron catalysts in FTS is catalyst attrition, especially when these catalysts are to be used in moving bed reactors such as slurry bubble column reactors (SBCRs).

Previous efforts from our group have succeeded in developing high attrition resistance Fe catalysts using spray drying [2-5] and have found that catalyst particle density was the key in determining catalyst attrition [5]. Although it was also found that type (binder or precipitated) and concentration of the structural promoter, SiO_2, determined directly the catalyst inner structure and hence catalyst particle density, the role of SiO_2 has not been well established due to the lack of the understanding of the use of precipitated SiO_2 alone. The first part of this study focused on developing a better understanding of catalyst attrition properties relating to the composition, in general, by investigating the use of precipitated SiO_2. Physical attrition of a series of spray-dried Fe catalysts prepared with only precipitated SiO_2 was evaluated using the jet cup attrition test. Changes in catalyst physical properties as well as surface morphology were investigated.

The second part of this study was to improve the physical strength of poor attrition resistant Fe catalysts by the use of pretreatment. Since, the presence of water vapor during

[*] Bracketed references placed on the line of text refer to the bibliography.

activation/reaction is well known to facilitate metal-support interactions in supported metal catalysts [6-8], it was hypothesized that it might increase the interactions between Fe and SiO_2 in poor attrition resistant Fe catalysts and, consequently, result in improved attrition resistance. Selected spray-dried Fe catalysts were pretreated with different gases (H_2 or CO) with or without the addition of water vapor. Their physical and chemical properties especially attrition resistance were studied.

The remainder of this research focused on the effect of different activations (H_2, CO, or syngas) of Fe catalysts on the development of site activity and concentration of surface reaction intermediates during CO hydrogenation as determined by steady-state isotopic transient kinetic analysis (SSITKA). Iron is well known to undergo extensive phase changes during activation as well as F-T reaction. Differently pretreated Fe catalyst samples were characterized for their changes in properties. CO hydrogenation at methanation conditions was used for the study since it has been proven to be an ideal system for isotopic transient kinetic investigations due to the ease of tracing isotopic labeled (^{12}C and ^{13}C) products by mass spectrometry [9-11].

The result of this research has not only provided a better understanding of the physical attrition of spray-dried Fe F-T catalysts but also has elucidated the nature of the active sites of these catalysts during reaction.

2.0 BACKGROUND

2.1 Fischer-Tropsch Synthesis

Fischer-Tropsch synthesis is basically the hydrogenation of carbon monoxide, producing mainly hydrocarbons (paraffins and olefins), alcohols, and small amounts of other oxygenated species [1,2]. This process provides a practical means to convert coal or natural gas into transportation fuel and also straight-chain high molecular weight alcohols and olefins for the chemical industry.

Ever since it was discovered in 1923, Fischer-Tropsch synthesis has remained a viable process for the production of liquid fuels and chemicals. Fischer-Tropsch fuels are considered to have superior quality with no sulfur contamination. Although the cost of the production of fuels from FTS is typically higher than from oil refineries, continuing research of this process has brought the production cost down significantly with developments in reactors, operating conditions, as well as catalysts. The recent research focus on FTS has been to develop both reactors and catalysts to achieve high yields of heavy weight hydrocarbons that can undergo hydrocracking and selective distillation to obtain high quality gasoline and diesel fuels [3].

By nature, FTS is a highly exothermic polymerization reaction using CH_x monomer insertion to create the chain growth of products [4], in which methane formation is thermodynamically favored. However, the distribution of hydrocarbon products from FTS can be varied significantly using different catalysts, promoters, H_2/CO ratios, reaction conditions, and types of reactor [5].

In an attempt to explain the mechanism of this multi-step reaction, many postulations of the reaction intermediates on catalyst surface for F-T reaction were proposed in the past. From the observation of carbon- and carbide-forming tendency on iron catalysts, Franz Fischer [6,7] introduced the surface carbidic carbon as reaction intermediates. This carbide form was thought to be hydrogenated to CH_2, which was then further polymerized to various hydrocarbons. This model was later discarded since no carbide phases were detected on Co and Ru catalysts. By noticing oxygen-containing organic F-T products, Storch, Golumbic, and Anderson proposed a mechanism where hydrogen atoms were added to absorbed CO to form an oxymethylene species [1]. Although this mechanism received much attention and some attempts have been made to support this hypothesis, no evidence supporting the existence of such species has been provided.

Later, Roelen [8] (who discovered the famous 'oxo synthesis'- a significant process for producing alcohols and aldehydes nowadays) proposed a mechanism for this process where alkyl ligands moved to create C-C bonds with absorbed CO ligands. Several researchers have suggested that C-C bond formation probably occurs similarly in FTS [9-11]. In the present day, while 'alkyl migration' stays as an alternative possibility, C-C bond formation through CH_2 insertion as the chain propagation step is accepted widely [12].

According to the CH_2-insertion model, Fischer-Tropsch kinetics is believed to begin with the dissociation of absorbed CO and H_2 molecules and the formation of absorbed methyl species on the catalyst surface via addition of hydrogen atoms to absorbed carbon atoms. These methyl species can either be terminated on the catalyst surface as methane or initiate chain growth by undergoing sequential insertion of surface methylene species (CH_2) [13]. The CH_2 is formed by the following reaction [12]:

$$CO + 2H_2 \rightarrow (CH_2) + H_2O \qquad (1)$$

The growth of hydrocarbon chains continues by this insertion while alkyl groups stay chemisorbed to the catalyst surface. At any point during the chain growth, the alkyl chains may be terminated to form predominantly linear α-olefins by β-hydrogen abstraction and n-paraffins by primary hydrogen addition [13-17]. This mechanism is not contradicted by the earlier argument against the carbide theory because the reaction intermediate now is surface bonded carbon, not the metal carbide phase as proposed in the carbide theory [18,19]

As mentioned earlier this synthesis produces a variety of different molecular sizes of hydrocarbons. These products conform to a statistical distribution α, which is defined as the probability of chain growth by C_1 monomer (CH_2) in this polymerization reaction [20]. In ideal polymerization regime the product distribution in molar unit decreases exponentially with carbon number, a so-called "Anderson-Schulz-Flory" (ASF) distribution. This diagram is typically used to characterize F-T products [12]. However, F-T product distributions reported in the literature often deviate from the ASF distribution due to secondary reactions of primary hydrocarbon products. Under normal process conditions, paraffins are relatively stable and assumed to be inert. On the other hand, α-olefins can re-enter the F-T chain growth process by reversing the chain termination step (so-called 'reinsertion') or alternatively undergo secondary reactions (hydrogenation, hydrogenolysis, and hydroformylation), leading to an increase in C_5+ selectivity and a decrease in CH_4 and olefin contents in F-T products [5,13-15]. These secondary reactions are potential causes of deviations from ASF product distribution. Remarkably strong deviations from this ideal distribution are found with alkalized iron catalysts, in which the products formed have been found to follow a "double ASF" distribution [15,21].

The highly exothermic nature of F-T synthesis can cause a severe heat transfer problem, which is significant to consider in reactor design for FTS. Without efficient heat removal, the temperature of the reaction can increase rapidly, and undesirable methane can be produced in a large amount, as it is thermodynamically favored at higher temperature. Recently, slurry bubble column reactors (SBCR) have gained more attention in commercial FTS due mainly to their excellent heat removal, simple design, and relatively low capital cost. Since the Fe catalysts used in this research were developed for use in SBCR, more details about this type of reactor compared to other commercial type F-T reactors are presented.

2.2 Fischer-Tropsch Reactors

Reaction temperature has a great effect on the performance of FTS. When the reaction temperature increases, it decreases average chain length as well as thermodynamically favors selective methane formation and carbon deposition, causing catalyst deactivation, especially for iron catalysts [12]. This thermodynamic limitation makes it difficult to increase reaction rate by simply increasing reaction temperature. Essentially, an isothermal condition is preferable for an efficient operation. A better isothermal process allows a reactor to operate at higher average temperature. However, an isothermal process cannot be easily obtained due to the highly exothermic nature of F-T reactions. Many models of F-T reactors have been invented and developed from time to time for better performances. Several models that are nowadays utilized in commercial practice are summarized as followings:

2.2.1 Fixed Bed Reactor (FBR)

Fixed bed reactors are usually used for low temperature Fischer-Tropsch (LTFT) synthesis, which produces mainly high molecular waxy hydrocarbons. These hydrocarbons are easily converted to diesel fuel of a high quality by hydrocracking process. The first model of fixed bed reactors operating commercially was developed by Ruhrchemie in early 1930s [12]. It was a box shape divided vertically by metal sheets and horizontally by cooling tubes crossing the sheets. The catalyst was loaded between these sheets and tubes. Heat generated by the reactions was removed by circulating cooling water. Later this model was improved for more efficient heat removal by using a bundle of tubes to contain catalyst particles and employing recycle gas at higher linear gas velocity [22]. This tubular fixed bed reactor (TFBR) led to the development of the 'iron medium pressure synthesis' or ARGE (Arbeitsgemeinschaft) process, which dominated as the only process for LTFT synthesis at Sasol from 1955 to 1993 [23]. The ARGE tubular fixed bed reactor, as shown in Figure 2.1, consists of 2050 single tubes of 12 m in length and 5 cm in diameter, packed with precipitated iron catalyst particles [22,23].

Heat generated from the process is removed by cooling water circulated on the shell side of the tubes. This process is operated at a shell side temperature about 220 °C and pressure at 25 and 45 bar [23]. Another process employing fixed bed reactors is the 'cobalt medium pressure synthesis', first developed by Fischer and Pichler [24] for the production of middle distillates and wax. This process is the basis of the novel Shell FT technology at the Bintulu Plant, built in 1993, with 500,000 t per annum capacity [13, 25]. Advantages of tubular fixed bed reactors commonly are: no expensive demonstration unit necessary for scale-up, no additional device

needed for separation of catalyst and liquid product, no catalyst attrition problem, and capability to operate with large loading of catalyst [13]. However, a couple of major disadvantages exist, such as high capital cost because of complex design, mechanical difficulty in scale-up, cumbersome catalyst replacement and laborious reactor maintenance causing a considerable down time during the operation [23].

2.2.2 Slurry Bubble Column Reactor (SBCR)

Due to the highly exothermicity of F-T reactions, slurry bubble column reactors (SBCRs) have recently gained interests due mainly to their excellent heat removal. Like other moving bed reactors, catalyst attrition in SBCRs has also been a concern, especially when operating with Fe-based catalysts. Catalyst attrition not only causes a loss of catalyst but also a filter-plugging problem, leading to an operational shutdown. This has led to efforts to produce a robust Fe catalyst for use in SBCRs. SBCR or slurry bed reactor or slurry phase distillate (SPD) reactor is considered as an improvement over the tubular fixed bed reactor for LTFT synthesis [26,27]. It was regarded by many authors as the most efficient process for the production of clean diesel fuel with low aromatics and no sulfur content [12]. Products obtained from SBCR have the same carbon distribution as those obtained from the TFB reactors, with Schulz-Flory distribution alpha values 0.95 and higher [28]. An SBCR, as shown in Figure 2.2, basically consists of a vessel containing a slurry of process-derived wax with catalyst particles dispersed of typical size smaller than 50 μm. This size of catalyst is small enough to eliminate intra-particle diffusion limitation. Cooling coils are installed in the reactor for heat removal via steam generation from cooling water. Syngas is bubbled through a gas distributor underneath, passing through the wax

with suspended catalyst. Reactant gases transport from the gas bubbles through wax and finally to the catalyst surface where they react. Heavy hydrocarbons and water form slurry in the reactor while light hydrocarbons in gas phase and unconverted syngas are removed at the top where they are separated by condensers.

SBCRs have been used on a commercial scale by SASOL since 1993 with a capacity of 2500 bbl/day. It is easier to construct and scale up than a TFB. A single SBCR has the capacity of 6 ARGE reactors while its construction cost is only 25% of that of the ARGE system with equivalent capacity [28]. Furthermore, it is possible to build an SBCR with higher capacity for high operating pressure process since the pressure drop across the SBCR is low (less than 1 bar) comparing to that across a TFBR (3-7 bar).

The SBCR is well known as providing excellent heat transfer and mass transfer during the reaction. Reactant gases and catalyst particles are well mixed in the reactor, giving more effective contact between catalyst and syngas. Well-mixing provides isothermal conditions in the reactor and, hence, allows operating at a higher average temperature, which results in higher reaction rates. Use of sufficiently small catalyst particles eliminates intra-particle diffusion limitation. Thus, all catalyst particles are used more efficiently, resulting in higher product yield per reactor volume and lower catalyst consumption at only 20 to 30 % comparing to that of TFBR [28]. In addition, catalyst can be added to or removed from the reactor during operation. This feature is very useful when Fe catalysts are used because of their low attrition resistance. It seems less important for Co catalysts because they have much longer life. However, this feature is also good for catalyst reactivation.

2.2.3 Fluidized Bed Reactor (FBR)

There are basically two types of fluidized bed reactor utilized commercially for FTS: the circulating fluidized bed reactor in which the catalyst is entrained with a fast moving gas stream and the fixed fluidized bed reactor in which the catalyst remains stationary with syngas passing upward through the catalyst bed.

2.2.3.1 Circulating Fluidized Bed Reactor (CFBR). The CFBR or riser reactor or entrained bed reactor was first developed by the Kellogg Company and later improved by Sasol for successful operation [12]. It is used in high temperature Fischer-Tropsch synthesis (HTFT), which is usually operated at 25 bar and 340°C. A schematic diagram of CFBR is shown in Figure 2.3.

During the operation, iron catalyst powder flows down through the standpipe, creating the highest pressure in the system above the slide valve [29]. After going through the slide valve, the catalyst is carried around the lower transfer bend into the vertical reactor section by the high velocity syngas stream. Heat of reaction is removed from the reactor section as steam through cooling coils suspended in the reactor section [28]. After leaving the reactor section, the catalyst passes through the upper transfer bend or gooseneck into the hopper and finally flows down the standpipe as it completes the cycle [29]. The suspended cyclone above the hopper functions to separate entrained catalyst before the gas exits the hopper. Scaling up this CFBR is the most challenging and also the most difficult task because of its complicated design. This complex reactor needs complex support system and complicated operating to handle the circulating catalyst loads and temperature differences, resulting in high operating cost.

2.2.3.2 Fixed Fluidized Bed Reactor (FFBR). This type of reactor is now being used as a replacement for the CFBRs in the HTFT process at Sasol, known as Sasol Advanced Synthol (SAS) process [12]. As seen in Figure 2.4, the FFBR is a conventional fluidized bed that is designed to operate under pressure between 20 to 40 bar at temperatures around 340 °C. The same Fe catalyst that is used in CFBR is also utilized in this reactor. The syngas is fed through the gas distributor at the bottom of the bed and fluidizes catalyst particles. The products in gas phase exit at the top of the reactor, where entrained catalyst particles are removed by cyclones. Cooling coils are used to remove heat of reaction by steam generating.

The FFBR gives similar product spectra to CFBR but more efficiently and cheaply [28]. The FFBR has many advantages over CFBR such as higher conversion, larger reaction zone, more efficient heat removal, and more energy efficiency [29]. Although, the catalyst consumption of these two reactors are about the same for a cycle run, less than half of catalyst in the CFBR is in the reaction zone while all of catalyst in the FFBR is in the reaction zone [29]. In order to scale-up the CFBR, all dimensions need to be considered, while only reactor diameter needs to be increased for larger capacity of FFBR [29].

The type of catalyst to be used in a reactor is very important to specify for reactor design and operation, since different catalysts will behave differently. With Fe catalysts, substantial tail gas (e.g., recycle ratio 2:1) is needed to supply due to limited conversion causing by water inhibition. With cobalt, no water inhibition occurs and the conversion per pass can be higher. Furthermore, with cobalt, the selectivity is strongly dependent on the partial pressures of CO and H_2. A sufficiently high CO partial pressure, even at the catalyst bed end, should be maintained in order to avoid excessive methane formation.

2.3 Fischer-Tropsch Catalysts

FTS is a heterogeneous reaction that is commonly catalyzed by group VIII metals such as Fe, Co, Ni and Ru. Fe and Co catalysts are currently utilized in commercial practice. Ni was discarded as a FT catalyst because it produces predominantly methane [22, 30] and loses its activity by carbonyl formation [22, 31]. Ru catalysts have gained more interest in laboratory study due to its high activity at low temperature, high molecular wax production, and simple catalytic system that is suitable for fundamental study of FTS [12]. Only its high price and limited world resources exclude its use on a commercial scale [12,30]. Typically, F-T catalysts include supports and promoters in addition to the active metal surface. The support enhances the active metal surface area by decreasing sintering of the active metal during preparation. Promoters are added to help in getting higher metal dispersion, to improve selectivity during reaction, and to prolong the life of the catalyst.

Among FT catalysts, cobalt (Co) and iron (Fe) based catalysts are presently utilized in industrial practice. Cobalt based catalysts provide high FT activity, high selectivity to long straight chain hydrocarbons, low water-gas-shift activity which makes them the preferred catalysts for the conversion of synthesis gas derived from natural gas reforming. In contrast, iron-based catalysts have high water-gas-shift activity that is suitable for the operation with synthesis gas derived from coal gasification. With Fe and Co catalysts, products can be markedly varied with varied promoters, operating temperature and pressure, H_2/CO ratios, and type of reactor [30]. These two commercial catalysts will now be discussed in more detail.

2.3.1 Fe FT Catalysts

In 1923, alkalized iron was first discovered by Franz Fischer and Hans Tropsch to catalyze the production of "synthol" (a mixture consisting mainly of oxygenated chemicals and a very small quantity of hydrocarbons) from CO and hydrogen [32]. Although the early development of iron catalysts for FTS did not achieve much successful results comparing to their competitors, cobalt catalysts, they have a significant advantage over cobalt catalysts in that Fe is easily available from many sources whereas the supply of cobalt is limited [32].

Fe catalysts provide low selectivity to undesirable methane and high water-gas-shift activity that allows operation with low H_2/CO ratio syngas because of the additional supplement of hydrogen, according to the following reaction:

$$CO + H_2O \rightarrow CO_2 + H_2 \qquad (2)$$

This property makes Fe a preferable catalyst for conversion of syngas derived from coal gasification. Fe has a lower cost than Co but has more catalyst attrition problems.

Fe catalysts are usually prepared either by precipitation or fusion. The latter preparation was found to produce more attrition resistance catalysts [30]. In general, precipitated Fe catalysts are prepared by precipitation of mixing solutions containing iron and other promoters. The precipitate is then washed, collected, and dried. For fused Fe catalysts, Fe together with promoters are melted in an arc furnace and cooled down in ingots. After cooling down, they are crushed to desired particle sizes. Fused Fe catalysts are the most suitable catalysts for the high

temperature Fischer-Tropsch process in circulating fluidized bed or fixed fluidized bed reactors, since other metals would produce high methane [29].

Typical promoters for Fe catalysts are potassium (K) and copper (Cu). Potassium functions to maintain the catalyst activity over long periods of time. Furthermore, not only does K strengthen the Fe-C bond, it also weakens the C-O and Fe-H bonds. Weakening C-O increases the rate of reaction since breaking the C-O bond is a rate-limiting step for FTS with Fe. Strengthening the Fe-C bond facilitates chain growth of products while weakening the Fe-H bond reduces H_2 adsorption on the catalyst surface, leading to less methane and paraffin formation. Other alkalis act similarly to K, but less effectively [30]. Copper substantially lowers reduction temperature, reduces sintering, and permits high surface area without affecting selectivity of the catalysts [30].

2.3.2 Co FT Catalysts

Co catalysts have more attrition resistance compared to Fe catalysts since they can be incorporated with strong supports to enhance the strength of the catalysts. Furthermore, advantages of Co catalysts over Fe catalysts are that they have high F-T activity, high selectivity to linear long chain hydrocarbons, and low water-gas-shift activity [33]. Thus, Co-based catalysts are preferable choices for the conversion of high H_2/CO ratio syngas as produced from natural gas. However, rapid deactivation of cobalt F-T catalysts is generally well known and needs improvement.

Many formulations of cobalt-based catalysts have been studied to improve their performance. Effect of different supports such as titania [34,35], silica [36], alumina [37,38],

zirconia and ceria [39,40] as well as influence of different catalyst precursors such as Co-EDTA complex [39], cobalt carbonyls [40,41], and cobalt acetate [42] on catalyst activity have been extensively investigated. Additionally, the impact of preparation variables such as temperature and pH value on catalyst performance has also been investigated [43,44]. Addition of a second metal such as Ru [45], Rh [46] and Pt [47] as a promoter has been reported to improve the reduction of cobalt by increasing hydrogen adsorption on the second metal. It was found that the presence of a second metal improved the regeneration of the deactivated catalyst [48].

With Co catalysts, products contain mainly straight-chain and monomethyl paraffins and olefins, and a very small amount of dimethyl- and ethyl- substituted species [49]. There are no traces of naphthenes, aromatics, diolefins, or acetylenes in the products [50]. Olefins, mainly α olefins, seem to be a major product of the synthesis on cobalt catalysts [49].

2.4 Catalyst Deactivation

Like for all catalysts, deactivation of Fischer-Tropsch (FT) catalysts inevitably occurs, resulting in inefficient production. Many factors can cause the deactivation of FT catalysts such as sintering, fouling, poisoning by sulfur or other chemicals, etc. Among these possible causes, carbon deposition is the most commonly encountered no matter what type of catalyst is used in the process. The deposition of carbon has also been found to depend on reaction temperature, pressure, particle size and hydrogen-to-carbon monoxide ratio of feed gas. In general, activity of catalysts declines due to the loss of active area. The following causes lead to the deactivation of FT catalysts:

2.4.1 Conversion of Active Phases to Inert Phases

Generally the active phase for FT catalysts is the metallic phase. The metallic phases of Co, Ni and Ru are more stable than that of Fe under FTS conditions. Under these conditions Fe_3O_4 always exists while the oxidation of Co, Ni and Ru is not thermodynamically favored [22]. Carbides of Co, Ni, and Fe are also formed during the synthesis. The stability of these carbides under syngas atmospheres depends on the relative rates of carbiding and reducing reactions since those carbides are readily reduced under a pure H_2 atmosphere [22]. During the synthesis with iron catalysts, the metallic phase is changed rapidly to magnetite (Fe_3O_4) and iron carbides. First unstable cementite (Fe_3C) is formed and then converted to Hägg carbide (Fe_5C_2). After several days another carbide phase appears, called Eckstrom Adcock (Fe_7C_3). However, there is no clear relation between catalyst activity and type of carbide formed [51]. These carbides can be further oxidized in the presence of oxidizing agents such as CO_2 and H_2O, which are the products of FTS. Phase changes of catalysts during FTS are inevitable and they cause loss of catalyst activity in some degree.

2.4.2 Sintering

Sintering causes loss of catalyst activity by inducing crystal growth in catalysts, resulting in a loss of an active surface area for the reaction. This is supported by the difference in x-ray diffraction pattern of fresh and used catalysts. The x-ray patterns of fresh catalysts are broad and indistinct, indicating small crystals, while those of used catalysts are much sharper, as a result of

crystal growth. The amount of refractory oxides used in catalyst preparation is associated with the resistance to sintering of the catalyst. When lower contents of these oxides (SiO_2, Al_2O_3, etc) are used in precipitated catalysts, activity declines more markedly [22]. Sintering of catalyst in fixed bed reactors can be found near the reactor exit. In this section, water, as a product from the reaction, is at its highest vapor pressure. It was observed that this water vapor enhances the rate of sintering of the catalyst [22].

2.4.3 Fouling

During the synthesis, liquid wax can fill catalyst pores and hence retard the rate of diffusion of synthesis gas to the catalyst active surface. This wax can be removed periodically by liquid extraction using a lighter solvent, leading to a sharp increase in activity. For Co catalysts, periodic hydrogen reactivation at high temperature around 673 K is commonly used to hydrocrack high molecular wax to volatile compounds, giving the same result as solvent extraction [22]. However, solvent extraction can be used to remove only high-molecular wax soluble in hydrocarbon products, but not insoluble carbonaceous deposits that decrease the number of active sites and constitute to the surface fouling of catalyst. These insoluble deposits can be potentially removed by hydrogen reduction at high temperature. Nevertheless, the rate of removal can be slow if these carbonaceous deposits have coked to a high degree [22].

2.4.4 Sulfur Poisoning

Sulfur compounds have been well known to cause a rapid deactivation of Fe, Ni and Co catalysts. Sulfur atoms are chemisorbed on the active metal sites, eliminating them from the

catalytic reaction. Generally, it is not possible to remove sulfur from poisoned catalysts under the conditions that will not destroy the catalysts [52]. Thus, the best way to avoid the sulfur contamination is to remove sulfur from the feed gas before using it in the synthesis. Fischer [53] gave the maximum allowable sulfur content in synthesis gas to be 1 to 2 mg/m^3. Nevertheless, the value should be 10 times lower than that in order to assure minimal poisoning from sulfur [22].

Some promoters, especially alkalis, are reported to improve sulfur poisoning resistance, but only to a small degree. Most catalysts containing Fe, Ni, Co and Ru are sensitive to sulfur poisoning. Molybdenum and tungsten can be used to develop sulfur-resistant catalysts; however, present catalysts have low activity and poor selectivity. Catalysts with high sulfur resistance may not be needed since products would be contaminated by sulfur during synthesis with high sulfur-content syngas.

2.4.5 Metal-Support Compound Formation

The formation of metal and support is one of the factors that cause the loss of catalyst activity by losing active surface areas. The supports used mostly for FT catalysts are alumina (Al_2O_3) and silica (SiO_2). Kobelbauer et al. [54] reported in their study with silica-supported Co catalysts that cobalt silicates, both reducible and nonreducible, were formed under normal FT condition and they were not completely reduced during TPR to 900 °C. Similarly, alumina-supported cobalt catalysts have been reported to have a metal-support interaction as $CoAl_2O_4$ during calcination [55]. Although this compound is not present in large portions nor does it contribute as a major factor for catalyst deactivation during synthesis, $CoAl_2O_4$ is not reducible at temperatures up to 1200 K [55].

2.4.6 Carbon Deposition

For Ni, Co and Ru based catalysts, much less deposition of carbon occurs compared to Fe based catalysts under normal FT conditions. Carbon deposition on Fe catalysts usually occurs at high temperatures, while at low temperature, below 523 K, Fe catalysts form carbides but no carbon depositions are found [20]. Deposited carbon comes from the dissociation of absorbed CO from the synthesis gas. This absorbed CO provides an oxygen atom when reacting with either CO to form CO_2 or H_2 to form H_2O and leaves carbon on the surface. This carbon can migrate into the metal lattice and form carbides. After carbide formation is completed, carbon will continue to accumulate on the catalyst surface, creating severe stresses that cause the breakage of catalyst particles. Deposition of carbon on a catalyst can cause swelling and disintegration of the catalyst particles. Fractured catalyst fines can cause a plugging problem in fixed bed reactors and in filters of slurry bubble column reactors.

2.4.7 Attrition

Attrition of catalysts can cause a plugging problem in fixed bed reactors as well as in downstream filters of slurry bubble column reactors, leading to activity decline because of the loss of catalyst from the reactor. Generally, Fe based catalysts cause more attrition problems than Co based catalysts. The strength of Co based catalysts can be enhanced by adding strong support materials. Fe based catalysts, however, are usually used without support material to gain sufficiently high activity. Severe attrition problems of Fe based catalysts in the FT process is

well known, especially when the catalysts are utilized in slurry bubble column reactors or moving bed reactors.

To improve the physical strength of Fe FT catalysts, the spray-drying technique has been used for catalyst preparation without lowering catalyst activity [56]. Recently, the spray-dried technique was used to prepare Fe FT catalysts having improved attrition resistance [57-59]. Recently, Zhao et al. [60] studied two series of Fe FT catalysts prepared by spray drying to investigate the effects of precipitated silica and binder silica on attrition resistance of Fe catalysts (see Figure 2.5). From their study, it was found that the silica source and concentration have a significant impact on the attrition resistance properties of catalysts; moreover, attrition resistance appears to correlate with the density of the catalyst.

Figure 2.5 shows that the catalyst with the highest attrition resistance, generating the lowest amount of fines lost, has a concentration of total SiO_2 about 11%. For catalysts with only binder silica (dotted line), the role of binder silica on attrition resistance shows clearly that the maximum attrition resistance appears at intermediate level of binder silica and then it decreases as silica concentration goes higher. However, the role of precipitation silica (solid line) is still questionable whether it causes higher fines loss because of higher amounts of precipitated silica added or because of the higher total silica concentration. A complete analysis for the role of SiO_2 addition can be achieved by determining the role of precipitated silica on attrition resistance of spray-dried Fe FT catalysts and comparing with the previous findings. This is one of the objectives of this research. The results will be discussed in later chapters.

2.5 Active Phase of Fe for FTS

Most other common F-T catalysts (Ni, Co, and Ru) beside Fe must undergo H_2 reduction to change from their oxide forms to the metal before becoming active for FTS. They then remain largely in the metallic state during synthesis under various process conditions [61]. For iron catalysts, such a straightforward activation does not apply. They undergo extensive phase changes during different activations (H_2, CO or syngas pretreatment) and F-T reaction.

Common activations for Fe F-T catalysts include CO, H_2, or syngas (CO + H_2). Either CO alone or CO + H_2 results in iron carbide formation on Fe catalyst surface [62,63]. Furthermore, any metallic iron formed by H_2 reduction of iron oxide catalysts is converted quickly to iron carbide once exposed to syngas [64]. Gradually, iron carbides are converted to a mixture of iron carbides and Fe_3O_4 during synthesis. The extent and rate of formation of the iron oxide phase depend upon the operating conditions such as CO conversion, water-gas-shift activity, promoter levels and time-on-stream [65]. Thus, iron in a "working, steady-state" is present as a mixture of oxide and carbide phases.

Several phases of iron have been found to exist under FTS conditions [66-,69] including metallic Fe (α-Fe), Fe oxides (hematite, α-Fe_2O_3, magnetite, Fe_3O_4, and Fe_xO), and Fe carbides. At least five different forms of iron carbides are known to exist. They can be categorized into two groups: O-carbides with C atom in octahedral interstices (ε-Fe_2C, ε'-$Fe_{2.2}C$, and Fe_xC) and TP-carbides with C atoms in trigonal prismatic interstices (χ-$Fe_{2.5}C$ and Fe_3C) [70]. The quantities of these phases present depend greatly on the reaction conditions, exposure time to reactants, as well as the type and initial state of the catalyst (metal, oxide, supported or

unsupported). However, the effect of each phase during the reaction has never been fully delineated and the active phase for FTS is still a controversy among researchers.

There has been much research in the past trying to determine the active phase of iron during FTS. Teichner and co-workers [71,72] in 1982 proposed that magnetite (Fe_3O_4) was the active phase since the proportion of Fe_3O_4 was found to fall continuously with time-on-stream while the activity of catalysts increased initially and then went down during the same time interval. This idea that magnetite is the active phase was supported by Kuivila et al. [73] and also Butt [74,75], who found that magnetite was active in the absence of carbides. Dictor and Bell [76] proposed that a mixture of χ and ε' carbides and Fe metal was instead the active form for FTS. Although Huang et al. [77] found that magnetite was the only crystalline phase present detectable by XRD in the catalyst when it reached the maximum activity, they concluded that magnetite was not necessarily an active phase since it was inactive when initially exposed to syngas.

Two models regarding the role of the carbide phase have been proposed in the literature. The first is the carbide model proposed by Raupp and Delgass [78] in which the active sites are believed to be located on the bulk carbide phase and the site density varies along with the formation of bulk carbide. The second model is called the competition model [69] where there is a competition for CO molecules between carbidization and hydrocarbon formation. In this model, Fe metal is inactive but rapidly transformed into carbides during the initial stage of reaction. This transformation is possibly the cause of the increase in activity of catalysts during initial reaction. Later, the decline in activity of the catalyst could possibly result from the formation of inactive carbon on the active carbide surface. Amorphous carbon may not deactivate the catalyst as much as graphitic carbon.

Identification of the type of deposited carbon [carbon on the surface (potentially inactive) and carbon in the iron phase (potentially active)] could lead to a better understanding of the active form of iron and solve this controversy. However, it requires a technique with sufficient spatial resolution. However, most of the techniques used to study iron catalysts, in the past, including Mössbauer spectroscopy, XRD, and XPS, are not capable of providing such a resolution [70].

2.6 SSITKA

Steady state isotropic-transient kinetic analysis (SSITKA), first developed by Happel [79], Bennett [80], and Biloen [81], is a powerful technique to study kinetics of catalytic reactions at steady state conditions. This is an *in situ* technique, which allows one to obtain kinetic information about reaction mechanism as well as reaction intermediates present on catalyst surface by tracking isotropic labeled species of a reactant versus time following a switch after steady state is reached. This switch is done while maintaining the surface reaction undisturbed (isothermal, isobaric, constant concentrations and flow rates of reactants and products). The distribution of isotropic species coming out in product stream is detected by mass spectroscopy. From the isotropic product analysis, kinetic surface reaction parameters at steady state, such as concentration of adsorbed reaction intermediates (N_i) and the mean surface resident time (t_i), can be determined [82]. Moreover, different kinetic information can be obtained using this technique, such as site heterogeneity, activity distribution, as well as identification of possible mechanisms [83]. A typical SSITKA system, as illustrated in Figure 2.6, consists of 2

reactants [labeled (R^*) and non-labeled (R)], a reactor, a switching valve, a gas chromatograph (GC) for effluent analysis, and a mass spectrometer (MS) for isotopic analysis [82]. Once a reaction reaches steady state, a particular isotropic-labeled species is switched quickly into the reactant stream. This rapid switch in combination with the pressure and flow rate balance results in essentially an undisturbed steady state reaction. A small amount of inert gas is used to determine the gas-phase holdup of the system by feeding it along with the reactant stream. The effluent is fed to the MS for isotropic analysis and to the GC for component analysis.

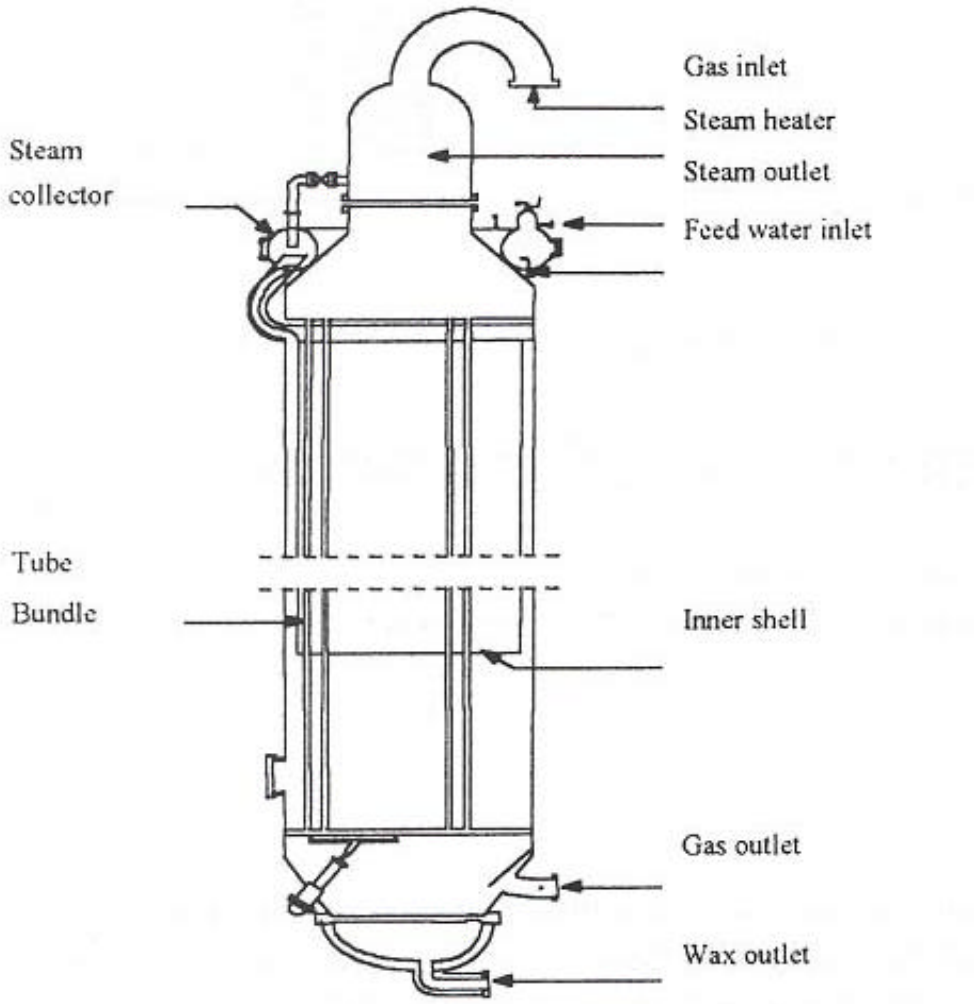

Figure 2.1 Tubular Fixed Be d (ARGE) Reactor [23].

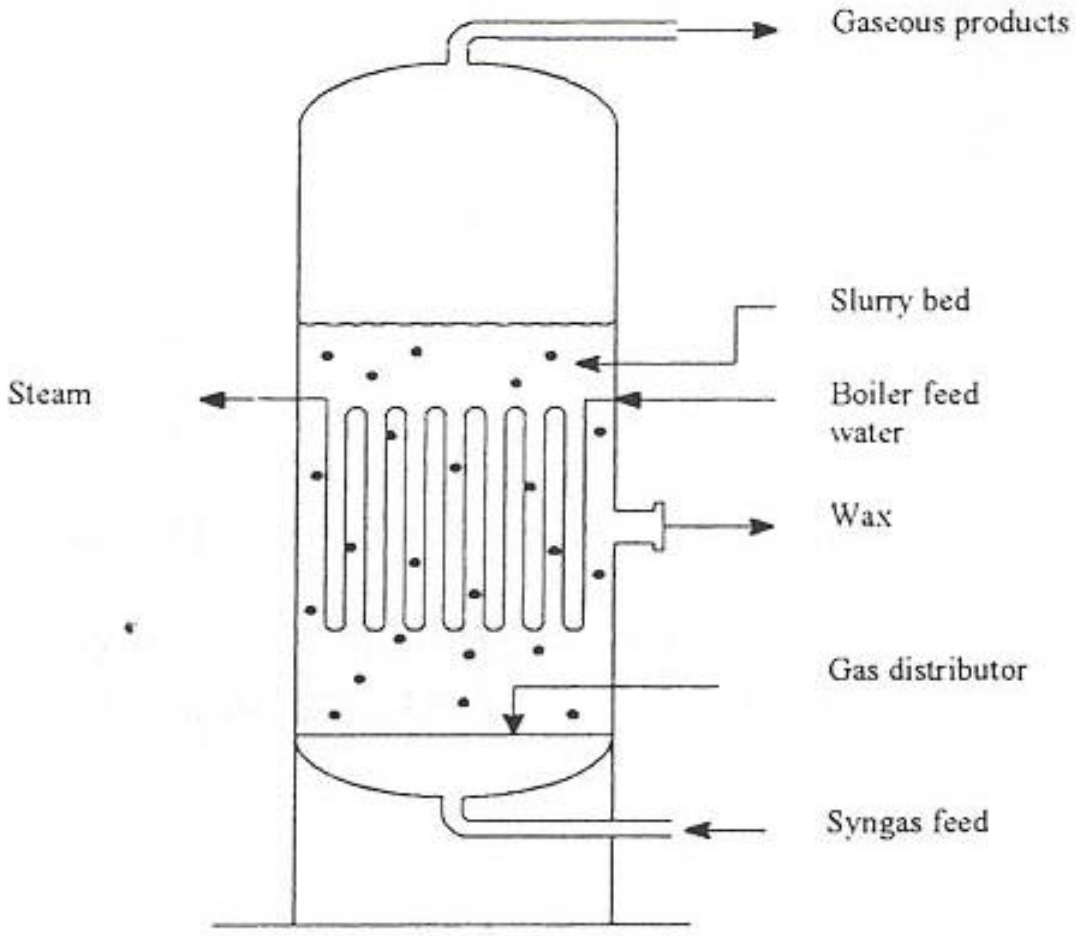

Figure 2.2 Slurry Bubble Column Reactor [23].

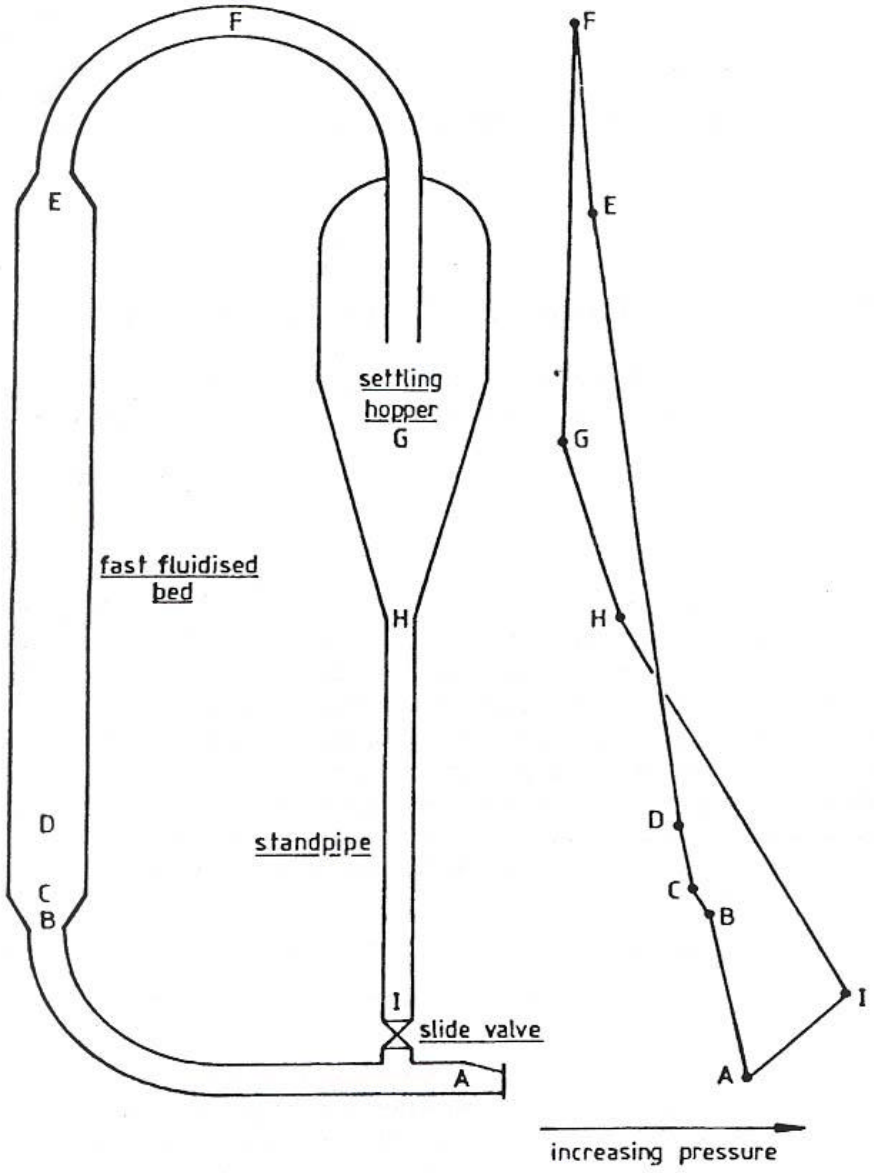

Figure 2.3 Circulating Fluidized Bed Reactor [28].

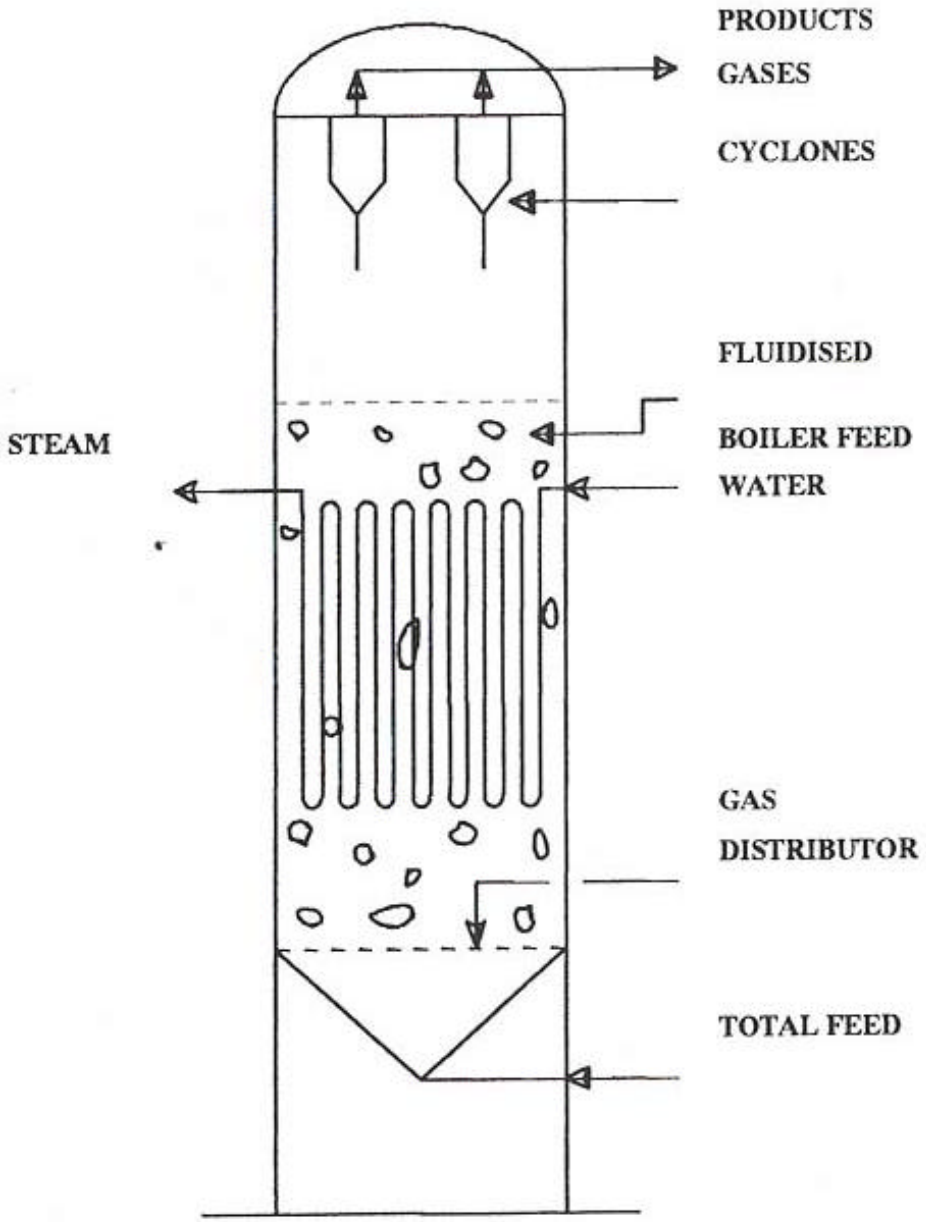

Figure 2.4 Fixed Fluidized Bed Reactor [28].

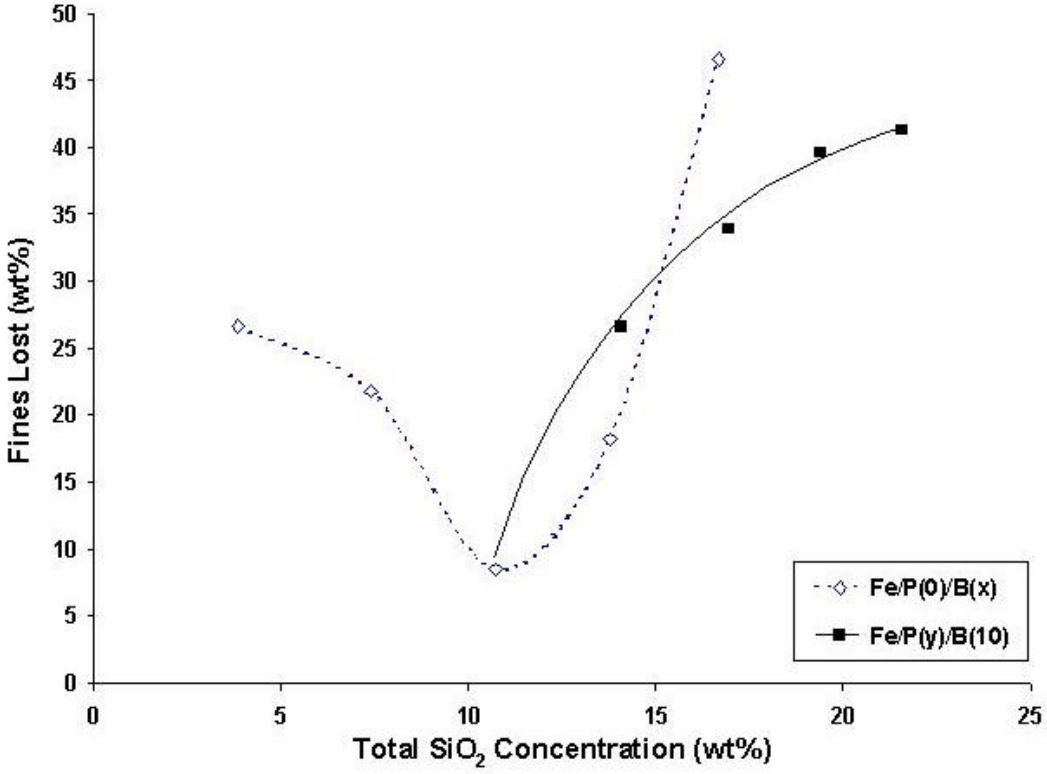

Figure 2.5 Attrition Test of Fe FT Catalysts [60].

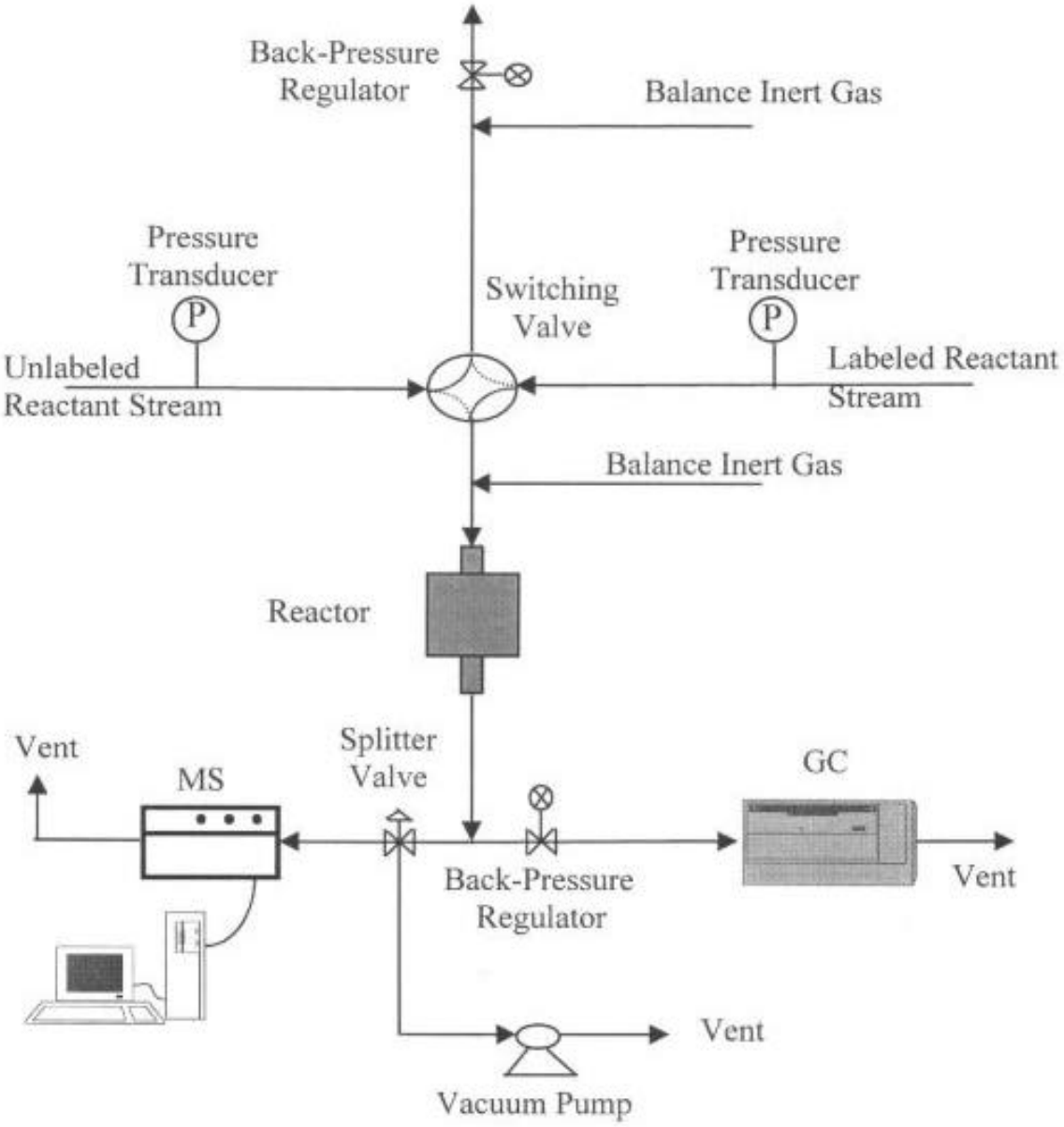

Figure 2.6 Schematic Diagram of Typical SSITKA System [82].

3.0 RESEARCH OBJECTIVES

The objectives of this research on Fe F-T catalysts can be divided into 3 major parts as follows:

3.1 Relating Catalyst Attrition and SiO_2 Composition

Attrition of spray-dried Fe F-T catalysts was found earlier to depend greatly on their particle density, which was determined by types (binder, precipitated or a combination) and concentrations of the structural promoters SiO_2. However the effect of only precipitated SiO_2 addition has not been studied. In this research, attrition of spray-dried Fe catalysts prepared with only precipitated SiO_2 in relatively low amounts was studied. Combining the results with previous findings resulted in a better understanding of the role of SiO_2 in catalyst attrition resistance.

3.2 Improving Physical Strength of Low Attrition Resistance Fe Catalysts

It was previously known that high attrition resistant spray-dried Fe F-T catalysts exhibited no significant changes in attrition properties due to pretreatments. Increased metal-support interactions in supported metal catalysts induced by pretreatments, especially in the presence of water vapor, suggested a possibility for improving the physical strength of poor attrition resistant spray-dried Fe catalysts. Selected spray-dried Fe catalysts that originally possessed low attrition resistances as prepared were pretreated

with either H_2, CO, H_2 + water vapor, or CO + water vapor. Their attrition resistance was evaluated using the jet cup attrition testing system. Physical and chemical properties changes due to the pretreatment of the catalysts were also assessed.

3.3 Understanding Activation of Fe Catalysts at the Site Level

Different pretreatments result in different Fe phases in the catalysts. Steady state isotopic transient kinetic analysis (SSITKA) was used to investigate *in situ* the intrinsic site active and concentration of surface reaction intermediates developed after activation and during CO hydrogenation. An Fe catalyst was pretreated differently with either H_2, CO, or syngas to obtain different Fe phases at the start of reaction. Physical and chemical properties changes of the catalyst samples due to the pretreatments were also investigated.

4.0 RESEARCH METHODOLOGY

The overview schematic of this research is shown in Figure 4.1. The methodologies applied are as follows:

4.1 Catalyst Preparation

Fe catalysts used in this research were prepared by precipitation of solutions containing $Fe(NO_3)_3 \cdot 9H2O$, $Cu(NO_3)_2 \cdot 2.5H_2O$, and $Si(OC_2H_5)_4$ (if added to obtain precipitated SiO_2) in the desired ratio with ammonium hydroxide. The precipitate was washed, filtered, and mixed with the desired ratios of $KHCO_3$. The resulting precipitate was slurried with binder SiO_2 if added, dried and, calcined.

4.2 Catalyst Pretreatment

4.2.1 Calcination

As standard conditions used in this study, Fe catalysts were calcined under air at 300°C for 5 h with ramping rate from room temperature of 1°C/min.

4.2.2 Passivation

Passivation is important in order to prevent the pretreated catalysts from rapid oxidation upon exposing to the air and preserve the catalyst bulk compositions. The passivation was done at room temperature after catalysts were pretreated using 2% O_2 in

He. An observed 2-5°C increase in catalyst bed temperature and then decrease to room temperature indicated sufficient passivation that created only a thin layer of oxides to protect the catalyst inner bulk composition.

4.2.3 Activation

Fe oxides precursors as prepared are not active for CO hydrogenation and, therefore needed to be activated before reaction. Common activations for Fe catalysts are pretreatments with either H_2, CO, or syngas (H_2 + CO, the ratio 2:3 v/v was used for this study). Activations in this study were done at 280°C for 12 h in a fixed bed reactor, ramping at 1 °C/min from room temperature. Three vol% of water vapor was used for those pretreatments with addition of water vapor.

4.3 Attrition Testing

Catalyst attrition was measured using a jet cup attrition testing system. The schematic diagram of the jet cup is illustrated in Figure 4.2. A catalyst sample was loaded in the jet cup and fluidized for 1 h with an air jet flow rate of 15 L/min. Elutriated fines and the remaining particles in the jet cup were collected and used to calculate attrition indices – weight percentage of fines lost. Detailed calculations are given in Appendix A.

4.4 Acid Leaching

Acid leaching was performed to leach out other metal components and obtain only structure of SiO_2 incorporated in the catalyst particles. A catalyst sample was dissolved in an HCl solution (pH = 1) for 48 h. Then it was washed, filtered, and dried under vacuum at room temperature to avoid any agglomeration induced by heat.

4.5 Catalyst Characterization

4.5.1 X-Ray Powder Diffraction (XRD)

XRD was used to determine the phase composition of Fe catalysts as prepared and after pretreatments. It was operated using a step scan mode at scan rate 2θ of 3 degree/min.

4.5.2 N_2 Physisorption

N_2 physisorption properties (BET surface area, pore volume, and average pore size) of catalysts were measured using a Micromeritics ASAP 2010. A 0.2 g catalyst sample was degassed at 100°C for 1 h and then at 300°C for 2 h prior to analysis. The analysis was done using N_2 adsorption at 77 K.

4.5.3 Chemisorption

H_2 and CO chemisorption were carried out to determine the surface Fe atoms using a Micromeritics ASAP 2010. A 0.5 g sample was pretreated in the system. H_2 chemisorption was performed at 35°C with an assumption of $H:Fe^0_s$ atom ratio of 1:1

while CO-chemisorption was conducted at 25°C and with an assumed stoichiometry ratio of CO:Fe^0_s = 1:2.

4.5.4 Temperature Programmed Reduction (TPR)

The reduction characteristics and total Fe reducibility were determined using an Altamira AMI-1 system. A 0.05 g catalyst sample was used. The analysis was performed from 40°C up to 860°C. The Fe reducibility calculation is presented in the Appendix B.

4.5.5 Scanning Electron Microscopy (SEM)

Particle sizes and surface morphology of catalyst particles were studied using SEM.

4.5.6 Energy Dispersive X-Ray Spectroscopy (EDXS)

A distribution of each element on the cross-sectioned catalyst particle can be determined using EDXS. A catalyst particle was embedded in a polymer and the cross-sectioned sample was obtained by microtoming.

4.6 CO Hydrogenation

CO hydrogenation at methanation conditions was performed to study reactivity of Fe catalysts. A 0.1 g of catalyst sample was pretreated in a fixed-bed micro reactor prior

to reaction. The product stream exiting from the reactor was analyzed by an online gas chromatograph. The reaction was carried out from initial to steady state.

4.7 Surface Reaction Parameters Measurement

Intrinsic site activity (t_M) and concentration of surface reaction intermediates (N_M) of catalyst samples were measured *in situ* at actual reaction conditions using steady state isotopic transient kinetic analysis (SSITKA). A step change was made during the switching between the 2 feed streams containing different isotopic labels (^{12}CO vs. ^{13}CO). The products were traced by mass spectrometry. Detailed calculations of t_M and N_M are given in Appendix C.

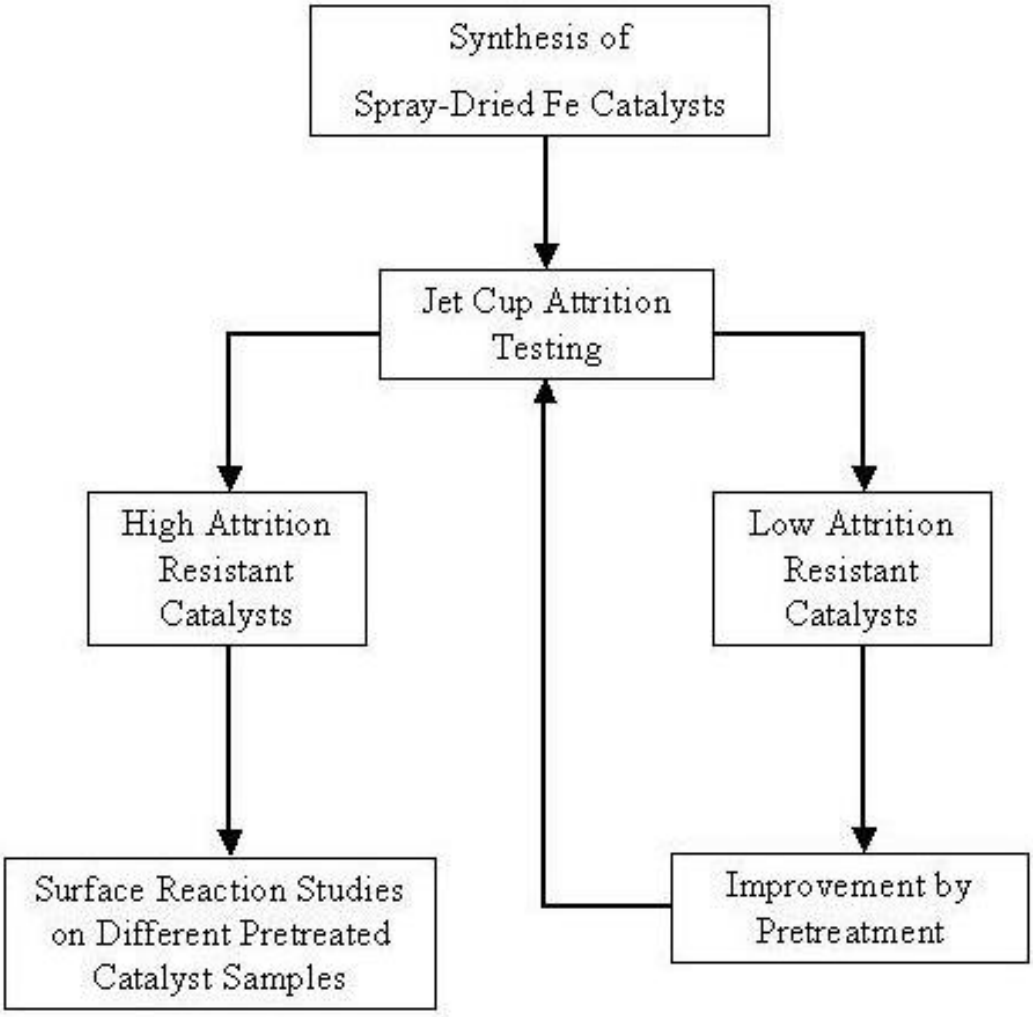

Figure 4.1 Research Overview.

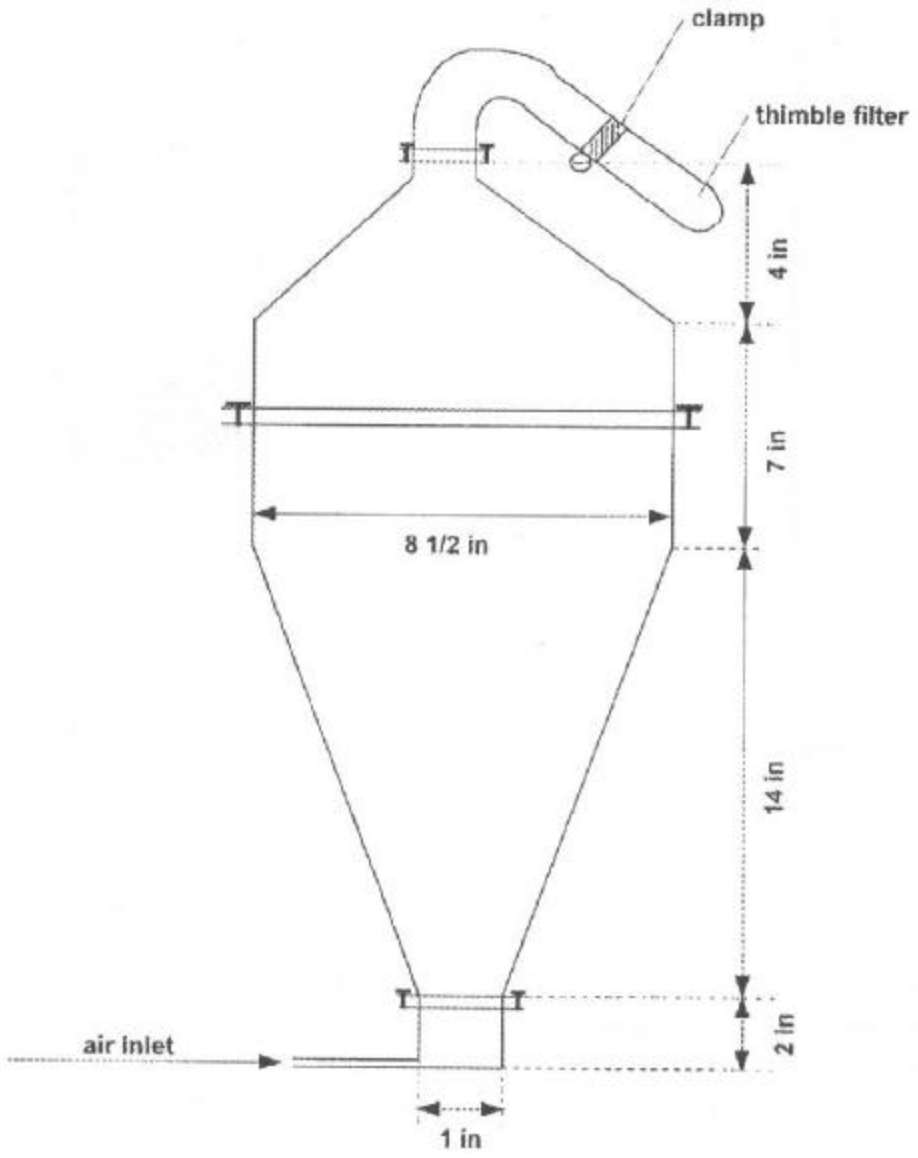

Figure 4.2 Jet Cup Attrition Testing System [11].

5.0 PREPARATION OF ATTRITION RESISTANT SPRAY-DRIED FE F-T CATALYSTS USING PRECIPITATED SIO_2

5.1 Introduction

Iron based catalysts are the preferred catalysts for hydrocarbon production via Fischer-Tropsch (FT) synthesis using low H_2/CO ratio syngas, such as derived from coal gasification or CO_2 reforming of natural gas [1]. This is due to the fact that they have not only high FT activity but also high water-gas-shift activity [2,3]. However, the low physical strength of structurally promoted bulk Fe catalysts (predominantly iron but usually containing lesser amounts of structural and chemical promoters), leading to attrition problems, has continuously been a concern for their application in moving bed reactors, such as fluidized bed and slurry bubble column reactors [4-7] Attrition resistant supported Fe catalysts can be made since silica or alumina supports can be prepared having very high attrition resistances and loading a metal on these supports does not greatly change their attrition resistances, as has been found for supported Co catalysts [8]. However, unlike cobalt-based catalysts, supported Fe catalysts are not preferred for commercial use because of low activity on a per gram basis [2,3,9-11] due to the greater difficulty in reducing/carburizing such highly dispersed Fe [1]. Moreover, with a large amount of support, interaction between the support and the alkali promoter required for these catalysts can also be a potential cause for their low performance [3]. Therefore, a high concentration of the Fe phase is needed to provide sufficient high activity. Nevertheless, use of iron alone (bulk Fe catalyst without a structural promoter) is not suitable because of its low active surface area.

The addition of a structural promoter such as alumina or silica to enhance and maintain higher Fe surface area is thus a common practice in the preparation of bulk Fe-based FT catalysts.

Recently, three-phase slurry bubble column reactors (SBCR) have drawn much attention for application to the highly exothermic FT synthesis (FTS) due to their excellent heat removal capability and ability to operate isothermally. As in other moving bed reactors, attrition of catalysts in SBCRs has also been encountered, especially when Fe-based catalysts have been used. Catalyst attrition in SBCRs can result in downstream filter plugging, product contamination, and/or low product quality. Moreover, catalyst attrition can result in an increase in viscosity of liquid waxy products from FTS in SBCRs during reaction, eventually leading to an operational shutdown to remove attritted particles from the slurry.

In the development of attrition-resistant catalysts, spray drying has been successfully used to prepare Fe FT catalysts with improved physical strength [1,12-17] Workers at Sasol used precipitation to prepare spray-dried Fe catalysts for use in an FT slurry bed reactor [18]. Catalyst surface area and pore structure can be varied greatly by controlling variables such as order of addition, rate of precipitation, temperature, and concentration and pH of solution [2]. Previous efforts by our group have shown that our optimum spray-dried Fe FT catalyst has an attrition resistance suitable for SBCR usage and, also, comparable activity and selectivity to the Rurhchemie Fe catalyst prepared by conventional precipitation [1,15,17]. Our spray-dried catalysts were found to have an evenly distributed SiO_2 phase instead of having a SiO_2 'egg shell' structure as found in attrition-resistant spray-dried vanadyl phosphate and multicomponent molybdate acrylonitrile catalysts developed previously by Dupont [19]. Thus, it was not surprising that attrition resistance of these catalysts was not directly related to their SiO_2 content, as was the case for the spray-dried catalysts with the SiO_2 'egg-shell' structure.

Further investigations [12-14] suggested that attrition resistance of our spray-dried Fe catalysts in their calcined and carburized forms is governed by particle density (particle mass divided by particle volume including all pore volumes). This finding strongly encouraged us to pursue the possibility of using lower precipitated SiO_2 concentrations (expecting higher particle densities). Previous preparations of spray-dried Fe catalyst have tended to have poor catalyst attrition resistances but also high SiO_2 concentrations (about 20-25 wt%). Type (binder vs. precipitated) and total concentration of SiO_2 incorporated into the catalysts were found to directly affect catalyst inner structure and consequently particle density [12-14]. However, the role of precipitated silica by itself on catalyst attrition has not previously been delineated, especially at low concentrations. This is the focus of the present chapter.

All catalysts studied were in their calcined form in order to focus on the effect of precipitated SiO_2 concentration on physical attrition properties. Fe phase change due to different catalyst activation conditions or to FTS itself can potentially induce chemical attrition of catalysts; however, attrition due to phase change either by different activation conditions [14] or by carburization [13] has not been found to play a significant role in spray-dried Fe catalysts having less than 12 wt% SiO_2.

5.2 Experiment

5.2.1 Catalyst

A series of spray-dried Fe FT catalysts having compositions of 100/Fe/5Cu/4.2K/*x*SiO_2 was used in this study. Six catalyst compositions in this series were prepared with precipitated SiO_2 at different levels: 0, 3, 5, 8, 10, and 12 wt% based on total catalyst weight. Fe/P(*y*) is used to refer to each catalyst composition according to its precipitated SiO_2 content incorporated; for instance, Fe/P(5) refers to the catalyst composition with 5 wt% precipitated SiO_2 added. The concentrations of Cu and K relative to Fe remained identical for all catalyst compositions; therefore, they are not used in the catalyst nomenclature. The details of catalyst preparation can be found elsewhere [1,17]. In brief, a solution containing the desired ratio of $Fe(NO_3)_3 \cdot 9H_2O$, $Cu(NO_3)_2 \cdot 2.5H_2O$, and $Si(OC_2H_5)_4$ (added to give precipitated SiO_2) was precipitated with ammonium hydroxide. An aqueous potassium promoter $KHCO_3$ was added to a slurry of the precipitate. The slurry was spray-dried at 250^{o}C in a Niro spray drier and was then calcined at 300 ^{o}C for 5 hours in a muffle furnace. The calcined catalysts were sieved between 38-90 μm before attrition testing and other characterizations.

5.2.2 Catalyst Characterization

Attrition tests were conducted using a jet cup system. The details of the system configuration as well as test procedure have been extensively described previously [20,21]. In

the jet cup test, 5 g of each calcined catalyst sample was evaluated for attrition resistance under identical testing conditions using an air jet flow of 15 *l*/min with a relative humidity of 60±5% at room temperature and atmospheric pressure. After 1 hr time-on-stream, the air jet flow was stopped and the weight of fines collected by the downstream filter was determined. "Weight percentage of fines lost" was calculated and used as one of the attrition indices. Particle size distribution before and after attrition testing was determined with a Leeds & Northup Microtrac laser particle size analyzer and used to calculate "net change in volume moment", the other attrition index used in our attrition studies [12-14,20]. Volume moment is a measure of the average particle size.

A Philips XL30 Scanning Electron Microscope (SEM) was used to observe the morphology of the catalyst particles, before and after attrition, and also the structure of the precipitated SiO_2 network in the catalyst particles, after acid leaching. Elemental analysis was carried out to determine surface composition and distribution of each element on cross-sectional surfaces of catalyst particles using Energy Dispersive X-ray Spectroscopy (EDXS). Powder XRD patterns of the catalyst samples was determined using a Philips X'pert Diffractometer. Catalyst BET surface areas and pore volumes were measured using a Micromeritics ASAP 2010 automated system. Each catalyst sample was degassed under vacuum at 100 ^{o}C for 1 hr and then 300 ^{o}C for 2 hrs before BET surface area and pore volume measurements. Average particle density (particle mass divided by its volume) of each catalyst was determined using low-pressure mercury intrusion. Detailed descriptions of sample characterization, handling procedure, as well as attrition indices have been described in our previous studies [12-14,20,21].

5.3 Results

5.3.1 Catalyst Attrition

Attrition results for all the catalysts studied are summarized in Table 5.1 and the plot of the two attrition indices, "weight percentage of fines lost" and "net change in volume moment" versus total silica concentration is shown in Figure 5.1. Weight percentage of fines lost was calculated based on the ratio of the weight of fines collected from the exit filter of the jet cup and the total weight of all particles recovered after the jet cup test. Net change in volume moment was the average particle size change during the attrition test. Since the average particle size decreases during attrition, net change in volume moment is always a positive number. Volume moments of the attritted catalysts were calculated based on both fines generated and particles remaining in the jet cup. Therefore, net change in volume moment is calculated by {[volume moment of fresh – volume moment of attritted (average bottom & fines)]/[volume moment of fresh]} x 100. Detailed calculations and significance of attrition indices have been given elsewhere [12,20]. High values of attrition indices indicate low attrition resistances of catalysts.

As shown in Figure 5.1, the catalyst without precipitated SiO_2 (Fe/P(0)) showed the highest attrition resistance (least attrition) among all the catalysts tested, while the lowest attrition resistance (highest attrition) was exhibited by the catalysts with the highest concentration of precipitated SiO_2. Figure 5.1 shows clearly that both attrition indices had similar trends with varying concentration of precipitated SiO_2. Effect of fluidization differences (as a result of particle density differences) on catalyst attrition in the jet cup has been considered and proved to be negligible by using an ultrasonic attrition test, an attrition test with no

fluidization involved [12,13,20,21]. Attrition results from the ultrasonic test were found to be comparable and reproducible within experimental error to those obtained with the jet cup test.

5.3.2 Catalyst Particle Properties

The BET surface areas and pore volumes (micro-and-meso pores) of the catalysts, measured by N_2 physisorption, are summarized in Table 5.2. It can be seen (Table 5.2) that BET surface areas fluctuated with the total concentration of SiO_2, and no relationship between these two parameters can be drawn. It should be noted that the experimental error of BET surface area measurement is ±5% based on multiple runs of the same sample. However, this error is increased to ca. ±10% by an added sampling error due to potential partial segregation of different particle sizes and densities within a powder sample. In addition, surface area of catalysts may fluctuate somewhat due to slight variations in a number of preparation parameters (especially precipitation pH). As expected, the catalyst with 0% SiO_2 had the lowest BET surface area. However, BET surface areas of all the catalysts tested did not change significantly during attrition, except for Fe/P(5) and Fe/P(8). The pore volumes of this catalyst series did not vary significantly with total SiO_2 content and remained essentially unchanged after attrition.

The XRD patterns of all the catalysts tested before and after attrition were found to be identical and confirmed that iron existed mainly as hematite (Fe_2O_3). Other components including precipitated SiO_2 were not detectable. The attrition process did not change the XRD patterns of hematite significantly. Thus, as to be expected, attrition affected only physical properties of the catalyst particles and not chemical ones.

Particle density (particle mass divided by its volume including all pore volumes) has been suggested to strongly govern attrition resistance of our spray-dried Fe FT catalysts in calcined, reduced, and carburized forms [12-14]. Therefore, in this present chapter the particle densities of some of the catalyst samples were measured to verify that density also plays a dominant role in determining attrition resistance of the catalysts containing only precipitated SiO_2. Particle density was determined based on low-pressure mercury intrusion in order to prevent mercury from penetrating into the pores of the particles. Mercury porosimetry was used to measure macro pore volumes of the catalyst samples. Particle density and macro pore volume results are summarized in Table 5.3. It can be seen that macro pore volumes of the selected samples were essentially similar within experimental error. The catalyst with no precipitated SiO_2 (Fe/P(0)) had the highest particle density. Particle density decreased as the concentration of precipitated SiO_2 increased.

5.3.3 Catalyst Morphology

SEM micrographs of all the catalyst samples before and after attrition are shown in Figures 5.2-5.4. The catalyst with no precipitated SiO_2 (Figure 5.2/Top) shows clearly non-spherical particles while the other catalysts with addition of precipitated SiO_2 have particles somewhat more rounded in shape and agglomerated. The figures show that breakage during attrition was mostly a break up of particle agglomerates since there was an obvious decrease in numbers of agglomerates after attrition. There was no evidence for the actual breakage of distinct catalyst particles. The presence of small chips and pieces caused by abrasion was observed in the fines collected at the top exit of the jet cup. Degree of breakage increased as the amount of

precipitated SiO_2 incorporated increased, which is in good agreement with changes in the attrition indices. It can also be observed that some particles had interior holes, seen only as dark spots on particles at higher magnification in Figures 5.2-5.4. Such holes, which have also been found for the spray-dried Fe catalysts studied previously [13], were probably produced because of the lower efficiency of a laboratory scale spray drier. Only a small minority of these catalyst particles had holes but they provided a means to determine if the silica structure was maintained during acid leaching of the catalyst particles, discussed in detail later.

To obtain a better understanding of the factors affecting attrition resistance, catalyst inner structure as well as distribution of each element in the catalyst particles are important to determine. The distribution of each element in the catalyst particles was determined using EDXS to analyze the cross-sectional area of catalyst particles prepared by microtoming. The elemental mapping results, an example being shown in Figure 5.5, were found to be similar for all catalyst compositions containing precipitated SiO_2. Iron, Cu and precipitated SiO_2 were found to be evenly distributed throughout the catalyst particles. Potassium, on the other hand, was found in higher concentration at catalyst surfaces as seen on the outer edge of the cross-sectioned particles.

The precipitated SiO_2 network incorporated in the catalysts can be seen by SEM after acid leaching, which dissolves Fe, Fe oxide, Cu, and K and leaves mainly the SiO_2 structure. Catalyst particles were treated with 30% HCl solution (pH=1) for 48 hours to ensure that those elements were leached out. The residue was washed thoroughly with deionized water under vacuum filtration and dried under vacuum at room temperature to avoid agglomeration by heating. Figure 5.6 shows typical SiO_2 structures seen with and without interior holes. Both structures showed a smoother texture of SiO_2 surface at this magnification, which differs from the more

porous SiO_2 structures seen in spray-dried Fe catalysts prepared earlier with either binder or binder + precipitated SiO_2 [12]. The SiO_2 structures obtained by leaching catalysts after attrition were identical, consistent with the fact that there was not a great deal of attrition and most was due to a break up of agglomerates (Figures 5.2-5.4).

5.4 Discussion

5.4.1 Catalyst Attrition Resistance

Although '<u>weight percentage of fines lost</u>' and '<u>net change in volume moment</u>' are both used as attrition indices, they have different physical meanings. While <u>weight percentage of fines lost</u> is a representative of the amount of fines generated and elutriated (ca. <22 μm), <u>net change in volume moment</u> represents a change of volume mean average particle size, weighted mostly towards the larger particles [12]. Therefore, a combination of these two attrition indices have been used in our attrition studies [12-14,20,21] to help delineate physical attrition both by, fracture (generating large broken particles) and abrasion/erosion (generating fines). Due to the difference in their physical meanings, it would not be surprising if the values of these two parameters were not identical with each other. However, for this spray-dried Fe catalyst series prepared with precipitated SiO_2 only, both attrition indices show similar trends in their relationship to the amount of precipitated SiO_2 added (Figure 5.1). These results suggest that the change in average particle size (mostly large particles) occurred in a similar degree as fines generated and possibly that the breakage of large particles facilitated the generating of fines.

Weight percentage of fines lost is, however, considered the most important attrition index in our studies since fines generated cause the aforementioned problems in SBCR operation and since these catalysts were developed for SBCR usage.

In our previous study [12] to determine the effect of SiO_2 type (binder vs. precipitated + binder) and concentration on attrition resistance of spray-dried Fe catalysts, the catalyst having only binder SiO_2 (Fe/P(0)/ B(11)) at the moderate concentration of ca. 11 wt% SiO_2 showed the highest attrition resistance (least attrition). Addition of precipitated SiO_2 to this composition (Fe/P(*y*)/B(10)) was found to reduce attrition resistance sharply. The use of precipitated silica alone at high loadings (20-25 wt%) is well known to result in poor attrition resistant Fe catalysts. However, the effect of having only precipitated SiO_2 at lower concentrations, especially in spray-dried Fe catalysts, was not determined. Thus, it is useful to compare the attrition results of the catalysts in this study (which had the same Fe/Cu/K ratios as those previously studied but were prepared with only precipitated SiO_2) with those from the previous study [12] (see Figure 5.7). Catalysts with only precipitated SiO_2 at concentrations ≤ 12 wt% showed significantly improved attrition resistance than other catalyst compositions. At a moderate total SiO_2 concentration about 11 wt%, the curves for the 3 catalyst series essentially intersect, indicating that some particle property of these spray-dried iron catalysts prepared with similar amounts but different types of SiO_2 could possibly have an influence on their attrition resistances.

The two catalysts having the lowest concentrations of binder SiO_2 seem to have had somewhat different attrition properties than the rest of the catalysts (Figure 5.7). This was possibly due to their being prepared at different solution pH and/or drying temperature, which may have caused lower particle densities than otherwise expected. This effect has been shown to be reproducible.

In the earlier studies [12-14], we found that catalyst attrition depended greatly on catalyst particle density and that this was not due to a bias in the attrition test. Figure 5.6 shows % fines lost versus particle density for catalysts prepared with only precipitated SiO_2 and for catalysts prepared with only binder SiO_2 or with binder + precipitated SiO_2 [12]. The results for the catalysts having only precipitated SiO_2 are completely consistent with the previous data and therefore confirm the strong relationship between these two parameters. Thus a catalyst with a high particle density exhibits low attrition or, in other words, has high attrition resistance. On the other hand, too dense catalysts, however, may not be fluidized well enough to obtain a good dispersion in reactor slurry, leading to poor contact between reactants and catalyst particles.

Thus, attrition resistance is not only the important factor in catalyst design for SBCR usage. High surface area and proper particle density are also needed to obtain high catalytic activity and good fluidization, respectively. The presence of SiO_2 in Fe FT catalysts enhances their active surface areas but lowers the density of the catalyst as well as their attrition resistances. Therefore, the amount of SiO_2 added must be optimized to obtain high catalytic activity, high attrition resistance, and good fluidization of catalyst particles when used in SBCRs.

5.4.2 SiO_2 Structure

After acid leaching, precipitated SiO_2 particles (Figure 5.6) were not found significantly changed in either size or shape from the original catalyst particles. Moreover, those particles with interior-hole structures maintained the same structure (with holes) after being acid leached. All these observed structures after acid leaching as well as the EDXS results suggest that the structure of precipitated SiO_2 in the catalyst particles was a continuously network (skeleton).

There is no evidence that suggests the SiO_2 existed as discrete, non-continuous parts in the original catalyst particles that somehow agglomerated during acid leaching. Although some SiO_2 particles were found to be have interior holes, in no way did they have an 'egg shell' structure [19]. Precipitated SiO_2 was evenly distributed, as shown by EDXS (Figure 5.5), through out the particles, similarly to Fe.

The surface morphology of the acid leached precipitated SiO_2 particles (Figure 5.6) both with and without interior holes was relatively more smooth compared to the porous SiO_2 structures resulting from acid leaching of the catalysts prepared with binder SiO_2 or binder + precipitated SiO_2 [12]. However, the difference in this morphology did not seem to be a major factor for the physical strength of the catalysts (Figure 5.7).

5.5 Conclusions

A series of spray-dried Fe catalysts prepared with different amounts of precipitated SiO_2 was investigated for their attrition resistances. Attrition of these catalysts was found to increase with increasing amount of precipitated SiO_2 added. Based on a comparison of these results with those from our previous study of catalysts with binder or binder + precipitated SiO_2 [12], it can be concluded that, in general, addition of SiO_2, regardless of the source, tends to decrease attrition resistance, especially as the total SiO_2 concentration exceeds 12 wt%. However, for catalysts with binder SiO_2, there appears to be a reproducible maximum in attrition resistance for 10-12 wt% binder SiO_2. For some reason yet to be fully known, use of binder $SiO_2 \leq$ 10-12 wt% as the sole source of SiO_2 produces catalysts with lower particle densities than at the optimum.

Our results clearly show that precipitated SiO_2 can be used in the preparation of attrition resistant spray-dried Fe catalysts when present in a proper amount (less than 12 wt%) so long as appropriate precipitation and spray-drying techniques are employed.

Attrition resistance of spray-dried Fe FT catalysts prepared with any SiO_2 type can be concluded to be governed by particle density. Addition of SiO_2 tends to decrease catalyst particle density resulting in lower catalyst attrition resistance. However, too dense catalysts may not be fluidized sufficiently to provide a good dispersion of catalyst particles in a reactor slurry. A catalyst that will perform well in a slurry bubble column reactor must have a proper particle density to fluidize well in the slurry and also have a high surface area for high catalytic activity. Therefore, addition of SiO_2 to spray-dried Fe catalysts must be optimized to provide high active surface area, suitable particle density for good dispersion in the slurry, and reasonably high attrition resistance. Based on our attrition results, the optimal amount of SiO_2 to be added to spray-dried Fe FT catalysts to meet those requirements appears to be ca. 10-11 wt% based on total catalyst weight.

Table 5.1 Jet Cup Attrition Results.

Catalyst	Total SiO_2 Concentration (wt%)	Fines Lost (wt%) [a,b]	Net Change in Volume Moment (%) [c,d,e]
Fe/P(0)	0.0	3.2	6.0
Fe/P(3)	2.7	6.4	18.4
Fe/P(5)	5.2	7.5	23.4
Fe/P(8)	7.6	8.6	27.1
Fe/P(10)	9.9	9.3	30.1
Fe/P(12)	12.1	7.7	27.8
Fe/P(16)	16.1	24.5	--
Fe/P(20)	19.8	29.9	--

(a) Wt% fines = weight of fines collected/weight of total catalyst recovered x 100%.

(b) Error = ±10% of the value measured.

(c) Net change in volume moment was determined with reference to the particle size distribution before attrition testing.

(d) Net change in volume moment (VM) = [(VM of sample after attrition test – VM of sample before test) / VM of sample before test] x 100%.

(e) Error = ±5% of the value measured.

Table 5.2 Summary of Attrition Test Conditions and Results.

Catalyst	BET Surface Area (m^2/g)[(a)]		Pore Volume (cm^3/g)[(b)]	
	Fresh	Attritted	Fresh	Attritted
Fe/P(0)	24	23	0.08	0.08
Fe/P(3)	69	63	0.12	0.11
Fe/P(5)	83	115	0.12	0.16
Fe/P(8)	48	69	0.11	0.14
Fe/P(10)	41	44	0.11	0.11
Fe/P(12)	76	84	0.11	0.12

(a) Error = ±5% of the value measured.

(b) Error = ±10% of the value measured.

Table 5.3 Macro Pore Volume and Particle Density of Selected Iron Catalysts.

Catalyst	Macro Pore Volume (cm^3/g) [(a)]	Particle Density (g/cm^3) [(b)]
Fe/P(0)	0.25	1.64
Fe/P(10)	0.26	1.40
Fe/P(12)	0.24	1.44
Fe/P(16)	--	0.81
Fe/P(20)	--	0.79

(a) Measured using mercury porosimetry, error=±10% of the value measured.

(b) Determined using low-pressure mercury displacement, error=±5% of the value measured.

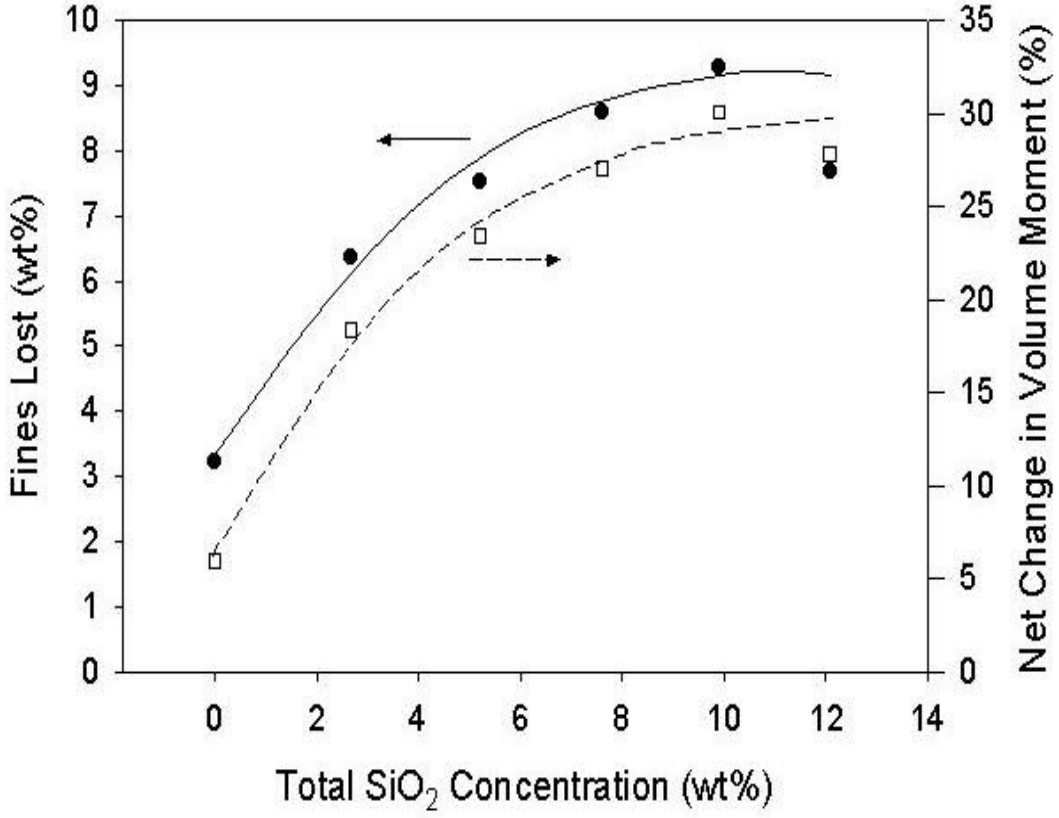

Figure 5.1 Jet Cup Attrition Results.

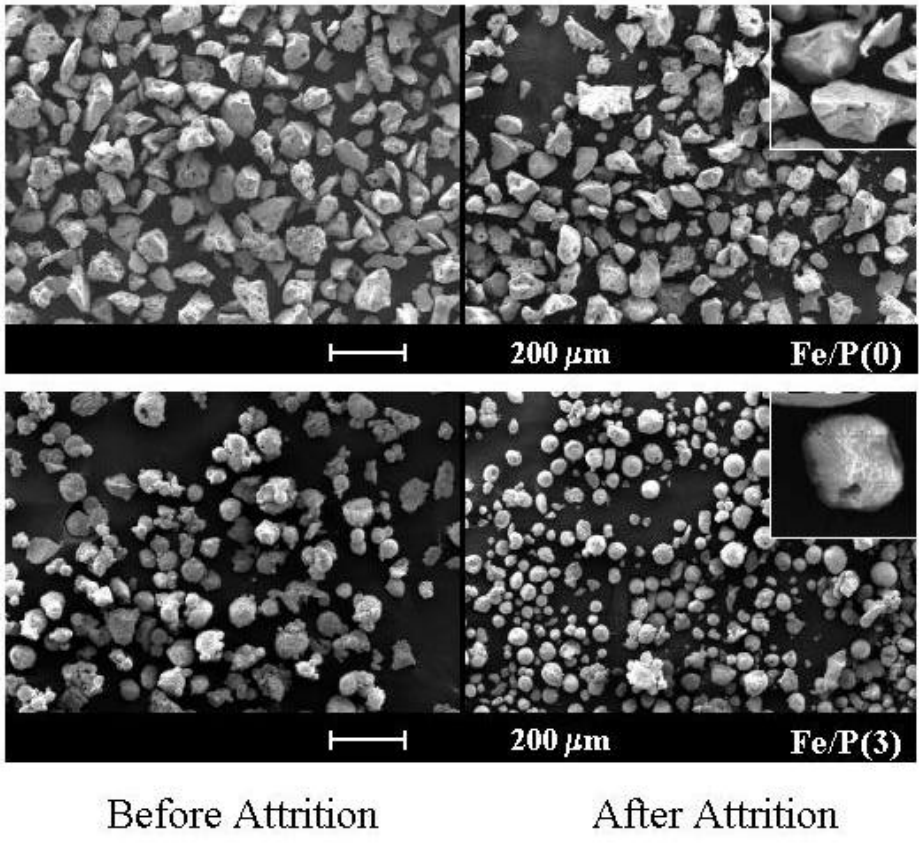

Figure 5.2 SEM Micrographs of Fe/P(0) and Fe/P(3) before and after Attrition.

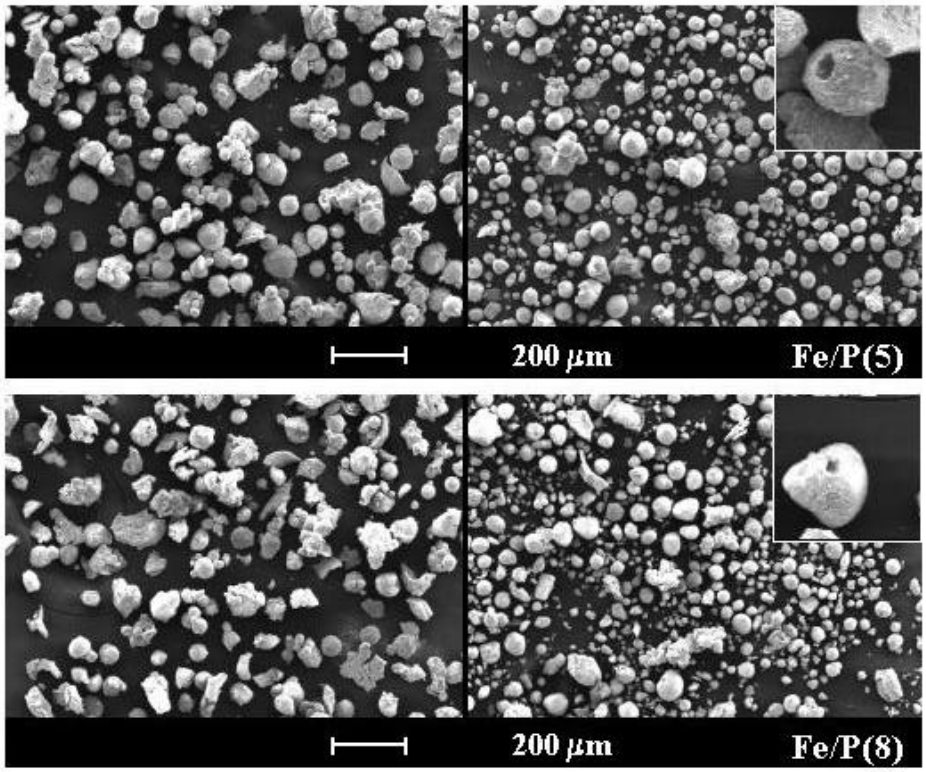

Figure 5.3 SEM Micrographs of Fe/P(5) and Fe/P(8) before and after Attrition.

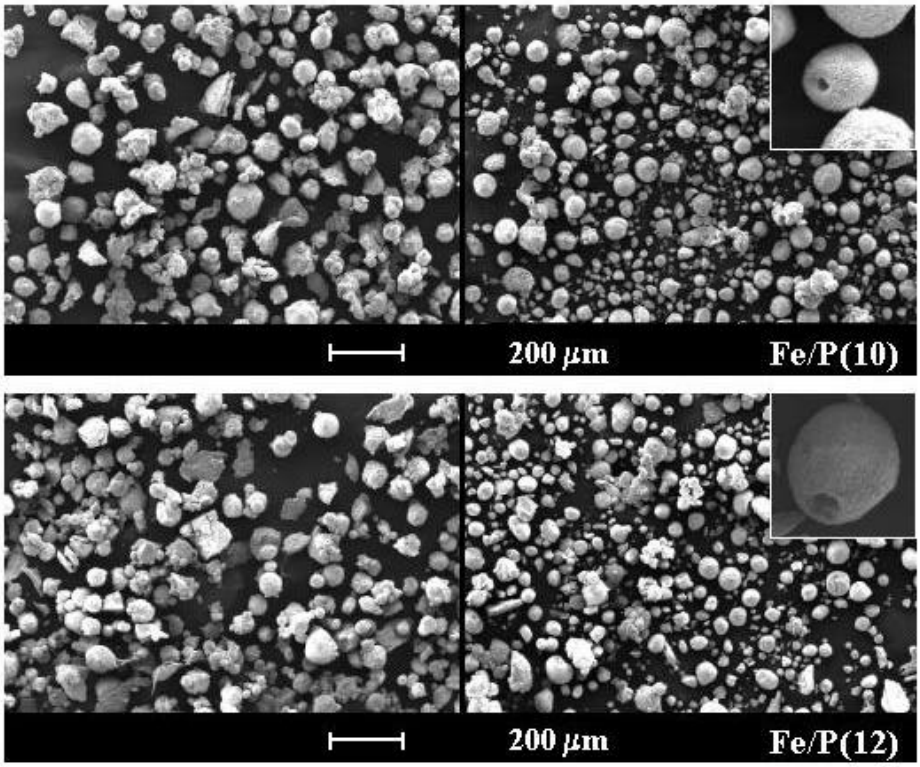

Figure 5.4 SEM Micrographs of Fe/P(10) and Fe/P(12) before and after Attrition.

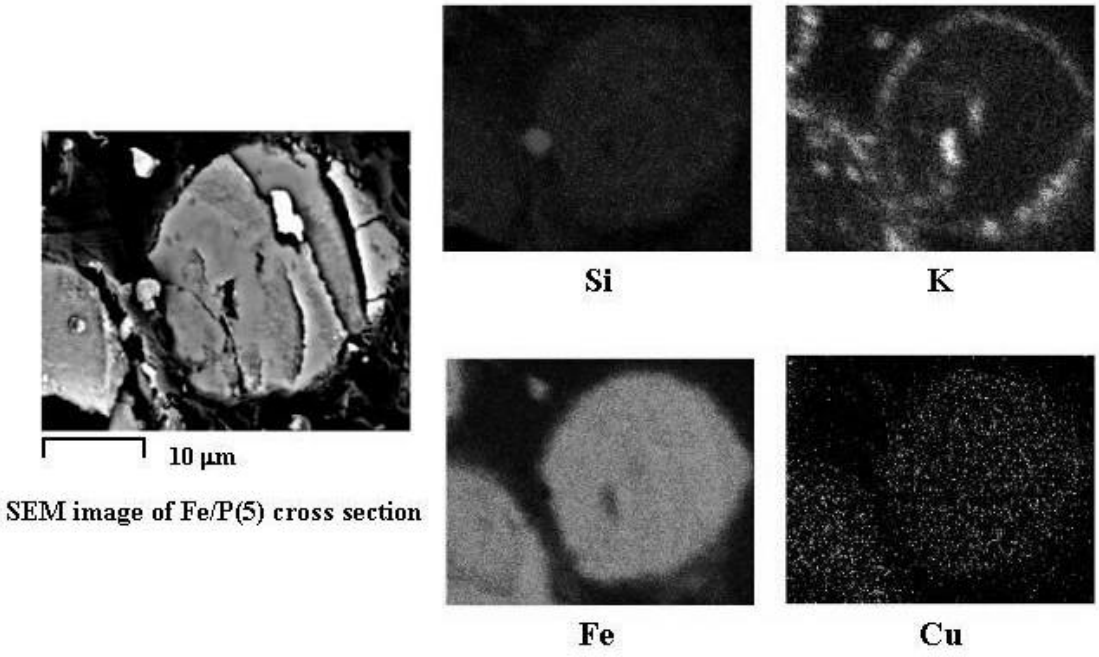

Figure 5.5 EDXS Results for the Cross Section of a Typical Fe/P(5) Particle.

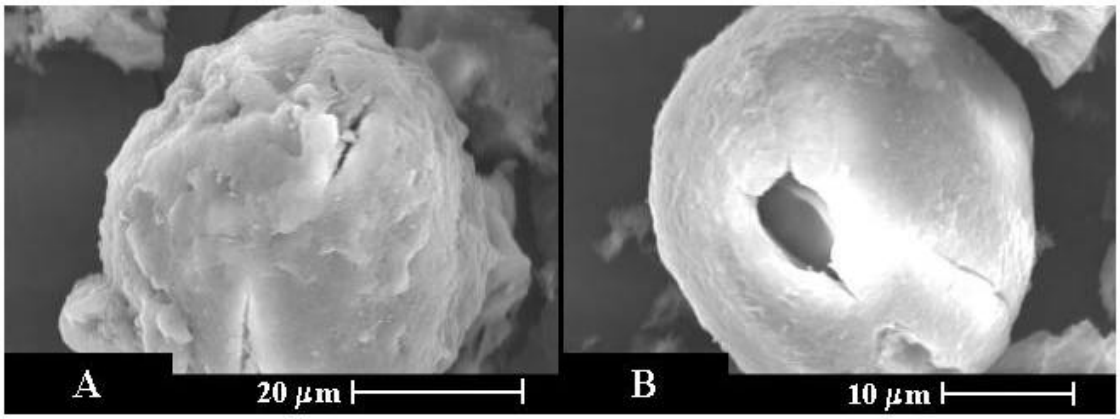

Figure 5.6 SEM Micrographs of Typical SiO_2 Structures after Acid Leaching [Fe/P(12)]: [A] Typical Structure, [B] Particle with Interior Hole.

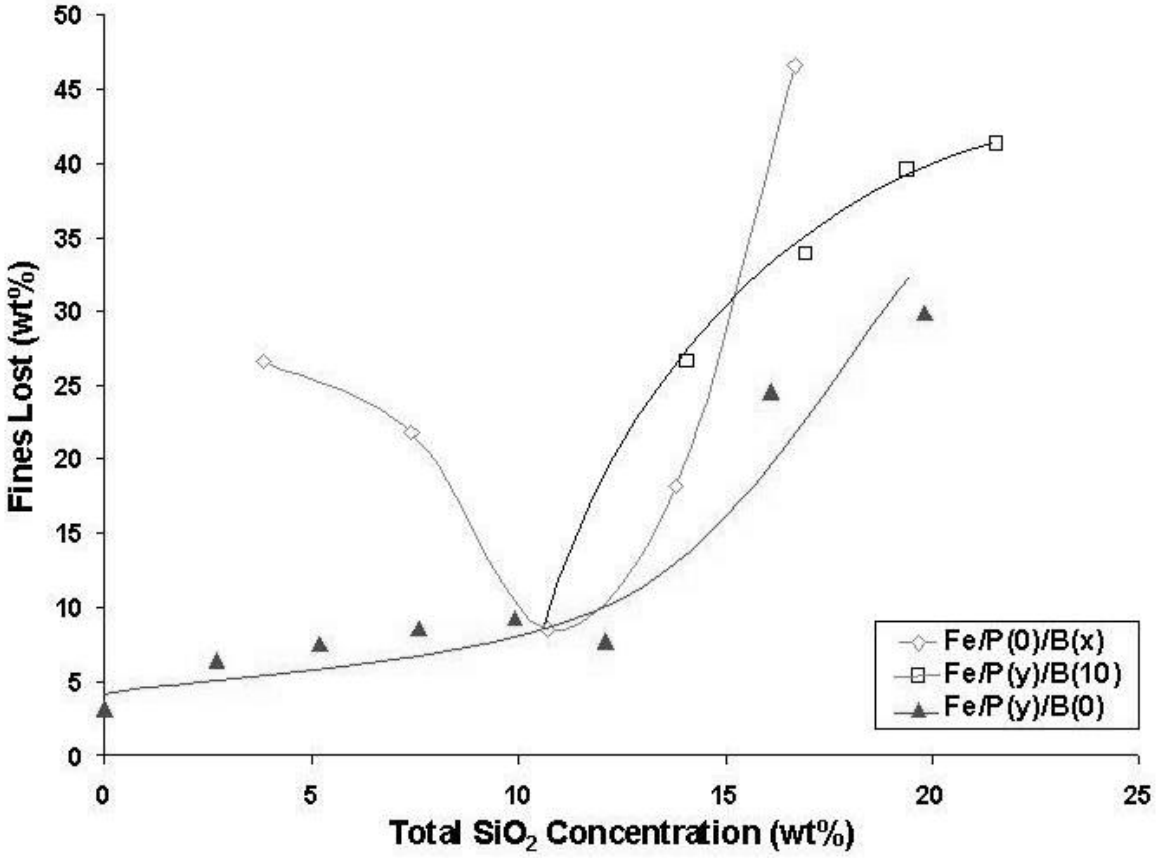

Figure 5.7 Weight Percentage of Fines Lost vs. Total Concentration of SiO_2 for Different Series of Spray-Dried Fe FT Catalysts: B Refers to Binder SiO_2, P Refers to Precipitated SiO_2, *x* and *y* Refer to the Amount of Binder and Precipitated SiO_2 Added, Respectively (Data for Fe/P(0)/B(*x*) and Fe/P(*y*)/B(10) from Reference [1]).

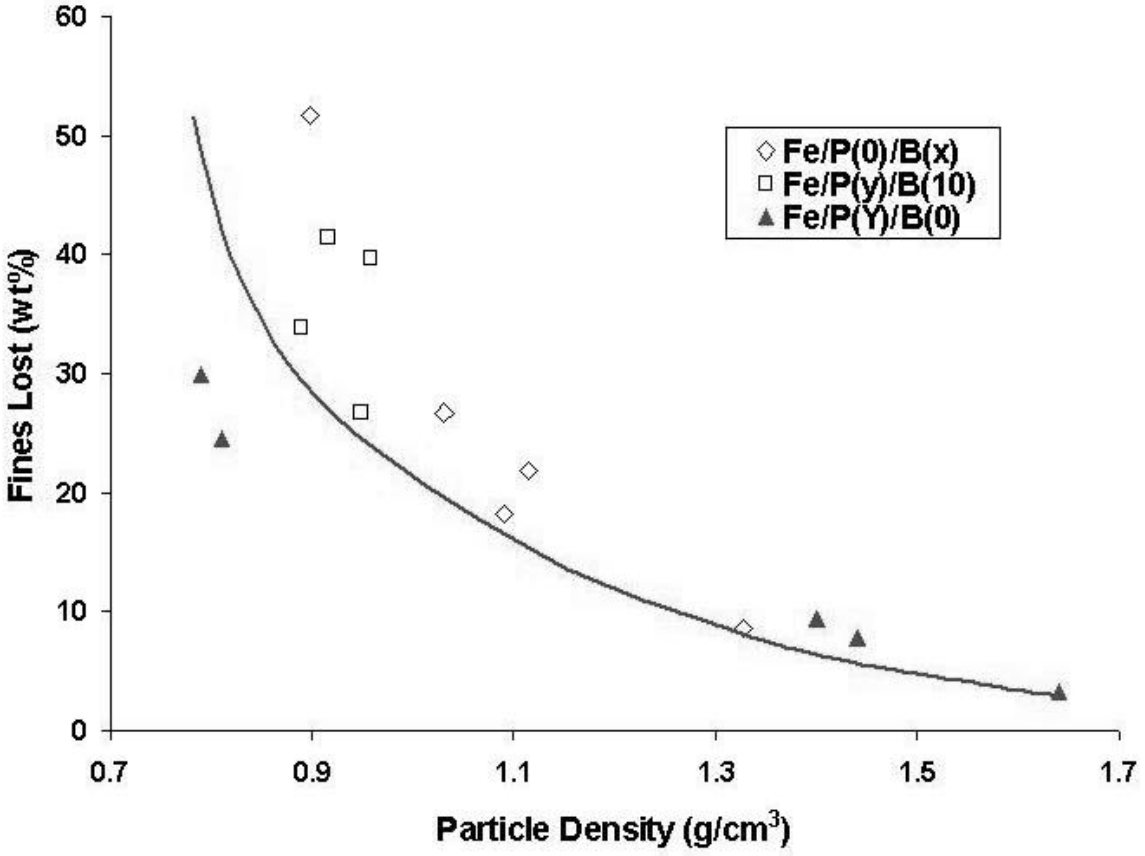

Figure 5.8 Weight Percentage of Fines Lost vs. Average Particle Density of Calcined Fe/P(y), Fe/B(x), and Fe/P(y)B(10) Catalysts.

6.0 SPRAY DRIED IRON FTS CATALYSTS: USE OF PRETREATMENT TO IMPROVE ATTRITION RESISTANCE

6.1 Introduction

Low physical attrition resistances of Fe FTS catalysts have been a major drawback for their application in moving bed reactors, i.e., fluidized bed and slurry bubble column reactors (SBCRs) [1-4]. In addition to physical attrition, Fe catalysts are also subjected to chemical attrition as they undergo extensive phase changes during activation and Fischer-Tropsch (F-T) reaction [1,5,6]. Common activation procedures for Fe F-T catalysts involve pretreatments with H_2 [7,8], CO [9,10], or H_2 + CO [11-13]. A large number of studies have been reported dealing with the effect of these activations on properties and performances during F-T reaction of Fe catalysts [8,14-19], however, few studies have addressed the effect of pretreatment on catalyst attrition [20-22].

Bulk precipitated Fe catalysts are well known to have poor resistance to not only physical attrition [23,24] but also chemical attrition [20], especially after activation and during F-T reaction. Activation of a precipitated Fe catalyst, without a proper structural promoter, either with H_2, CO, or syngas has been reported to reduce markedly the BET surface area of the catalyst as a result of the collapse of the highly porous iron structure [8]. Addition of refractory SiO_2 to precipitated Fe catalysts not only increases the initial surface area but also enhances catalyst stability during activation and reaction by preventing sintering of the iron pore structure. Less surface area loss after different activations has been shown by the same research group for a

precipitated Fe catalyst with 25 wt% SiO_2 [16]. However, such a large amount of SiO_2 can impair catalyst physical strength, causing severe attrition problems.

Recently, spray-drying was successfully used to prepare high attrition resistant Fe catalysts without sacrificing their reactivities [25,26], but high attrition resistance was only achieved for certain formulations. These spray-dried catalysts in the calcined state were found to have physical attrition resistances strongly related to particle density, which was determined by the type (precipitated, binder, or a combination) and concentration of the structural promoter, SiO_2, incorporated [27]. Zhao et al. [21] found that chemical attrition due to carburization was negligible when the amount of SiO_2 incorporated in a spray-dried Fe catalyst was higher than 9 wt%. The effect of pretreatment on both physical and chemical attrition was found to be negligible for a high attrition resistant catalyst prepared with 9 wt% binder SiO_2 [22]. No significant changes in particle size, BET surface area, pore volume, or particle density of this catalyst were detected. The importance of particle density as the key in determining catalyst attrition resistance remained true for spray-dried Fe FT catalysts after carburization [21] or other pretreatments [22]. Recognition of this strong relationship between particle density and catalyst attrition resistance has led us to successfully develop highly attrition resistant Fe catalysts prepared using only precipitated SiO_2 [28].

The effect of pretreatment on spray-dried SiO_2-containing Fe catalysts having low attrition resistance has not been delineated, especially when water vapor is present during pretreatment. Water vapor can be a byproduct of pretreatment of calcined metal catalysts with any gas containing H_2. In addition, the presence of water vapor is known to facilitate metal-support compound formation in metal catalysts, including metal silicate [29-37]. The formation of iron silicate has been reported to occur during reduction at temperatures equal to or higher

than 500°C [38,39]. The presence of water vapor in a pretreatment gas, thus, might increase the interactions between Fe and the structural promoter SiO_2 present in spray-dried Fe catalysts having low attrition resistance and, thereby, increase attrition resistance.

This paper addresses the effects of pretreatment and the presence of water vapor on the attrition resistance of a spray-dried SiO_2-containing Fe catalyst having low attrition resistance in the calcined state. Changes in physical, especially attrition resistance, and chemical properties of the catalyst due to the pretreatments are addressed and discussed.

6.2 Experiment

6.2.1 Catalyst

A spray-dried Fe catalyst was prepared having a composition of 100Fe/5Cu/4.2K with 8 wt% precipitated SiO_2 and 8 wt% binder SiO_2. The details of catalyst preparation including incorporation of different types of SiO_2 have been described elsewhere [25,40,41]. In brief, a solution containing nominal atomic ratios of Fe, Cu, and Si (added to give precipitated SiO_2) was precipitated at room temperature with ammonium hydroxide. The resulting precipitate was filtered, washed, and then mixed with the desired ratio of $KHCO_3$ solution. Binder SiO_2 was added to the reslurried precipitate before spray drying at 250°C in a Niro spray drier. Calcination was then carried out at 300 °C for 5 h in a muffle furnace. The calcined catalyst was sieved to particle sizes between 38-90 μm before pretreatment, attrition testing, and other characterizations.

6.2.2 Pretreatments

The four pretreatments studied were based on H_2 or CO, with or without 3 vol% water vapor addition. Each 1.9 g catalyst sample was pretreated under identical conditions in a fixed-bed quartz reactor at ambient pressure with a pretreatment gas flow rate of 3.0 NL/g-cat/h. The treatment temperature was increased from room temperature to 280°C at 1°C/min and held at that temperature for 16 h. Following reduction/carburization, the catalyst was cooled down to room temperature under He and passivated with 2% O_2 in He, both at constant gas flow rates of 3.0 NL/g-cat/h. During passivation, the catalyst bed temperature initially increased ca. 2-5°C and then cooled down again to room temperature under the passivation gas flow. This indicates the formation of a thin layer of Fe oxides, enough to prevent severe oxidation upon exposure to air and yet preserve the bulk compositions of the catalyst samples after pretreatment [42]. After passivation, a part of each catalyst sample was removed from the reactor and, without further sieving, stored in a sealed container for characterization. The rest of the passivated catalyst was recalcined under air using a ramp rate of 1°C/min from room temperature to 300°C and holding at that temperature for 5 h with an air flow rate of 3.0 NL/g-cat/h. After cooling down under air to room temperature, the recalcined catalyst was then removed from the reactor and, without further sieving, put into another sealed container.

6.2.3 Catalyst Nomenclature

The following nomenclature is used to refer to the four different pretreatments and also the pretreated catalyst samples: [H] for H_2-, [Hw] for (H_2 + H_2O)-, [CO] for CO-, and [COw] for

($CO + H_2O$)-pretreatments and pretreated samples. The original calcined catalyst, with no pretreatment applied, is used as a benchmark and is referred as P8B8 to indicate that it contains 8 wt% precipitated (P) and 8 wt% binder (B) SiO_2. Each pretreated sample was prepared from the same P8B8 catalyst. The concentrations of Fe, Cu, and K were identical and are not included in the catalyst nomenclature.

6.2.4 Catalyst Attrition

All pretreated catalyst samples were recalcined before attrition measurement in order that they could all be studied in the same stable state. Attrition measurements were carried out using a jet cup system. The details of the system configuration and testing procedure, previously described in detail [1], remained identical for this study, except as specified below. Briefly, all attrition tests were conducted under identical conditions using an air jet flow of 15 NL/min with a relative humidity of 60±5% at ambient temperature and pressure. Accumulated fines lost, collected at the jet cup exit, was measured every 10 min during 1 h time-on-stream (TOS) and used to calculate the attrition index, "weight percentage of fines lost". Due to the amounts of catalyst needed to study the different pretreatments, a 1 g catalyst sample was used for attrition measurement in this study instead of the 5 g used in previous studies. Attrition measurements for 1 g catalyst samples were found to be highly reproducible (error = ±3.3% of the value measured), comparable, and efficient. Prediction of the exact amount of catalyst attrition during TOS in an SBCR was not the issue here as it had been in reference [1].

6.2.5 Catalyst Characterization

Powder XRD patterns of the catalyst samples were obtained with a Scintag 2000 x-ray diffractometer with monochromatized Cu K_α radiation (40 kV, 40 mA) and a Ge detector using a step scan mode at a scan rate of 0.02^o ($2q$) per second from 10^o-80^o. XRD peak identification was done by comparison to the JCPDS database software.

Catalyst BET surface areas, pore volumes, and pore sizes were measured by N_2 physisorption using a Micromeritics ASAP 2010 automated system. Each catalyst sample was degassed under vacuum at 100 ^{o}C for 1 h and then 300 ^{o}C for 2 h before each measurement.

Average particle density (particle mass divided by its volume) of each catalyst was determined using low-pressure mercury intrusion by the Materials Analysis Laboratory (MAL) of Micromeritics Instrument Corporation.

The reducibilities of the pretreated iron catalysts after recalcination were determined by temperature programmed reduction (TPR) using an Altamira AMI-1 system and a 0.05 g sample of each sample. The TPR measurements were conducted using 5% H_2 in Ar with a total flow rate of 30 cc/min and a temperature ramp from 40^oC up to 860^oC at 5^oC/min. H_2 consumption was measured by analyzing the effluent gas using an equipped thermal conductivity detector. The reduction of Ag_2O was used to calibrate the detector output.

A Hitachi S-3500N Scanning Electron Microscope (SEM) was used to observe the surface morphology of the catalyst particles, and also the silica structure from the catalyst particles after acid leaching. The SEM was operated using secondary electron detection (SE mode) at 15kV and a working distance of 15 mm. Acid leaching was done by dissolving 0.2 g of catalyst sample in an HCl solution having a 30% concentration (pH = 1) for 48 h and then

washing several times with deionized water under vacuum filtration. The residual particles were dried under vacuum at room temperature to avoid any agglomeration induced by heat.

6.3 Results

6.3.1 Catalyst Attrition

The attrition index, "weight percentage of fines lost", is calculated based on the percentage ratio of fines collected to total particles recovered (fines and bottoms) after 1 h of a jet cup test [1]. For all attrition measurements in this study, fines collection was made every 10 min in order to follow attrition of a sample during 1 h time-on-stream. Detailed calculations and significance of weight percentage of fines lost as an attrition index have been given elsewhere [1,27]. Basically, a high value of the attrition index means a high catalyst attrition or, in other words, low catalyst attrition resistance. Fluidization differences in the jet cup attrition test due to different particle densities of catalysts have been determined previously to have a negligible effect on attrition measurement [21,1-28]. This was proved using an ultrasonic attrition test for comparison that involved no fluidization yet gave comparable attrition results to those obtained in the jet cup test.

The attrition result for the selected spray-dried Fe catalyst in the calcined state used for this study (P8B8) is shown in Figure 6.1 along with 3 different attrition trends related to type and concentration of SiO_2 in spray-dried Fe catalysts found previously in our attrition studies [27,28,43]. It should be noted that the attrition results presented in Figure 6.1 were measured by

jet cup using 5 g catalyst samples. Subsequent attrition data presented in this paper were all measured using 1 g catalyst samples. Figure 6.1 basically shows that P8B8 had very low attrition resistance (i.e., high attrition) in its initial calcined state.

Figure 6.2 shows attrition results with TOS of P8B8 both in the original calcined and pretreated forms. Attrition of calcined P8B8 was reproducible within experimental error, even when the frequency of fines collection was different (5 vs. 10 min). The total amount of attrition after 1 h was slightly lower than when 5 g samples were used (Figure 6.1) due to fewer collisions of the particles at lower concentration in the jet cup. Unlike high attrition resistant spray-dried Fe catalysts, for which pretreatments essentially had no effect in changing their attrition properties [22], P8B8 showed clear improvements in physical strength after the different pretreatments. Attrition resistances of all pretreated samples of P8B8 were higher than that of its original calcined form and increased in the following order of pretreatment: [None] < [Hw] < [COw] < [CO] < [H].

6.3.2 Phase Composition

The calcined P8B8 catalyst as prepared can be expected to consist mainly of hematite, Fe_2O_3. However, its XRD pattern (Figure 6.3) showed no observable peaks of hematite. Since the XRD pattern after recalcination of the calcined P8B8 was identical (not shown here), insufficiency of the first calcination during preparation was not the cause of the relatively amorphous XRD pattern. Instead, it is speculated that the SiO_2 present formed a network structure in the catalyst granules and prevented Fe_2O_3 from crystallizing into sizes large enough to be detected by XRD.

The pretreated catalyst samples after passivation were used for the determination of Fe phase composition in the catalyst after different pretreatments. The resulting powder X-ray diffraction patterns of differently pretreated samples are also shown in Figure 6.3. The diffraction peaks at $2q$ of ca. 44.8° and 65.2° indicate the presence of Fe metal in the [H] sample while the peaks at 39.4°, 41.0°, and 43.7° indicate a mixture of Fe carbides in [CO]. The peaks cited are the most intense peaks for these compounds. Identification of the exact phase of Fe carbides is usually difficult due to the overlapping of their diffraction peaks [20]. Moreover, the dominant peak in [CO] at about 43-44° has been reported to be characteristic of both the ε'–$Fe_{2.2}C$ and χ–Fe_5C_2 phases [15]. Therefore, the Fe carbide mixture formed is suggested to be a combination of these two carbide phases. Addition of water vapor during either H_2 or CO pretreatment resulted in the formation of Fe_3O_4 in both [Hw] and [COw], as indicated by the presence of the two strongest Fe_3O_4 peaks at $2q$ of ca. 35.6° and 62.9°. No trace of iron metal was found by XRD in [Hw], while a mixture of Fe carbides, as found in [CO], was also detected in [COw] but in a lesser amount.

As mentioned previously, all pretreated P8B8 samples were recalcined before attrition testing and other characterizations than XRD in order to facilitate ease of handling and to have the same basis for comparison purposes. The diffraction patterns of the differently pretreated and recalcined P8B8 samples (Figure 6.4) with peaks at $2q$ of ca. 35.6°, 63.0°, 30.1°, 56.9°, 43.0°, and 53.4° (marked with upside down triangles) indicate only the presence of Fe_3O_4. Although the identical calcination conditions were used to recalcine the pretreated and passivated catalyst samples, the different Fe phases in those samples appeared to be oxidized to only Fe_3O_4, and not Fe_2O_3 as expected. This was possibly due to the dry precipitate as prepared having a highly porous structure of FeOOH that could be oxidized to Fe_2O_3 more easily than either Fe metal or

Fe carbides in the pretreated samples under the calcination conditions used. Iron silicate and the oxides of Cu, K, and even Si were not detectable by XRD for calcined or any pretreated P8B8.

6.3.3 Surface Area, Porosity and Density

BET surface areas, pore volumes, and pore sizes of P8B8 in its calcined and pretreated forms were measured using N_2 physisorption and the data are presented in Table 6.1. It has been proven extensively in our previous studies [1-28] that these catalyst properties remain essentially unchanged after jet cup attrition testing. Therefore, in this study, these properties were only measured before attrition testing. As shown in Table 6.1, calcined P8B8 had a BET surface area slightly higher than 200 m^2/g, pore volume of ca. 0.4 cm^3/g, and average micro-meso pore size of ca 75 Å.

These properties changed significantly after pretreatment and passivation: BET surface area decreased by more than 50%, pore volume decreased significantly, and pore size increased 80-90%. After recalcination, both BET surface areas and pore volumes of all pretreated samples were found to decrease even more, especially those of [H] which decreased more than a factor of 5. Based on the results in Table 6.1, the properties of [H] and [CO] apparently changed the most from the original calcined P8B8. [Hw] had significantly higher BET surface and pore volume than [H] in both passivated and, especially, recalcined forms.

In earlier studies [1-28], particle density (particle mass divided by its volume, including all pore volumes) has been shown to be a key parameter in determining spray-dried Fe catalyst attrition resistance. Particle densities of the catalysts were determined using low-pressure mercury intrusion. The results, plotted vs. "weight percentage of fines lost" during jet cup

attrition for 1h in Figure 6.5, were found to be completely comparable to previous findings [21,22,27,28], indicating that Fe catalyst attrition resistance is strongly related to particle density. As seen in Figure 6.5, the calcined P8B8 had the lowest particle density, resulting in the highest attrition (the highest wt% fines lost during a 1 h jet cup attrition test), whereas hydrogen pretreatment resulted in the catalyst [H] having the highest particle density as well as the lowest attrition (highest attrition resistance). It should be noted that the CO-pretreatment of P8B8 in this study resulted in a marked decrease in BET surface area and increase in catalyst particle density comparable to what was found previously by carburization of other low-density spray-dried Fe FT catalysts [21].

6.3.4 Fe Reducibility

In order to detect any increase in Fe-SiO_2 interactions induced by pretreatment, Fe reducibilities of the pretreated Fe catalyst samples were measured and compared to that of the original calcined P8B8. The Fe reducibility data as determined by H_2 TPR are presented in Figure 6.6 and Table 6.2. The TPR peaks are categorized into 2 groups: low temperature peaks (located below 450°C) and high temperature peaks (located above 450°C). The total Fe reducibility is the summation of Fe reduced in both the low and high temperature peaks. It should be noted that all pretreated catalyst samples were recalcined under the aforementioned recalcination conditions before TPR measurement.

The TPR profile (Figure 6.6) of the calcined P8B8 catalyst shows a 2-step reduction, similar to our previous results [44] as well as to others in the literature [16]. The first step (peak at 327°C) is suggested to be the reduction of Fe_2O_3 to Fe_3O_4, which is facile, while the second

step (peak at ca. 600°C) is the reduction of Fe_3O_4 to Fe metal and happens much slower [16]. The shoulder on the peak at 327°C is probably the reduction of the promoter CuO [16]. This was confirmed by TPR of Fe_2O_3 (hematite, 99.8%-Fe, Strem Chemicals) and Fe_2O_3 + CuO, prepared by impregnating Fe_2O_3 with $Cu(NO_3)_2 3H_2O$ (98-102 %, Alfa Aesar) solution, drying, and then calcining under the identical conditions that were used to prepare the calcined P8B8 catalysts (Figure 6.6). The reduction of Fe_2O_3 to Fe_3O_4 ($Fe_2O_3 + 1/3\ H_2 \rightarrow 2/3\ Fe_3O_4 + 1/3\ H_2O$) consumes only 1/9th or 11.1% of the H_2 consumed by total reduction of Fe_2O_3 to Fe metal ($Fe_2O_3 + 3\ H_2 \rightarrow 2\ Fe^0 + 3\ H_2O$). This number is in a good agreement with the 12% Fe reducibility of Fe_2O_3 at low temperature (Table 6.2), confirming that its first reduction peak is related to the reduction of Fe_2O_3 to Fe_3O_4. It can also be seen that the TPR profile of Fe_2O_3 + CuO (Figure 6.3) shows the reduction of CuO prior to 243°C, followed by the first step in the reduction of Fe_2O_3 at 281°C. The presence of Cu shifted the first reduction peak for Fe_2O_3 to significantly lower temperature when compared to Fe_2O_3 without the Cu promoter. The shifting to lower temperature of the first reduction peak by Cu addition was also found for the calcined P8B8, although this was to a lesser degree than it was in Fe_2O_3 + CuO. TPR of recalcined [H] and [CO] gave two low temperature peaks between 243°C and 375°C. Addition of water vapor during either H_2- or CO-pretreatment ([Hw] and [COw]) resulted in only one major low temperature TPR peak. That of [Hw] was located at about 325°C while that of [COw] was at 243°C.

The peak areas of the H_2 TPR profiles were used to calculate the Fe reducibility data that are presented in Table 6.2. As shown in Table 6.2, most pretreated P8B8 samples showed decreases in Fe reducibility at lower temperature (< 450°C), especially [CO] whose reducibility

decreased ca. 50%. On the other hand, total Fe reducibility remained largely similar for all the samples.

6.3.5 Particle Morphology and SiO_2 Structure

SEM micrographs (Figure 6.7) show typical catalyst particles of calcined and pretreated P8B8. As can be seen in part in Figure 6.7, particle size and surface morphology of the original calcined P8B8 catalyst were not significantly changed by any of the pretreatments (and subsequent recalcination).

Structure and surface morphology of the calcined and pretreated samples after acid leaching were also studied with SEM (Figure 6.8), where all the components in the catalyst had been leached out except SiO_2. Although these samples underwent the same acid-leaching procedure, the resulting acid-leached particles looked quite different. Various sizes of the acid-leached particles were observed ranging from the size of the original calcined catalyst particles up to agglomerates slightly larger than 1 mm (Figure 6.8, left column). Agglomerates were formed for all of the acid-leached P8B8 samples, even though they were dried at room temperature to avoid agglomeration induced by heat. At higher magnification (Figure 6.8, right column), acid-leached SiO_2 particles of calcined P8B8 were shapeless with relatively flat surfaces. This similar structure was also found in acid-leached [Hw]. However, acid-leached [CO] and [H] formed agglomerates from primary rounded SiO_2 particles having a more defined structure. Acid-leached [COw] particles were different from the other pretreated P8B8 samples since they contained both shapeless and rounded SiO_2 structures.

6.4 Discussion

Unlike the case for high attrition resistant spray-dried Fe catalysts [22] where attrition resistance remained essentially constant following pretreatment, pretreatments with either H_2 or CO significantly improved the attrition properties of low attrition resistant spray-dried Fe catalyst (Figures 6.2), although [H] showed slightly better attrition resistance than [CO]. This improvement was mainly due to significant sintering of Fe metal ([H]) and Fe carbides ([CO]) upon pretreatment, as evident in the tremendous loss of surface area and pore volume (Table 6.1). This decrease in catalyst pore volume (meso- and micro-pores), as determined by N_2 physisorption, surprisingly correlated well with increasing particle density as well as catalyst attrition resistance (Figure 6.9) although this pore volume did not include the macro-pore volume. Furthermore, the loss of surface area in [H] and [CO] also resulted, to some degree, in shifting of the reduction of Fe_2O_3 to Fe_3O_4 to higher temperature (Figure 6.6) due to less accessibility of Fe by H_2 during TPR.

It was initially hypothesized that the addition of water vapor during pretreatments might increase the interaction between Fe and SiO_2, possibly including formation of iron silicate, and thus, better strengthen the catalyst particles. Surprisingly, the results show that, to the contrary, water vapor inhibited the improvement in catalyst attrition resistance, resulting in lower attrition resistant catalyst samples than both [H] and [CO] (Figure 6.2). Furthermore, there were no XRD peaks of iron silicates in either [Hw] or [COw] (Figure 6.3) and also no trace of increased Fe-SiO_2 interaction as revealed by TPR (Table 6.2), since the Fe reducibilities of both [Hw] and [COw] were found to be higher than those of [H] and [CO] (probably due to the high surface areas of the former samples).

Based on thermodynamic data for the iron metal/iron oxide system [45], a H_2O/H_2 ratio > 0.03 provides oxidizing conditions under which the Fe_3O_4 phase is thermodynamically stable. Therefore, the 3 vol% water vapor added during either H_2- or CO-pretreatment under the conditions used in this study probably maintained a partially oxidizing environment during the pretreatment, as evident in bulk Fe_3O_4 formation in both [Hw] and [COw] passivated samples (Figure 6.3). This partially oxidizing condition hindered the formation of iron metal (during H_2 reduction) and iron carbides (during carburization) and, consequently probably decreased sintering (i.e., loss of surface area). Thus, catalyst porosity was maintained (Table 6.1), resulting in lower particle density as well as lower attrition resistance.

The similar behavior of water vapor in retarding reduction [8] and carburization [19] has also been reported to cause less efficient catalyst activation due to the formation of relatively inactive Fe_3O_4. Thus, the presence of water vapor plays an important role in determining Fe phases formed during pretreatment or FT reaction [7,10,46] and, therefore, catalyst performance. Although water vapor may be consumed partly by the water-gas-shift (WGS) reaction during CO-pretreatment, it is unlikely to have been totally converted at 280°C.

The plot of catalyst attrition vs. particle density of differently pretreated P8B8, Figure 6.5, shows a strong relationship between these two factors. This plot was found to be completely comparable to our previous results [21,22,27,28] (Figure 6.10), which have demonstrated the importance of particle density as a key in determining catalyst attrition resistance. Therefore, particle density of spray-dried Fe FT catalysts remains the most significant factor in determining catalyst attrition, regardless of catalyst formulation.

While there were significant changes in the catalyst properties due to the various pretreatments (Table 6.1), the shape, size, and surface morphology of all of the catalysts tested

(Figures 6.7) were shown to be very similar at the magnifications studied. Yet, the SiO_2 structures of the differently pretreated samples after acid leaching (Figures 6.8) were found to be quite different. The SiO_2 structure of calcined catalysts (Figures 6.8) was found to be shapeless with smooth flattish surfaces, which is very different from the rounded shape of the original calcined catalyst before acid leaching (Figures 6.7). It should be noted that none of these SiO_2 structures observed after acid leaching (Figures 6.8) are exactly like the SiO_2 networks in either calcined P8B8 or any of the pretreated samples. The structures seen after acid leaching only can be said to indicate differences in the original SiO_2 structures. Thus, considering the morphologies of the acid-leached samples, the more defined structure of round-shaped SiO_2 particles present in the 2 highest attrition resistant samples ([H] and [CO], Figure 6.2) appears to relate to SiO_2 in a high attrition resistant structure.

Based on the results reported herein, physical strength of poor attrition resistant spray-dried Fe catalysts can, in fact, be improved significantly by pretreatment. Combining this finding with our previous results with a high attrition resistant Fe catalyst [22] suggest that pretreatment can improve catalyst attrition resistance only within a certain limit for a particular catalyst composition. This limit was found to be narrow for a high attrition-resistant spray-dried Fe catalyst since it was already dense as prepared and, unlike the poor attrition resistant catalyst of this study, its density could not be significantly changed during common pretreatment conditions.

6.5 Conclusions

All pretreatments applied were found to increase the physical attrition resistance of the poor attrition-resistant Fe spray-dried catalyst studied. There was no evidence of any significant chemical attrition. H_2 and CO pretreatments were found to improve significantly catalyst physical attrition resistance, however, this improvement seemed to be inhibited by the presence of water vapor during pretreatment. The improvement in attrition resistance of the catalysts tested was due to an increase in particle density, which, for the pretreated P8B8 samples, seemed to relate correspondingly to decreases in their meso- and micro-pore volumes. Particle density remained a key parameter in determining attrition resistance of spray-dried Fe FT catalysts. No significant changes in particle size and surface morphology of catalysts could be observed by SEM at the magnifications studied. However, after acid leaching the SiO_2 structures remaining were quite different, but probably none of them represented the actual SiO_2 network formed in P8B8. Yet, the more defined SiO_2 structure observed for the highest physical strength catalyst samples ([H] and [CO]) may to some extent be an indication of the SiO_2 in a high attrition resistant structure.

Although their physical strength can be improved significantly by pretreatments, these pretreated catalyst samples still have attrition resistances lower than high attrition resistant catalysts and possibly still too low for extended use in an SBCR. High performance Fe catalysts for SBCR usage need to have reasonably high active surface area, high attrition resistance, and also proper density for a good fluidization. From this study, CO activation was found to optimize those catalyst parameters for low SiO_2-containing Fe catalysts.

Table 6.1 N_2 Physisorption Results after Different Pretreatments.

Catalyst	Pretreatment	N_2 Physisorption[a]					
		BET S.A.(m^2/g)		***Pore Vol. (cm^3/g)***		***Average Pore Size (Å)***	
		After pretreatment[b]	Recalcined	After pretreatment[b]	Recalcined	After pretreatment[b]	Recalcined
P8B8	Org. calcined	206		0.39		75	
	[H]	61	11	0.22	0.03	141	123
	[Hw]	85	74	0.29	0.23	137	126
	[CO]	64	46	0.22	0.12	138	104
	[COw]	67	44	0.23	0.16	136	148

[a] Error = ±5% of the value measured.
[b] Passivated after treatement.

Table 6.2 TPR Results for the Calcined Spray-Dried Iron Catalysts.

Catalyst	Pretreatment	Fe Reducibility during TPR[a] (%)		
		Low T Peaks[c]	High T Peaks	Total
Fe_2O_3	N/A	12	42	54
Fe_2O_3+CuO	N/A	11	52	63
P8B8	Org. calcined	28	43	71
	[H]	23	44	67
	[Hw]	19	54	73
	[CO][b]	15	55	70
	[COw]	18	54	72

[a] Error = ±5% of the value measured.
[b] Based on 3 replications.
[c] Peaks at temperature lower than 450°C.

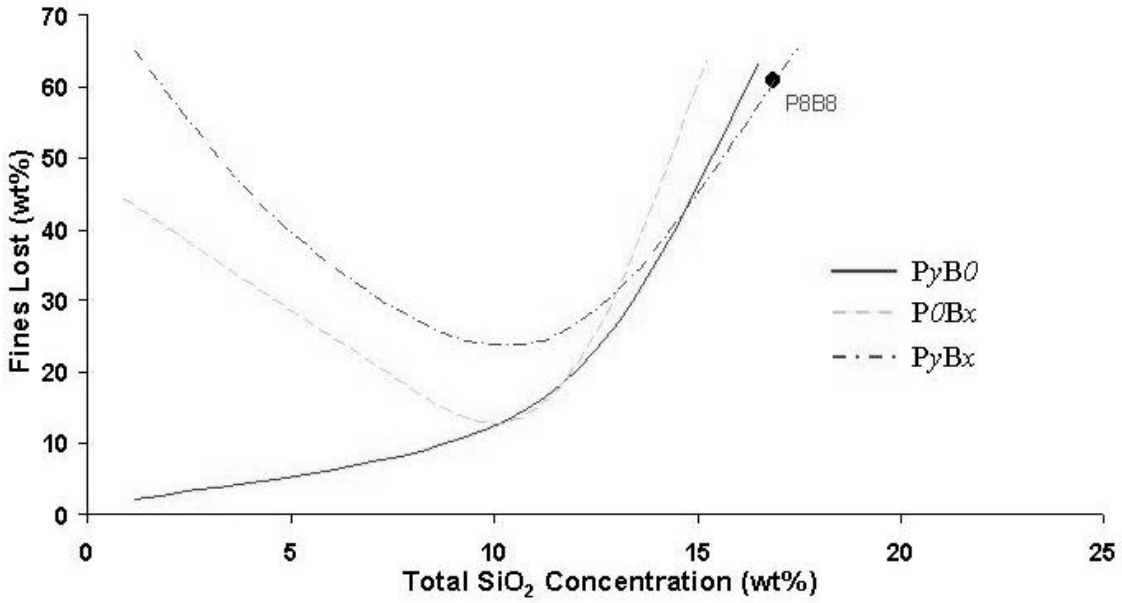

Figure 6.1 Attrition of P8B8 in the Initial Calcined State Referenced to Other Spray-Dried Fe Catalyst Formulations.

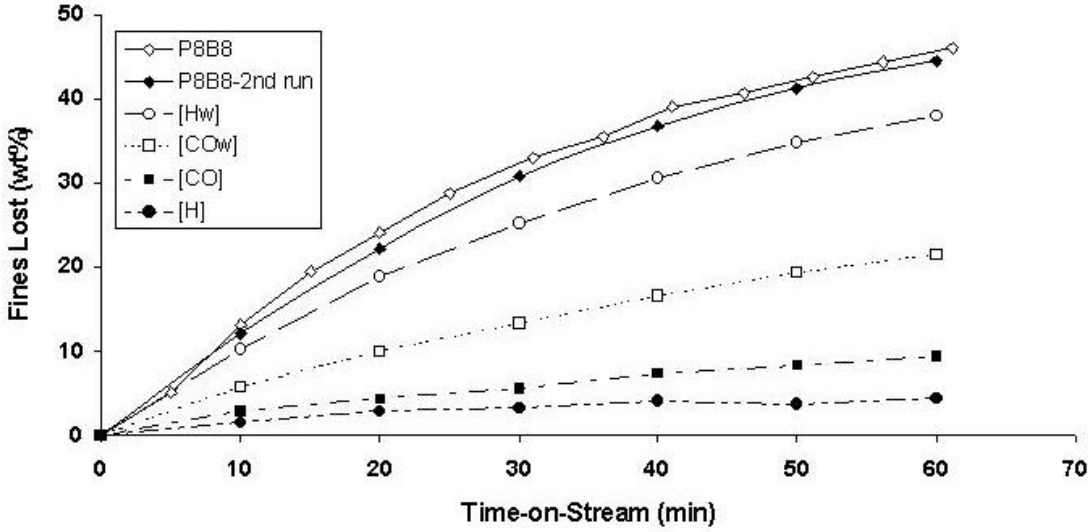

Figure 6.2 Attrition of Calcined and Differently Pretreated P8B8 Catalysts.

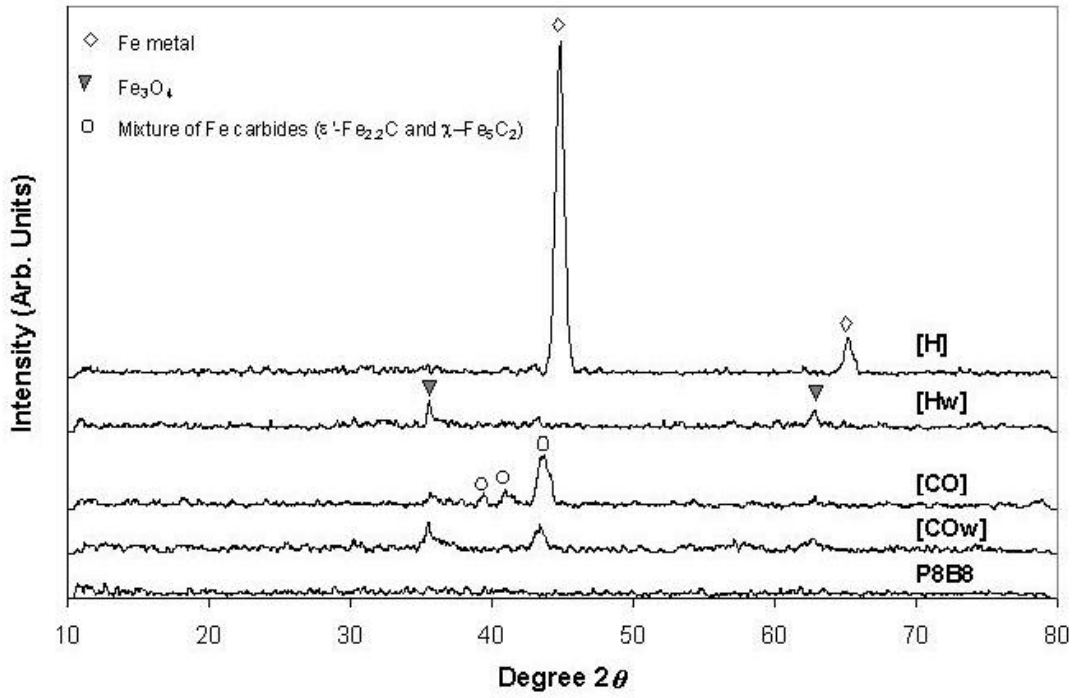

Figure 6.3 XRD Patterns of Calcined and Differently Pretreated P8B8 Catalysts After Passivation.

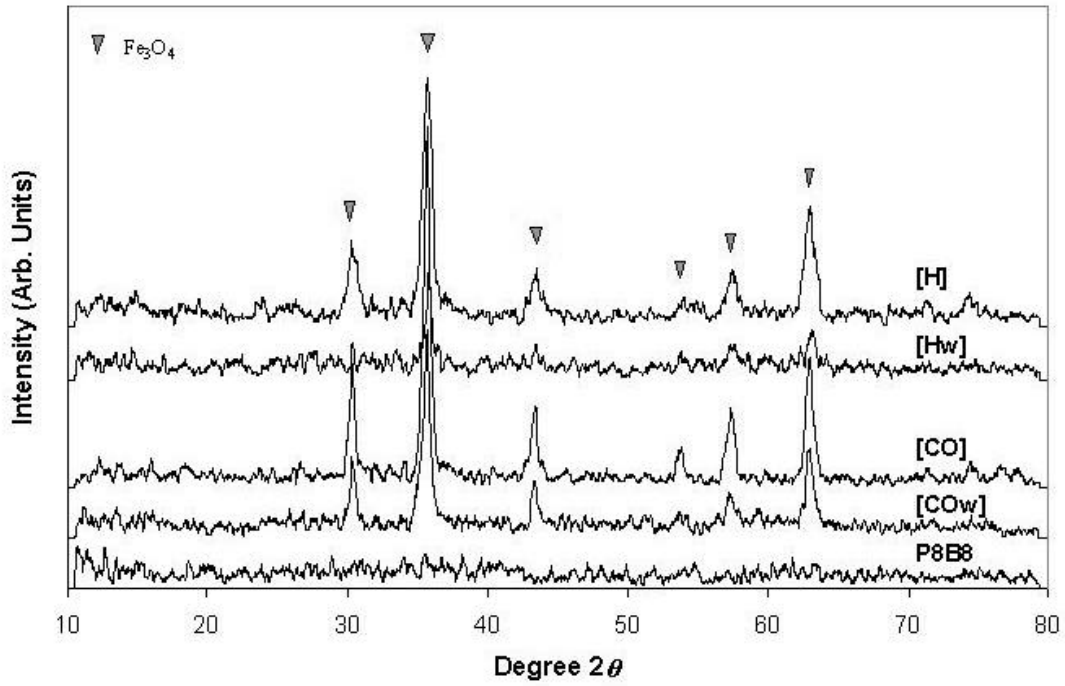

Figure 6.4 XRD Patterns of Calcined and Differently Pretreated P8B8 Catalysts after Recalcination.

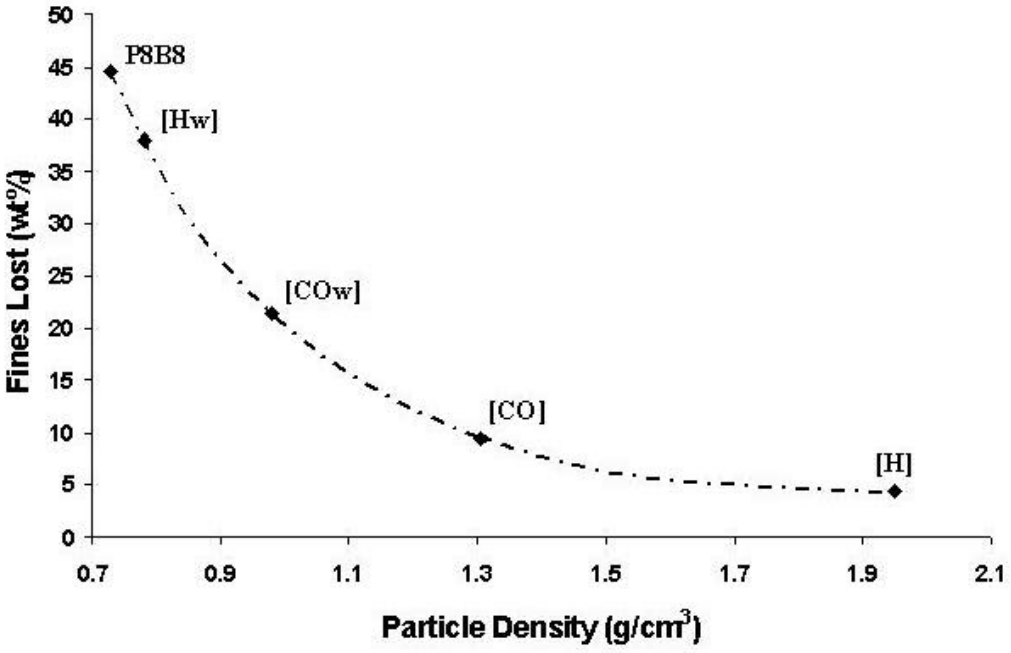

Figure 6.5 Attrition of Differently Pretreated P8B8 (after Recalcination) vs. Particle Density.

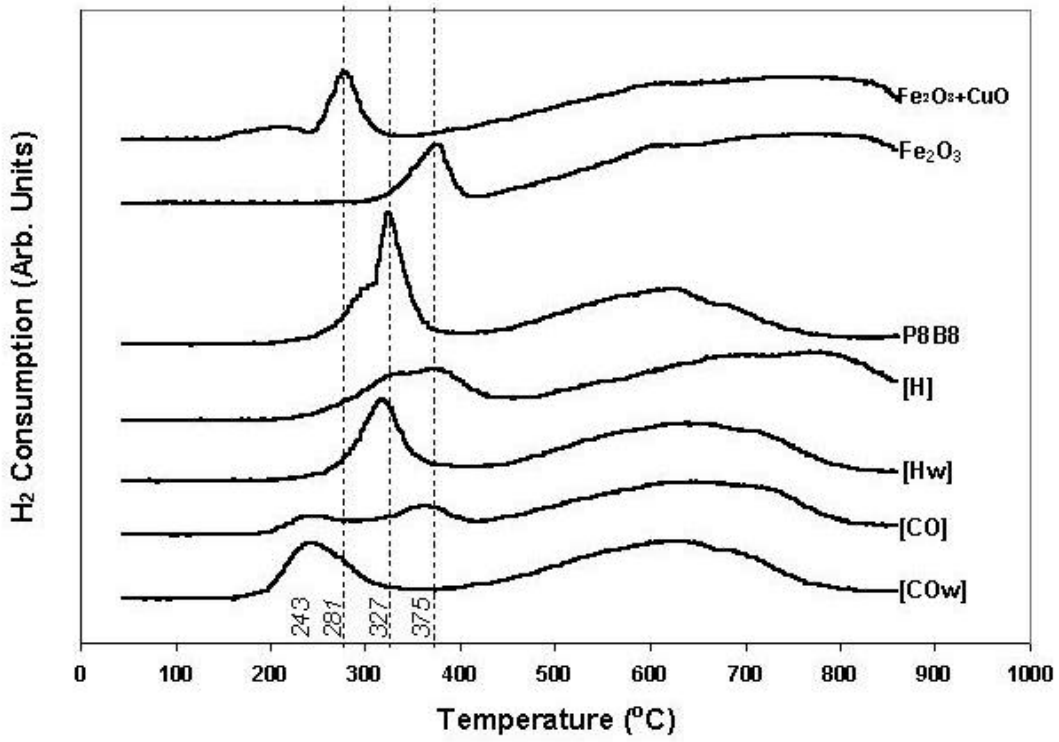

Figure 6.6 TPR Profiles of all Catalyst Samples Studied.

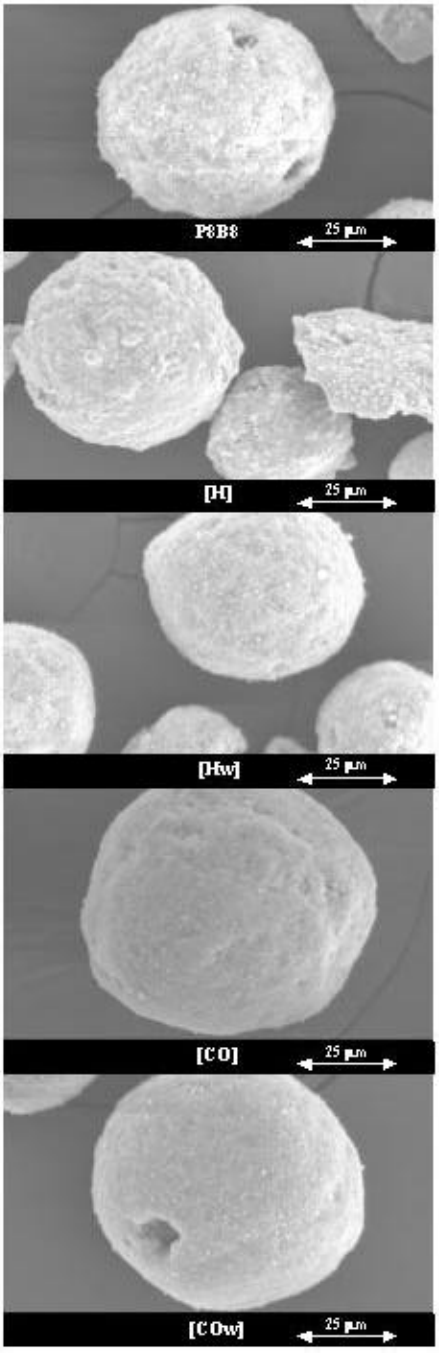

Figure 6.7 SEM Micrographs of Calcined and Pretreated Samples of P8B8.

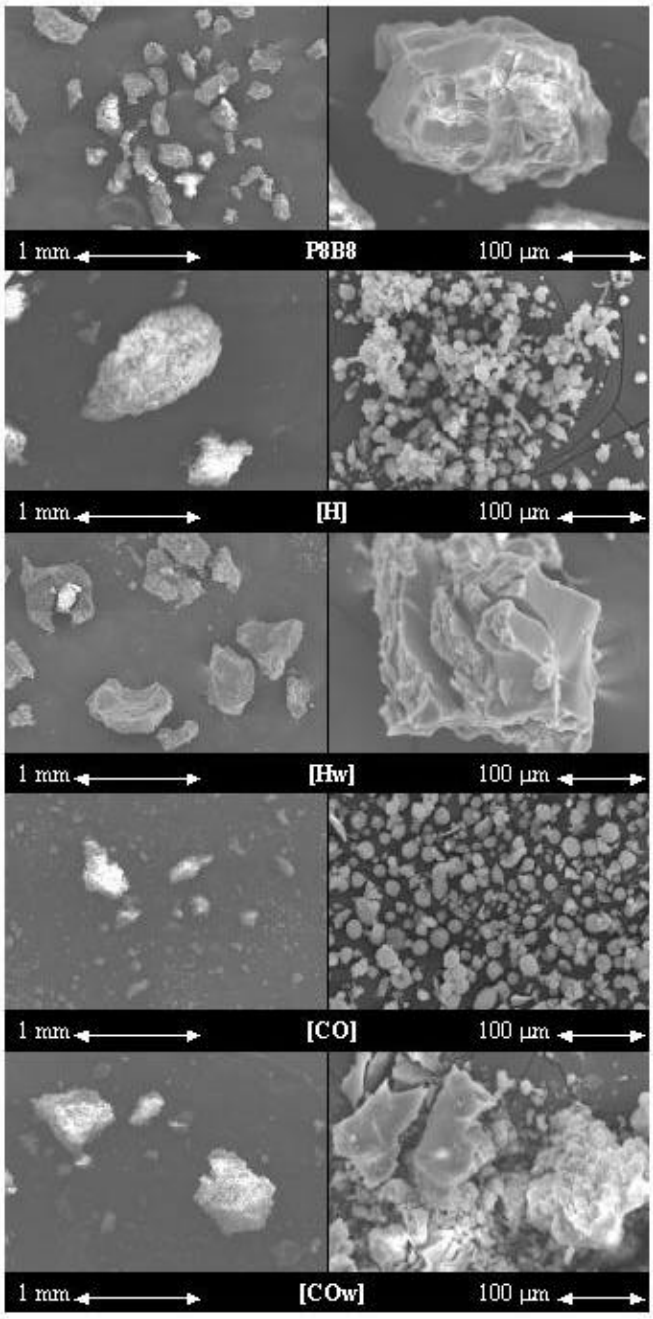

Figure 6.8 SEM Micrographs of Calcined and Pretreated Samples of P8B8.

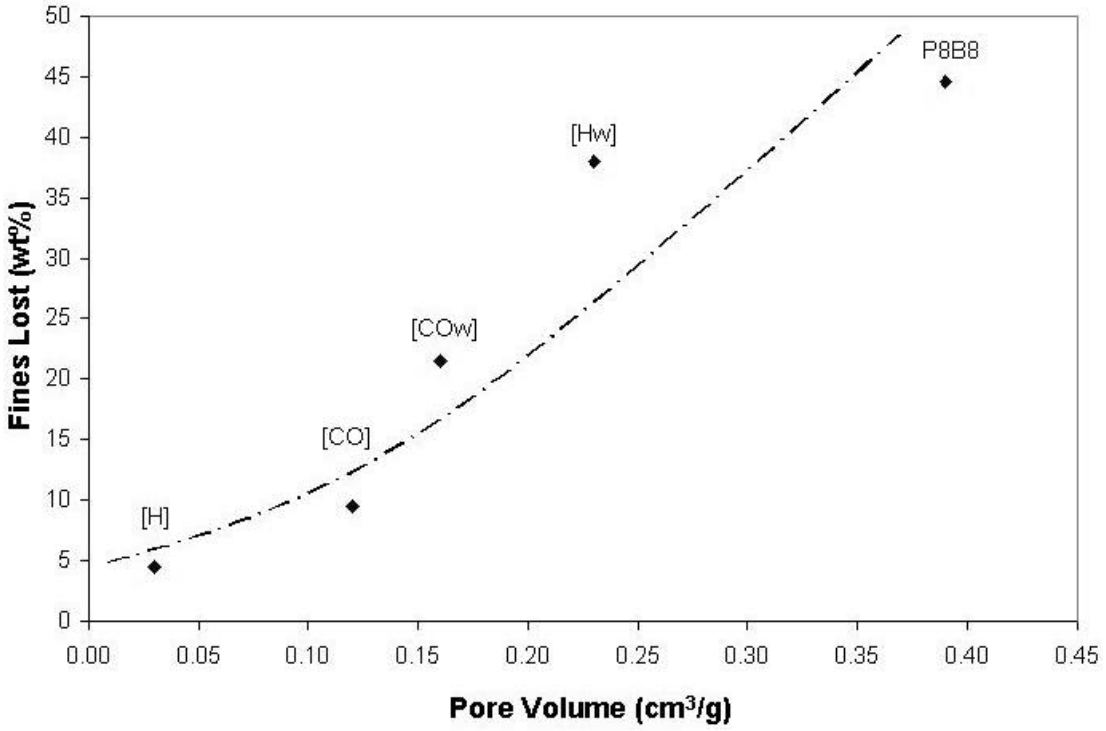

Figure 6.9 Micro-Meso Pore Volume vs. Fines Lost of Differently Pretreated P8B8 Samples.

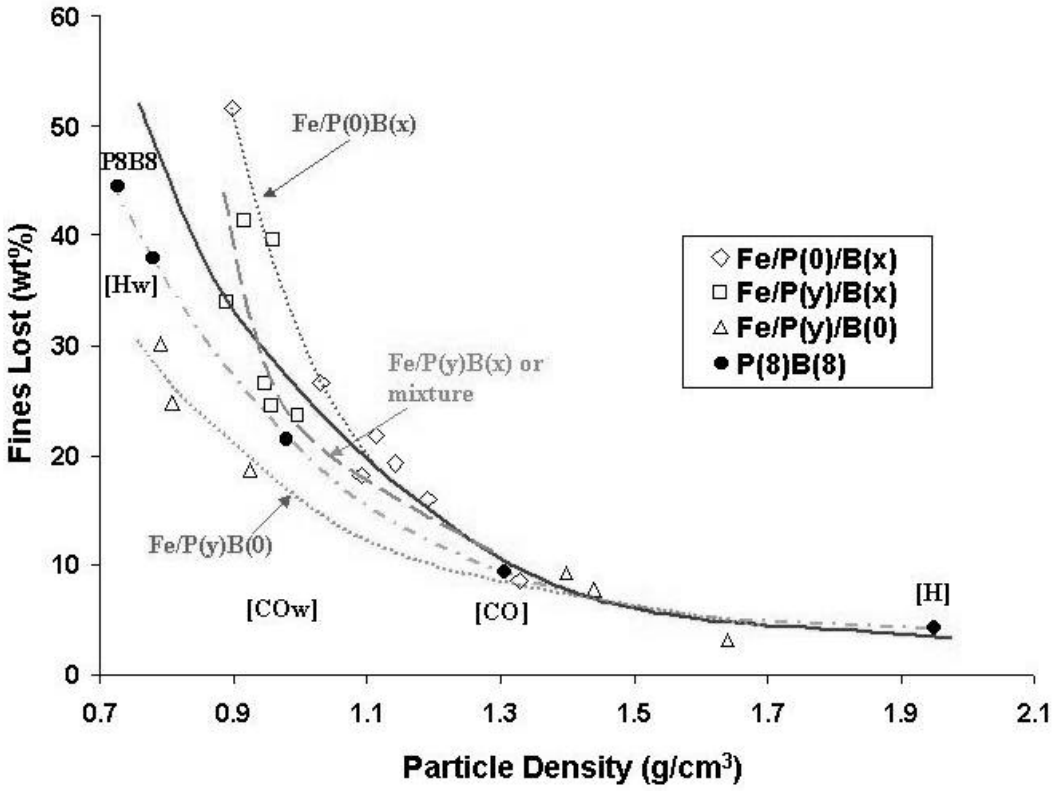

Figure 6.10 Attrition vs. Particle Density of Pretreated P8B8 Plotted with Previous Results.

7.0 SPRAY-DRIED FE FT CATALYSTS WITH LOW SiO_2 CONTENT: EFFECT OF CARBURIZATION ON ATTRITION RESISTANCE

7.1 Introduction

Iron (Fe) is one of the most active catalytic metals for Fischer-Tropsch synthesis (FTS). Application of Fe Fischer-Tropsch (FT) catalysts on an industrial scale in moving bed reactors, such as slurry bubble column reactors (SBCRs), has been greatly hindered by attrition problems [1-4]. Our efforts over the past years in improving the attrition resistance of Fe FT catalysts show that high attrition resistant Fe catalysts can be prepared by spray drying [5,6]. These catalysts have comparable activities to commercial catalysts [7].

Successful use of Fe catalysts depends greatly on successful activation. Common activations for Fe FT catalysts are pretreatments with H_2 [8,9], CO [10,11], or H_2 + CO [12-14]. It was suggested in a previous chapter (Chapter 6) that CO pretreatment is the best activation method for Fe catalysts, as it results in reasonably high surface area for high activity and significantly improved physical strength for a low attrition resistance catalyst. However, the previous study was done with only one catalyst composition that had high SiO_2 content and low attrition resistance. The effect of CO pretreatment (carburization) on the properties of poor attrition resistant catalysts with low SiO_2 content has never been explored and, hence, is the focus of this chapter. It should be noted that high attrition-resistant spray-dried Fe F-T catalysts previously showed no significant changes due to any pretreatment [15].

7.2 Experiment

7.2.1 Catalyst

Three spray-dried Fe catalysts were prepared having identical compositions by weight of 100Fe/5Cu/4.2K but different types and concentrations of SiO_2 (1.1 wt% binder, 0.6 wt% binder + 0.6 wt% precipitated SiO_2, and 15 wt% precipitated SiO_2 based on the Fe weight). The details of catalyst preparation including incorporation of different types of SiO_2 have been described elsewhere [25,16,17]. In summary, a solution containing nominal atomic ratios of Fe, Cu, and Si (added to give precipitated SiO_2) was precipitated at room temperature with ammonium hydroxide. The resulting precipitate was filtered, washed, and then mixed with the desired ratio of $KHCO_3$ solution. Binder SiO_2 was added to the reslurried precipitate before spray drying at 250^{o}C in a Niro spray drier. Calcination step was then carried out at 300 ^{o}C for 5 h in a muffle furnace. The catalyst was sieved to sizes between 38-90 μm before pretreatments and other characterizations.

7.2.2 Carburization

Each 1.9 g catalyst sample was carburized in a fixed-bed quartz reactor at ambient pressure with a specific CO flow rate of 3.0 NL/g-cat/h. The temperature was programmed to increase from room temperature to 280^{o}C at 1^{o}C/min and held at that temperature for 16 h. Then, each of the pretreated catalyst samples was cooled down to room temperature under He

and passivated with 2% O_2 in He, both at constant gas space velocities of 3.0 NL/g-cat/h. During passivation, the catalyst bed temperature increased ca. 2-5^oC and then cooled down again to room temperature under the passivation gas. The passivated catalyst was recalcined under air using a ramp rate of 1^oC/min from room temperature to 300^oC and holding at that temperature for 5 h with an air specific flow rate of 3.0 NL/g-cat/h. The recalcined catalyst was then removed from the reactor and kept separately in a sealed container without further sieving.

7.2.3 Catalyst Nomenclature

P*y*B*x* is used as a nomenclature to refer to different catalyst compositions containing different types of SiO_2: precipitated (P) and binder (B) in their original calcined state, as prepared. The values *y* and *x* indicate the concentrations of precipitated and/or binder SiO_2 in the catalyst, respectively. It should be noted that *y* and *x* are calculated based on the total catalyst weight, not on the Fe weight. [CO] is used to indicate the CO-pretreated samples. For example, P0.5B0.5-[CO] is representative of the CO-pretreated sample of the catalyst containing both precipitated and binder SiO_2, 0.5% of each SiO_2 type. The amounts of Fe, Cu, K in every catalyst compositions were identical; therefore, they are not used in the nomenclature.

7.2.4 Catalyst Attrition

All pretreated catalyst samples were recalcined before attrition measurement in order that they could all be studied in the same stable state. Attrition measurements were carried out with 1 g catalyst samples using a jet cup system. The details of the system configuration and testing procedure have been previously given in Chapter 6.

7.2.5 Catalyst Characterization

A Scintag 2000 x-ray diffractometer with monochromatized Cu K_α radiation (40 kV, 40 mA) and a Ge detector was used to determine powder XRD patterns of the catalyst samples. Each sample was analyzed, using a step scan mode at a scan rate of 0.02^o ($2q$) per second from 10^o-80^o. XRD peak identification was done by comparison to the JCPDS database software.

BET surface areas, pore volumes, and average pore sizes of the catalyst samples were measured by N_2 physisorption using a Micromeritics ASAP 2010 automated system. Each catalyst sample was degassed under vacuum at 100 ^{o}C for 1 h and then 300 ^{o}C for 2 h prior to each measurement.

Acid leaching was done with approximately 1 g catalyst samples. The catalyst sample was dissolved with HCl acid (pH = 1) for 48 h. Then, the sample was washed, filtered, and dried at room temperature under vacuum to avoid any agglomeration induced by heat. This acid leaching procedure has been previously shown to remove all other metal components in the catalyst and leave only the SiO_2 structure [27].

Particle size and surface morphology of the catalysts were studied using a Hitachi S-3500N Scanning Electron Microscope (SEM). The SEM was operated using secondary electron detection (SE mode) at 15kV and a working distance of 15 mm.

7.3 Results and Discussion

Significance of the attrition index "weight percentage of fines lost" has been discussed in the previous chapters. Detailed calculation of weight percentage of fines lost is given in the Appendix A. Basically, a high value of attrition index indicates more fines lost and a low attrition resistance.

Figure 7.1 shows attrition results for all the spray-dried Fe catalysts studied previously in their calcined state, grouping by different types of SiO_2. Attrition measurement using the jet cup is highly reproducible with experimental error ca. ± 5% of the values measured as shown in Table 7.1. Thus, attrition data scatter seen in Figure 7.1 is mainly due to variations in the controlled parameters during catalyst preparation (prepared by different technicians) rather than error of measurement. In addition, a strong influence of the controlled parameters during precipitation including precipitation rate, temperature, concentration, and pH on the properties of Fe catalysts has been previously found [7,18].

Attrition results for the catalysts studied here are presented in Figure 7.2 long with the attrition trends for catalysts with 3 different types of SiO_2. Figure 7.2 basically shows that B1, P0.5B0.5, and P12 had relatively poor attrition resistances. P12 was tested as a benchmark in order to compare between catalysts with low (1%) and moderate (12%) SiO_2 contents. It should be noted that all the attrition results presented in Figure 7.1 and 7.2 were done with 5 g catalyst samples. The rest of the attrition data reported in this chapter were measured using 1 g catalyst samples.

Similarly to what was previously found for P8B8 (Chapter 6), CO-pretreated B1, P0.5B0.5 and P12 showed significantly improved attrition resistance (lower attrition) (Figure 7.3). This is due mainly to the sintering of the Fe structure, resulting in significant decreases in both surface area and pore volume (Table 7.3). Powder XRD patterns of all the calcined catalysts as prepared show their major Fe phase as Fe_2O_3 as expected (Figure 7.4). All catalysts showed primarily the Fe_3O_4 phase after carburization and recalcination, confirming that all catalyst samples tested were in the same crystallite state before attrition testing. This eliminated any factor due to differences in Fe phase and crystallinity on attrition properties.

Carburization has been reported by Zhao et al. [19] to cause chemical attrition (nano-scale attrition due to stress in catalyst particles induced by phase change of Fe during carburization) in spray-dried Fe catalysts, prepared with SiO_2 lower than 9 wt%. Surprisingly there was no chemical attrition observed for any of the catalysts studied. Furthermore, there were no significant changes in average particle sizes of the catalysts due to CO pretreatment (Figure 7.5) or in catalyst surface morphology (Figure 7.6). However, the structures of SiO_2 after acid leaching in the original calcined and CO-pretreated catalyst sample were quite different for all catalysts tested (Figure 7.7). These structures were found comparable to acid-leached P8B8 SiO_2 particles both calcined and after CO-pretreatment, especially for those of P12. Acid-leached SiO_2 particles of B1 and P0.5B0.5 were found in tremendously smaller numbers than P12 and they were relatively small because of the low concentration of SiO_2 present in those catalysts (1%). The acid-leached SiO_2 particles from the calcined catalysts were shapeless with relatively flattish surface while those of CO-pretreated samples had a more defined structure, rounded in shape. None of these SiO_2 particles represented the actual SiO_2 network formed in the catalyst particles since their size and shape were not similar to the original

catalyst particles, especially for those that formed agglomerates have also been found previously in Chap 6 to be different from original catalyst particles. However, the rounded-shape SiO_2 could probably be used as an indication of the structure that resulted in high attrition resistance since it was found in the catalyst samples that exhibited a significant improved physical strength.

Changes in catalyst physical properties due to carburization for the selected catalysts prepared with various types of SiO_2 in this study were found to be very similar to those of P8B8. Therefore, it could be surmised that these catalysts would probably respond to other pretreatments the same way as P8B8 did. In other words, the effect of pretreatments on catalyst properties as reported for P8B8 (Chapter 6) would also be true for other spray-dried Fe catalysts regardless of the type and concentration of SiO_2.

7.4 Conclusions

Unlike high attrition resistant catalysts, carburization resulted in significantly improved physical strength for catalysts with low attrition resistances regardless of the amount of SiO_2 present. Carburization also caused significant decreases in catalyst surface and porosity, which also suggests that the improvement in attrition resistance by carburization resulted from the sintering of Fe in the catalysts. Particle size and surface morphology of the catalyst particles remained essentially unchanged. However, the acid-leached SiO_2 particles of fresh calcined and pretreated catalyst samples were found to be quite different as those of original calcined catalysts which were shapeless while those of CO-pretreated were rounded-shape and more defined.

Although these SiO_2 particles probably did not represent how silica was structured in the catalyst particles, the more-defined rounded shape SiO_2 particles could be used as an indication of an improved physical strength catalyst.

Since different catalyst compositions, either prepared with low (B1 and P0.5B0.5) or moderate (P12) SiO_2, responded to carburization similarly, it is suggested that the influence of carburization on different catalyst compositions that possessed low attrition resistances is similar. Since these catalysts responded to carburization similarly to P8B8 as well, conclusions about the effects of other pretreatments determined for P8B8 would probably also apply to these catalysts.

Table 7.1 Reproducibility Data for Jet Cup Attrition Testing.

Material	Flow Rate (L/min)	Fines Lost (wt%)	Avg. Fines Lost (wt%)	Error (%)
Puralox M1760[a]	15[c]	12.6	13.3	***-5.3***
		13.5		***1.5***
		13.8		***3.6***
B6[b]	10[d]	10.1	10.15	***-0.5***
		10.2		***0.5***
B6	15[d]	16.0	15.9	***-0.6***
		15.8		***0.6***

[a] An alumina.

[b] Spray-dried Fe catalyst containing binder SiO_2: 100/Fe/5Cu/4.2K/7SiO_2.

[c] Measured on 04/07/00 at Pittsburgh.

[d] Measured on 08/26/01 at Clemson.

Table 7.2 N_2 Physisorption Results for all Catalyst Samples Studied.

Catalyst Sample	N_2 Physisorption[a]		
	BET S.A.(m^2/g)	***Pore Vol. (cm^3/g)***	***Average Pore Size (Å)***
B1	75	0.18	157
B1-[CO]	*47*	*0.12*	*97*
P0.5B0.5	97	0.24	100
P0.5B0.5-[CO]	*52*	*0.18*	*80*
P12	165	0.27	64
P12-[CO]	*77*	*0.15*	*78*

[a] Error = ±5% of the value measured.

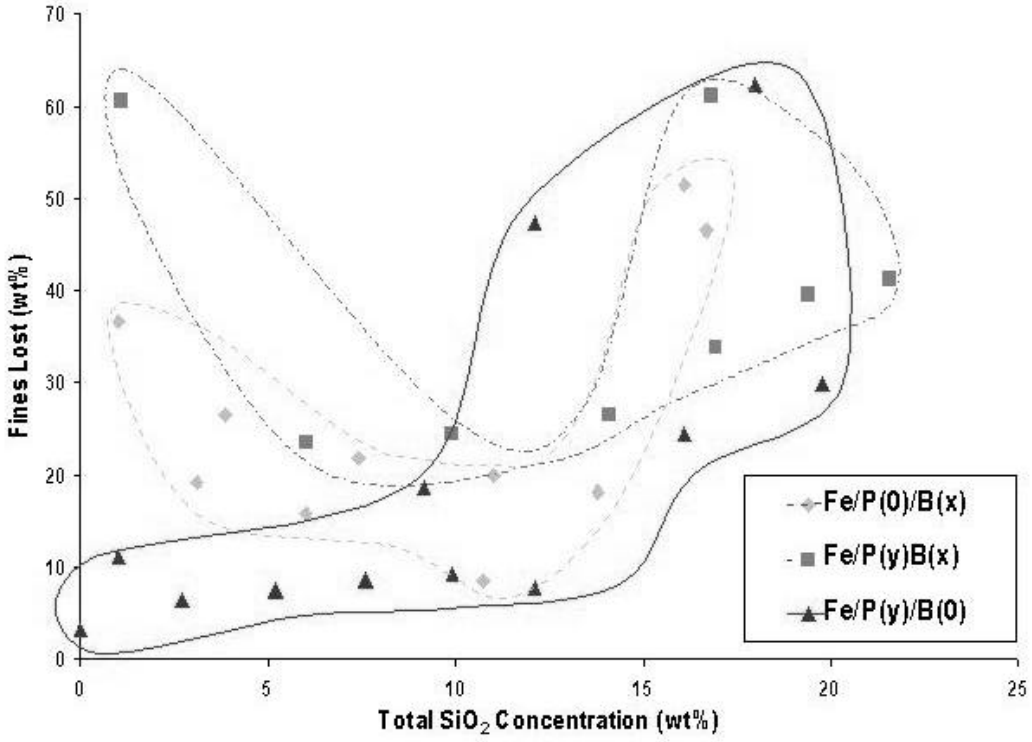

Figure 7.1 Attrition of all Spray-Dried Fe Catalysts in the Calcined State Previously Studied.

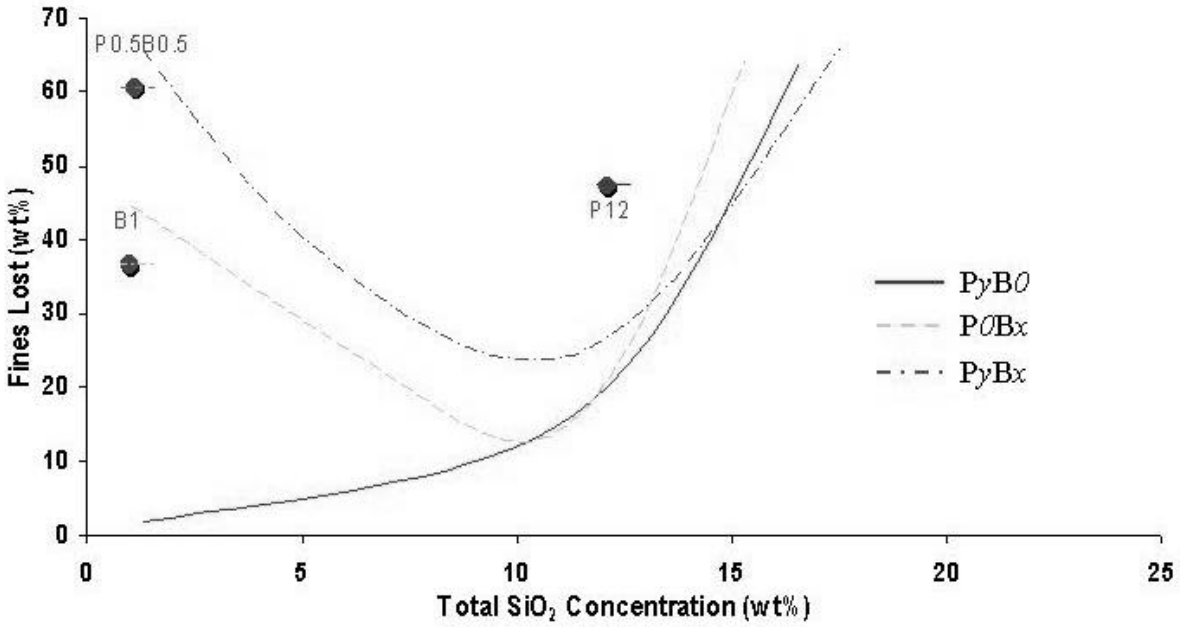

Figure 7.2 Attrition in the Calcined State of the Catalysts Selected for this Study.

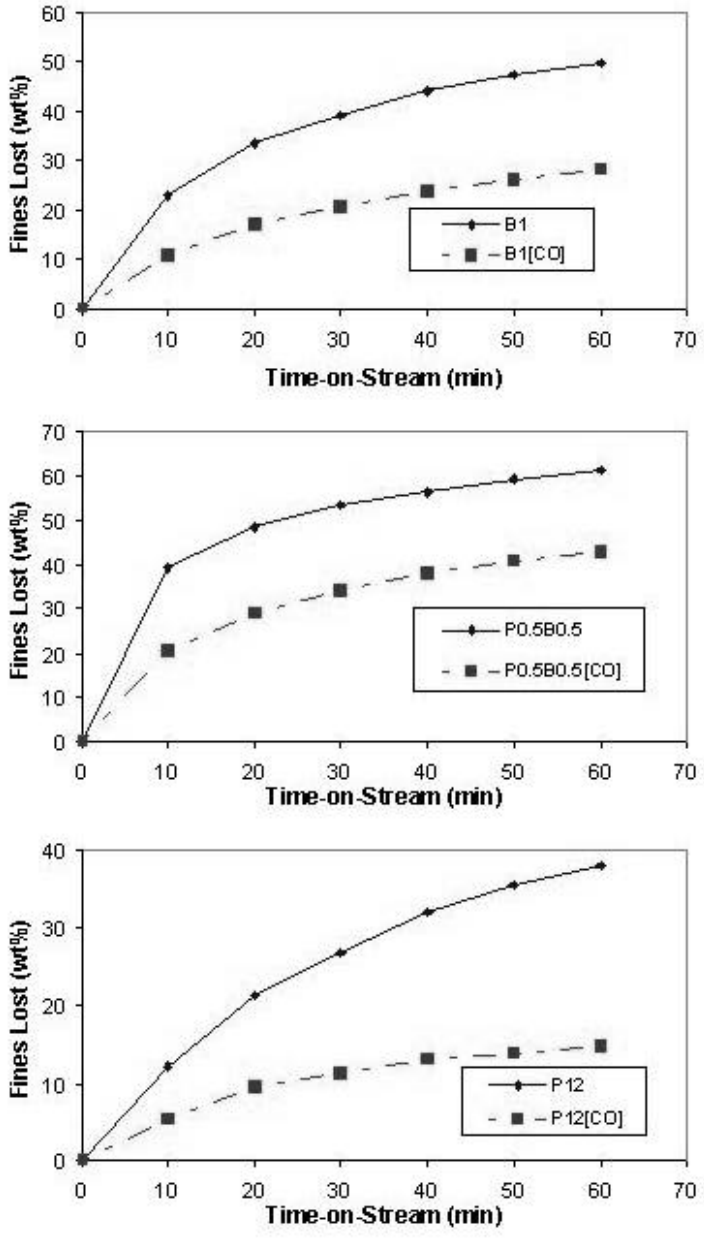

Figure 7.3 Attrition of B1, P0.5B0.5 and P12 Catalysts in both the Original Calcined and CO-Pretreated Forms.

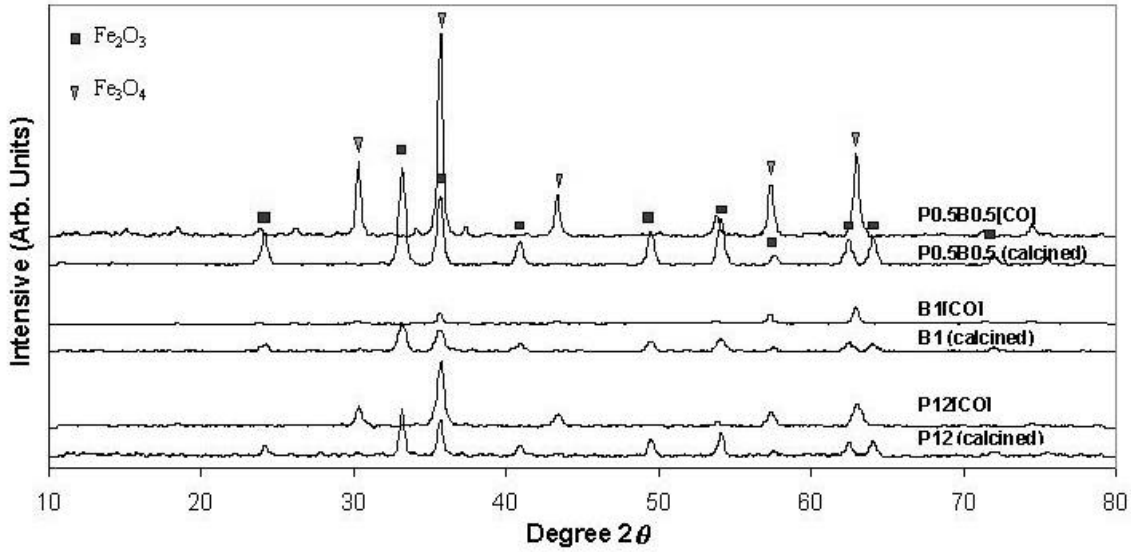

Figure 7.4 XRD Patterns of B1, P0.5B0.5, and P12 Catalysts in both the Original Calcined and CO-Pretreated Forms after Recalcination.

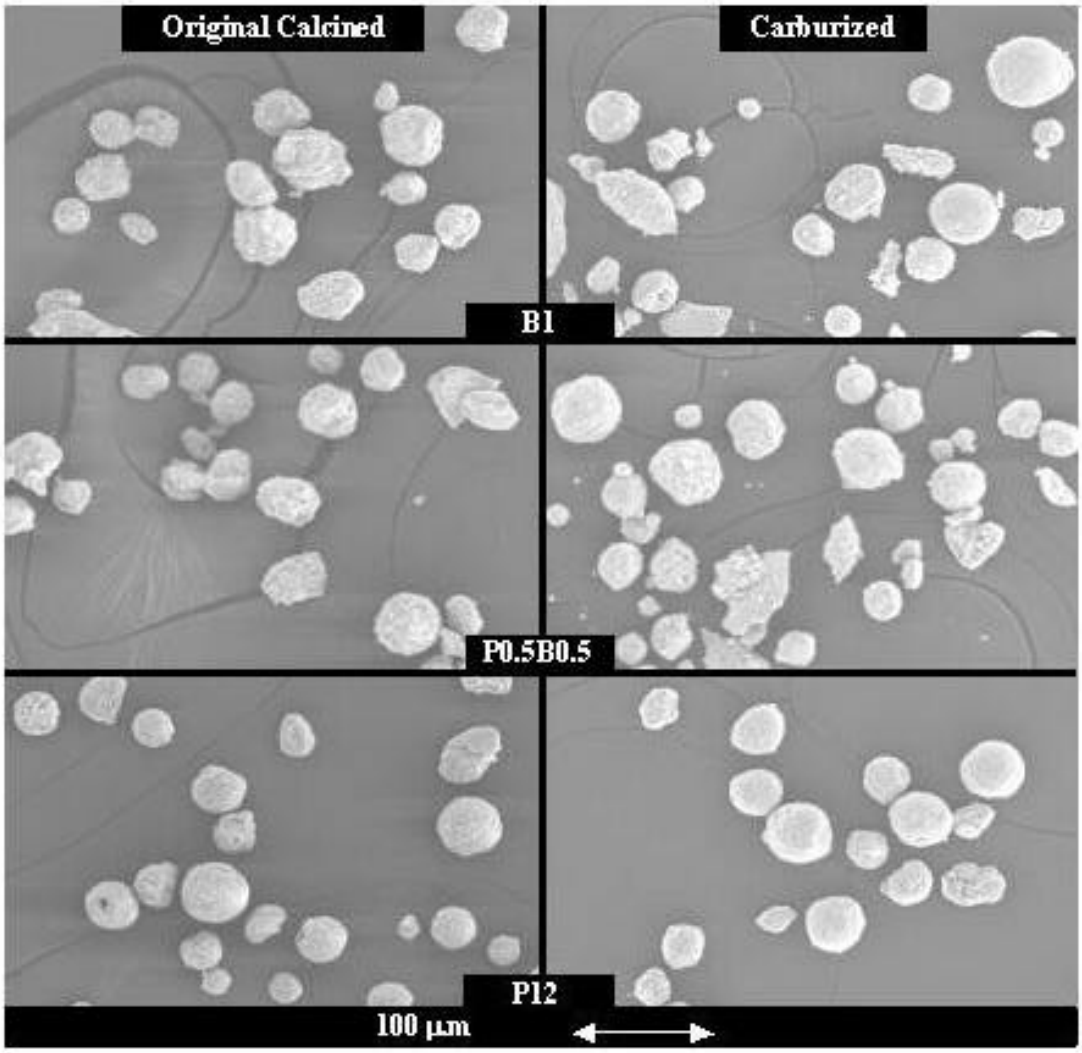

Figure 7.5 SEM Micrographs of all Catalysts Studied, Comparing their Original Calcined and CO-Pretreated Forms (Low Magnification).

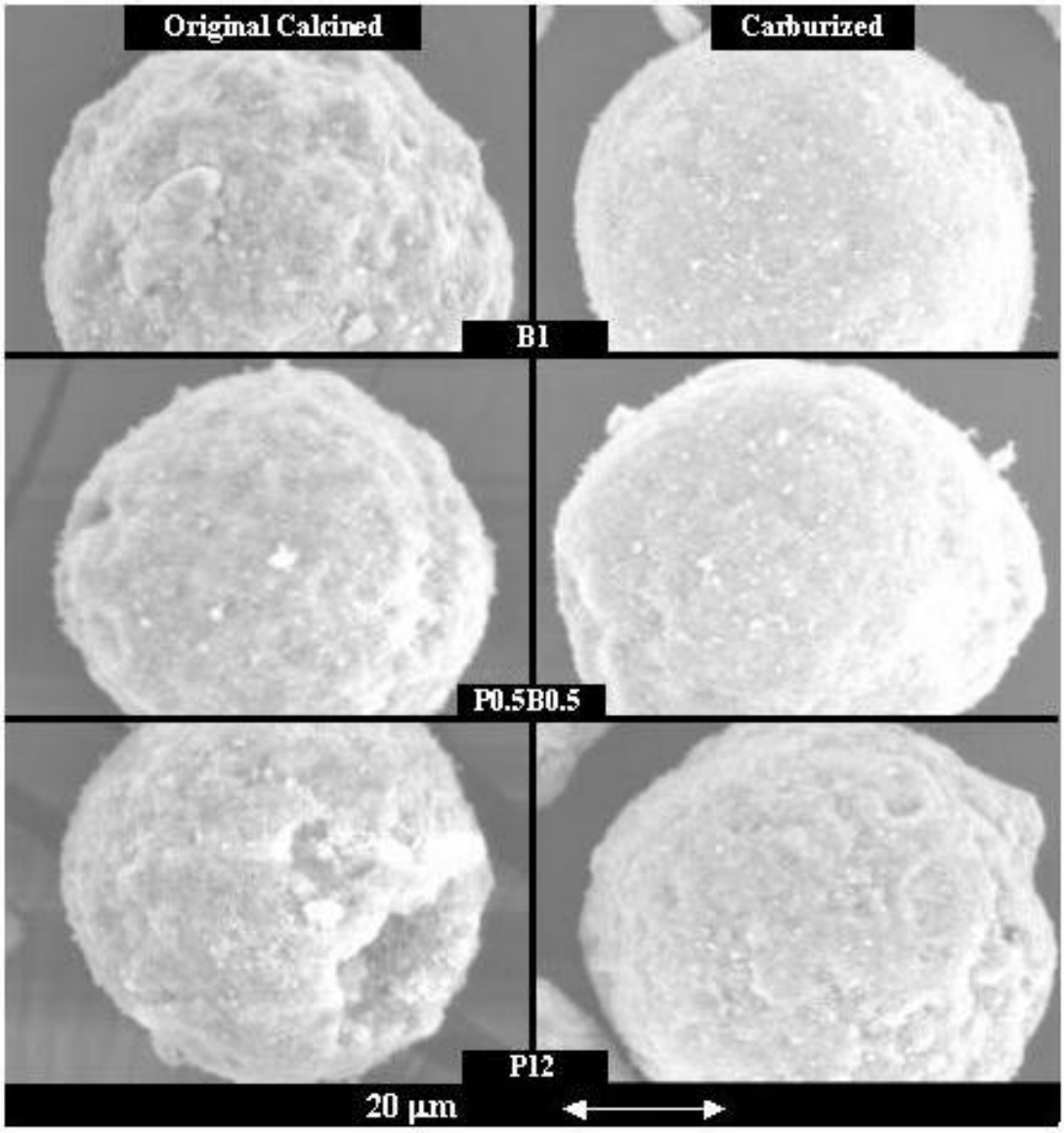

Figure 7.6 SEM Micrographs of all Catalysts Studied, Comparing their Original Calcined and CO-Pretreated Forms (High Magnification).

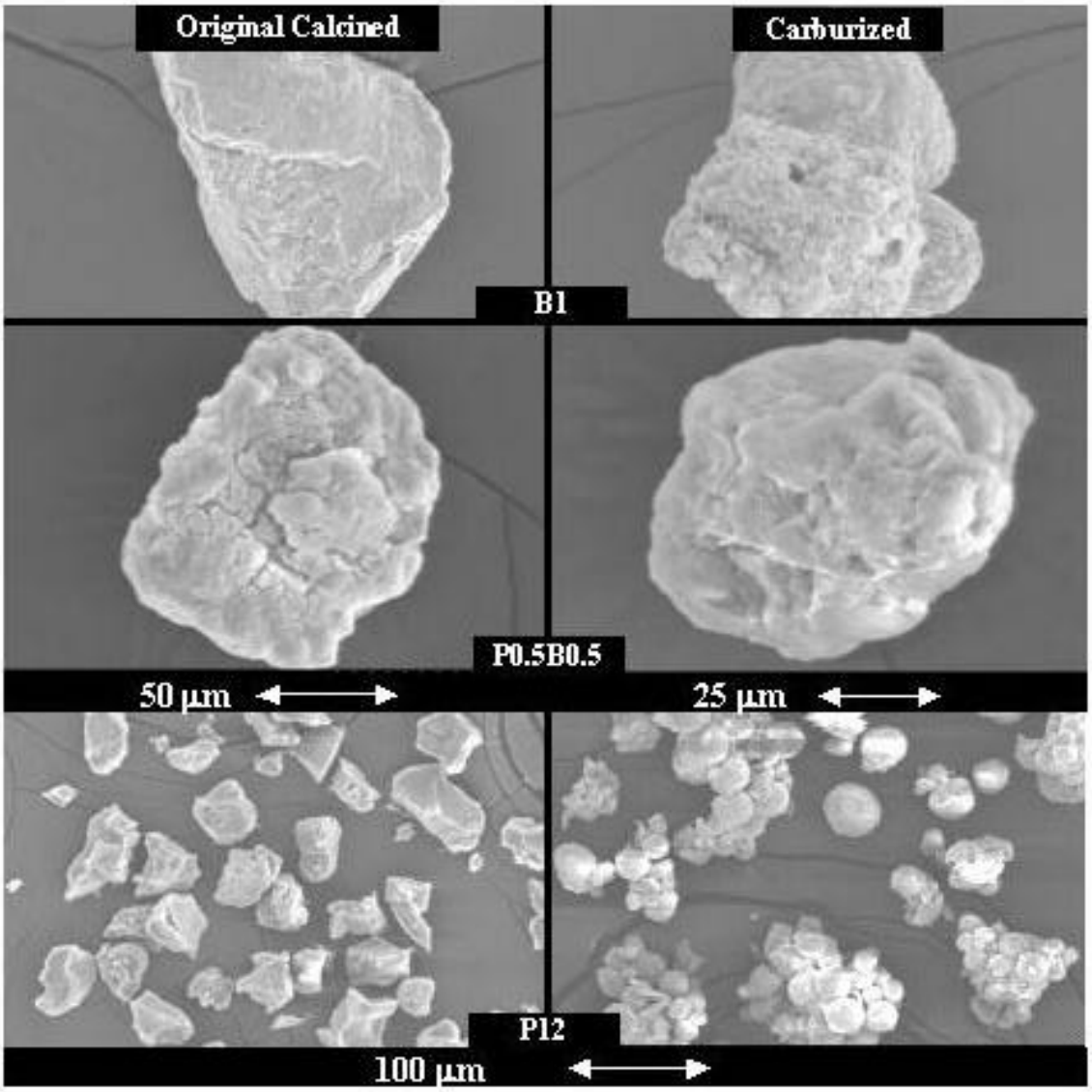

Figure 7.7 SEM Micrographs of the Original Calcined and CO-Pretreated Catalysts after Acid Leaching.

8.0 ACTIVATION AND DEACTIVATION OF FE FTS CATALYSIS: INVESTIGATION AT THE SITE LEVEL USING SSITKA

8.1 Introduction

Extensive phase changes of Fe F-T catalysts during activations and especially during FTS make Fe the most complicated system among F-T catalysts (including Ni, Co, and Ru). The catalytically active phase of the other metals is well known to be the metal state. Several phases of iron have been found to coexist during F-T reaction [1-4], including metallic Fe (α-Fe), Fe oxides, and Fe carbides [5]. The proportion of these Fe phases can be varied, depending upon reaction conditions and activation procedures, which determine the initial state of the catalyst before reaction. The catalytically active phase(s) in a working Fe catalyst for FTS has been debated extensively by researchers. The active Fe phases have been concluded to be mainly Fe oxides-Fe_3O_4 [6-10], Fe carbides [11-14], and Fe metal [4]. However, other possible active Fe phases have also been suggested, such as a surface phase on Fe_3O_4 [15].

Due to the above complexity, investigation into the active forms of Fe in a working catalyst requires an *in situ* technique with sufficient spatial resolution. Unfortunately, most of the techniques used to study iron catalysts in the past, including Mössbauer spectroscopy, XRD, and XPS, are not capable of providing such a resolution [5]. The conclusion has been reached by some [16-18] that the exact relationship between Fe phase composition and reactivity of the catalyst cannot be made.

The focus of the research reported herein was on characterizing the nature of the active sites of an Fe catalyst pretreated in different ways. The effect of different activations (H_2, CO, or syngas) were investigated. It was desired to determine how the active sites generated changed with reaction time-on-stream (TOS). Steady state isotropic-transient kinetic analysis (SSITKA), first developed by Happel [19], Bennett [20], and Biloen [21], is a powerful technique capable of *in situ* assessing the surface kinetics of catalytic reactions. Previously, this isotopic tracing technique had been successfully used to study the product chain growth during CO hydrogenation on Fe [22,23] and the carbon pathways on Fe/Al_2O_3 [24]. However, neither of these studies investigated the effect of pretreatment on Fe activity. The results of this study permit us to better understand activity development at the site level of an Fe catalyst after activation and during FTS. By using this isotopic tracing technique, the intrinsic site activities and concentrations of surface intermediates developing with TOS during Fe FTS are revealed for the first time.

8.2 Experiment

8.2.1 Catalyst

The Fe catalyst used for this study was prepared by precipitation and then spray drying. The relative compositions by weight percentage were $100Fe/5Cu/4.2K/11SiO_2$. The details of catalyst preparation have been given elsewhere [25-27]. Briefly, a mixture containing the desired ratios of Fe, Cu, and Si was precipitated at room temperature with ammonium hydroxide

solution. The resulting precipitate was filtered, washed, and then mixed with the desired ratio of $KHCO_3$ solution. The reslurried precipitate was then spray dried at 250°C in a Niro spray drier and calcined at 300 °C for 5 h in a muffle furnace. The calcined catalyst was sieved to particle sizes between 38-90 μm before use.

8.2.2 Catalyst Nomenclature

The following nomenclatures are used to refer to the three different pretreatments and pretreated catalyst samples: [H] for H_2-, [CO] for CO-, and [S] for syngas-pretreated samples. The original calcined catalyst is referred as P9 to indicate that it contains 9 wt% precipitated (P) SiO_2.

8.2.3 Catalyst Characterization

A Scintag 2000 x-ray diffractometer with monochromatized Cu K_α radiation (40 kV, 40 mA) and a Ge detector was used to determine powder XRD patterns of the pretreated and passivated catalyst samples. Each sample was analyzed, using a step scan mode at a scan rate of 0.02° (2q) per second from 10°-80°. XRD peak identification was done by comparison to the JCPDS database software.

BET surface areas, pore volumes, and average pore sizes of the pretreated and passivated catalyst samples were measured by N_2 physisorption using a Micromeritics ASAP 2010 automated system. Each catalyst sample was degassed under vacuum at 100°C for 1 h and then 300°C for 2 h prior to each measurement.

Both H_2 and CO chemisorptions on the reduced Fe catalyst samples were done for both [H] and [CO] with a Micromeritics Chemisorption ASAP 2010 automated system. H_2 chemisorption was performed at 35^{o}C following the procedure used in reference [28] assuming the ratio H chemisorbed:Fe atom = 1:1. Prior to H_2 chemisorption, the catalysts were evacuated to 10^{-6} mm Hg at 100^{o}C for 60 min., pretreated in flowing (50 cc/min) H_2 for [H] or CO for [CO] at 100^{o}C for 5 min., pretreated in flowing H_2 or CO at 280^{o}C for 12 hours after ramping up at a rate of 1^{o}C/min, and then evacuated at 10^{-6} mm Hg and 280^{o}C for 90 min to desorb any hydrogen or CO. For CO chemisorption, the catalyst sample was treated under the same condition as described above prior to the measurement but the analysis was carried out at 25^{o}C. It should be noted that CO chemisorption on Fe as suggested by Emmett and Brunauer in 1937 [29] was done at -183 ^{o}C assuming an average CO:Fe stoichiometry of 1:2. However, due to the limitation of the Micromeritics system, chemisorption at that low a temperature was not possible; thus, the CO chemisorption reported in this study was done at 25 ^{o}C.

8.2.4 SSITKA System

A schematic diagram and the detailed configuration of the SSITKA system used in this study have been given elsewhere (30). In brief, a quartz micro-reactor with ID of 4 mm was used with a thermocouple installed on the top of the catalyst bed for temperature readings. A pneumatic valve operated electrically was used to switch between two feed streams into the reactor having the same flow rates but containing different isotopic labeling of the reactant species (^{12}CO vs. ^{13}CO). The flow rate and pressure of the two feed streams were maintained constant during the switching using two backpressure regulators installed on the reactor effluent

line and a vent line. The gas lines used in the system were designed to be as short as possible to minimize gas phase holdup in the system. The gas lines exiting from the reactor were maintained at 220^{o}C to prevent blockage by heavy hydrocarbon deposits. The effluent gas was analyzed by an online gas chromatograph (Varian CP-3800) and a quadruple mass spectrometer (Pfeiffer Vacuum) equipped with a high-speed data-acquisition system interfaced to a personal computer using Balzers Quadstar 422 v 6.0 software (Balzers Instruments).

8.2.5 Kinetic Measurements

All the gases used for this study were ultra high purity grade. A 0.1 g catalyst sample was loaded into the reactor and pretreated with either H_2, CO, or syngas (H_2:CO = 2:3). Each pretreatment was carried out under identical conditions at 280^{o}C for 12 h with a ramp rate of 1^{o}C/min from room temperature, a gas flow rate of 5 cc/min, and a total pressure of 1 atm. After pretreatment the catalyst bed was purged with 30 cc/min of He for 15 min while the temperature was maintained 280 ^{o}C. At this temperature, the reaction mixture containing 2 cc/min of CO, 20 cc/min of H_2, and 80 cc/min of He was then introduced to the reactor. The system was pressurized to 1.8 atm and maintained at this pressure. A step change was made between ^{12}CO and ^{13}CO as the reaction proceeded with TOS, without disturbing the other reaction conditions. It should be noted that 5 vol% of Ar was added to ^{12}CO in order to determine the gas phase holdup in the reaction system. The details for calculation of SSITKA parameters [the average surface lifetime (t) and the concentration of surface intermediates (N)] are given elsewhere [35].

8.3 Results and Discussion

8.3.1 Catalyst Properties

Table 1 shows the N_2 physisorption properties and the major phases of Fe after different pretreatments. XRD patterns of all the catalyst samples studied are shown in Figure 1, with the most intense diffraction peaks for each Fe phase evident indicated. As expected, the fresh calcined catalyst as prepared was in form of hematite, Fe_2O_3. The major Fe phases of [H] were found to be Fe metal and magnetite, Fe_3O_4, while those of [CO] and [S] were mostly Fe carbides with only a small trace of Fe_3O_4 (its most intense peak being at $2q$ of ca. 35.5°). The presence of this small amount of Fe_3O_4 was even much clearer in a previous study for a different composition of spray-dried Fe catalyst [31]. Identification of exact carbide forms is usually difficult due to the overlapping of their diffraction peaks [32]. For example an intense peak between $2q$ of 43-44° has been reported to be characteristic of both ε'-$Fe_{2.2}C$ and χ-Fe_5C_2 [33]. Both carbide phases have been found after similar pretreatments (although not identical conditions) by other researchers using XRD and Mössbauer effect spectroscopy [32,34]. Therefore, it is concluded that in this study [CO] and [S] contained a mixture of these two carbides as majority phases after pretreatment.

BET surface area (Table 1) of the catalyst was found to decrease by more than 50% for all pretreatments while the porosity remained almost unchanged. The average pore size of the catalyst was found to be significantly larger in all pretreated samples. These changes in N_2 physisorption properties after pretreatment for precipitated Fe catalysts are commonly known to

result from sintering of the iron pore structure. The results for P9 were found to be in good agreement with our results for precipitated Fe catalysts reported previously [31].

Both H_2- and CO-chemisorption data of [H] and [CO] are summarized in Table 2. These measurements for [S] were not carried out since the equipment was not set up to pretreat with syngas. As shown in Table 2, [H] had higher values of total gas chemisorbed for either H_2 or CO. It should be noted that the total amount of H_2 chemisorbed for [H] was higher than the total CO chemisorbed. However, [CO] was found to exhibit the opposite, with more CO being adsorbed than H_2.

8.3.2 Catalyst Performance during Methanation

Both total rate (rate of CO converted) and rate of methane formation vs. TOS of the differently pretreated samples are presented in Figure 2. Although the same catalyst was used, the resulting rates (total and methane formation rates) after the different pretreatments were found to be significantly different, indicating that the pretreatments had a significant influence on the Fe catalyst that affected directly catalyst performance during reaction. The methane selectivity vs. TOS of each of the differently pretreated samples is shown in Figure 3. The initial rates of the differently pretreated samples (Figure 2) seemed to be about the same, although that of [H] was found to be slightly higher than those of [CO] or [S]. The activity of [H] increased rapidly and reached a maximum ca. 1.4 μmol/g-cat/s within the first hour of the reaction and then decreased rapidly due to a high deactivation rate. However, the deactivation rate slowed significantly as it approached steady-state operation after 13 h TOS. The higher activity of [H] than [CO] and [S] under these reaction conditions remained at steady state. [CO] also showed an

initial increase in rate as well, but an order of magnitude less than [H]. [S], on the other hand, did not seem to show any significant change in rate from its initial value and basically its activity remained essentially unchanged over 21 h TOS. This is probably due to the fact that the active sites of [S] were developed to the relatively stable state situation during the 12 h syngas activation.

Comparing the results of the different pretreatments, the rates of [CO] and [S] were found to be very similar at steady state. Throughout the whole course of reaction, [H] exhibited a significantly higher rate of CO conversion and methane formation than [CO] or [S] (Figure 2) although its methane selectivity was found to be significantly lower (Figure 3).

8.3.3 Surface Reaction Parameters

Steady state isotopic transient analysis (SSITKA) allows one to measure *in situ* under actual reaction conditions the intrinsic surface residence time (t) and the concentration of the most active surface reaction intermediates (N). Typical isotopic transients collected by mass spectrometry after isotopic switching for this Fe catalyst are shown in Figure 4. Surface residence time of active intermediates of a specie was calculated based on the difference in the peak area of that specie and the peak area of Ar, since Ar was not involved in the reaction and can be used to determine the average gas phase holdup in the entire reaction system. Detailed calculations of surface reaction residence time and concentration of active intermediates can be found elsewhere [35].

Figures 5 shows the reproducibility in measurements of methanation rate and surface lifetime (t_M) of active intermediates to form methane for selected runs with H_2 pretreated

samples. The data were highly reproducible, with the largest error in t_M of ca. ± 0.3 sec. Other runs (not shown here) were found to have the same degree of reproducibility. Figure 6 shows a comparison of the pseudo-first-order intrinsic activity (k_M), which is the inverse of the average surface residence time of the surface intermediates leading to methane (t_M), with TOS of the differently pretreated samples. A comparison of the concentrations of methane intermediates (N_M) with TOS is presented in Figure 7. It is clear from Figures 2, 6, and 7 that the higher activity of the [H]-pretreated catalyst was due to having a higher concentration of active intermediates – related to having undoubtedly more active sites. While the site activity (k_M) did become slightly higher for [H] than [CO] or [S], the difference was relatively small. Given that any H dependency appears in k_M rather than N_M, these k_M values can be considered to indicate that site activities on all the variously pretreated catalyst samples were identical. This suggests that the active sites on all the samples were essentially identical. This leads one to conclude that the active site of an Fe catalyst for FTS is unique – be it metal, carbide, or oxide. As seen from Figure 7, N_M of [H] increased rapidly within the first hour TOS as the catalyst started to be carburized once exposed to reactants. Figure 2 shows that the activity decreased rapidly within 1-4 h interval TOS and then continued to decline slowly to reach steady state after 20 h TOS, as a result of partial deactivation. Thus, deactivation was caused by a significant loss of concentration of surface methane intermediates from 1-4 h TOS (Figure 7) while the nature of active sites did not change significantly within that period (Figure 6). Although [CO] showed small increases in both k_M and N_M with TOS (Figures 6 and 7), these parameters were essentially constant. Both k_M and N_M of [S] were found to be essentially constant over 21 h TOS and exhibited similar values to those of [CO] throughout the whole course of reaction, taking into the

account of the error of measurements. Considering all these results, it can be suggested that the active F-T site is located on a (partially?) carburized Fe surface.

8.4 Conclusions

This study explored for the first time the effect of pretreatment and TOS on site activity and surface reaction intermediates on an Fe F-T catalyst, as determined by SSITKA. It was found that activity was primarily determined by the number of active intermediates, which were quite different for different pretreated samples at the beginning of the reaction. However, at steady state, the number of intermediates of [CO] and [S] were quite similar while that of [H] remained higher than the others. Taking into account the error of measurements, [H], [CO] and [S] exhibited essentially identical intrinsic site activity, suggesting that the active sites were all identical. The results supported the previous conclusion that the active sites for CO hydrogenation on Fe catalysts are probably on the carburized Fe surface.

Table 8.1 Catalyst Properties after Pretreatment and Passivation.

Pretreatment	**Fe Phase[a] (After Pretreatment)**	**N_2 Physisorption[b]**		
		BET S.A. ***(m^2/g)***	***Pore Volume*** ***(cm^3/g)***	***Average Pore Size*** ***(Å)***
Original calcined	Fe_2O_3	148	0.15	40
[H]	$Fe^0 + Fe_3O_4$	56	0.19	129
[S]	Fe carbides + Fe_3O_4	58	0.14	98
[CO]	Fe carbides + Fe_3O_4	76	0.13	68

[a] Determined by XRD.
[b] Error = ±5% of the value measured.

Table 8.2 Chemisorption on the Pretreated P9 Catalyst.

Pretreated Catalyst Samples	CO-Chemisorption[a]		H_2-Chemisorption[a]	
	Total (mmol CO/g-cat.)	Metal Dispersion[b] (%)	Total (mmol H_2/g-cat.)	Metal Dispersion[b] (%)
[H]	26.7	2.6	41.2	4.0
[CO]	8.0	0.8	4.5	0.4

[a] ±5% of values measured.
[b] Based on total Fe content in the catalyst as prepared, assuming $H/Fe^0_s = 1$ and $CO/Fe^0_s = 0.5$.

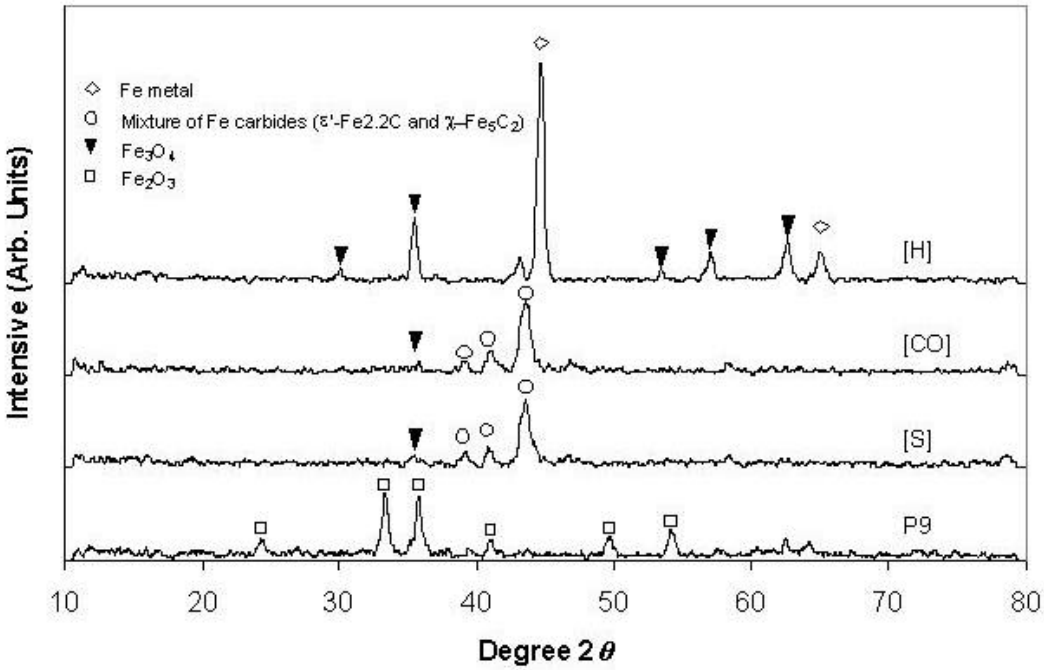

Figure 8.1 XRD Patterns of the Original Calcined and Differently Pretreated Catalyst Samples.

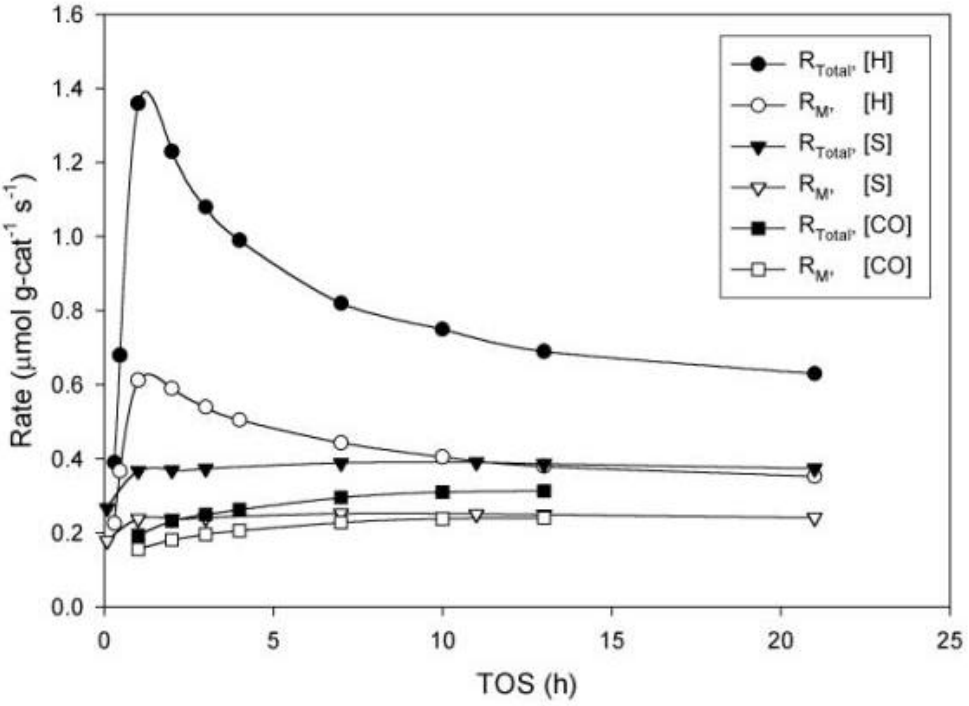

Figure 8.2 Total Rate and Rate of Methane Formation vs. TOS on the Differently Pretreated Samples.

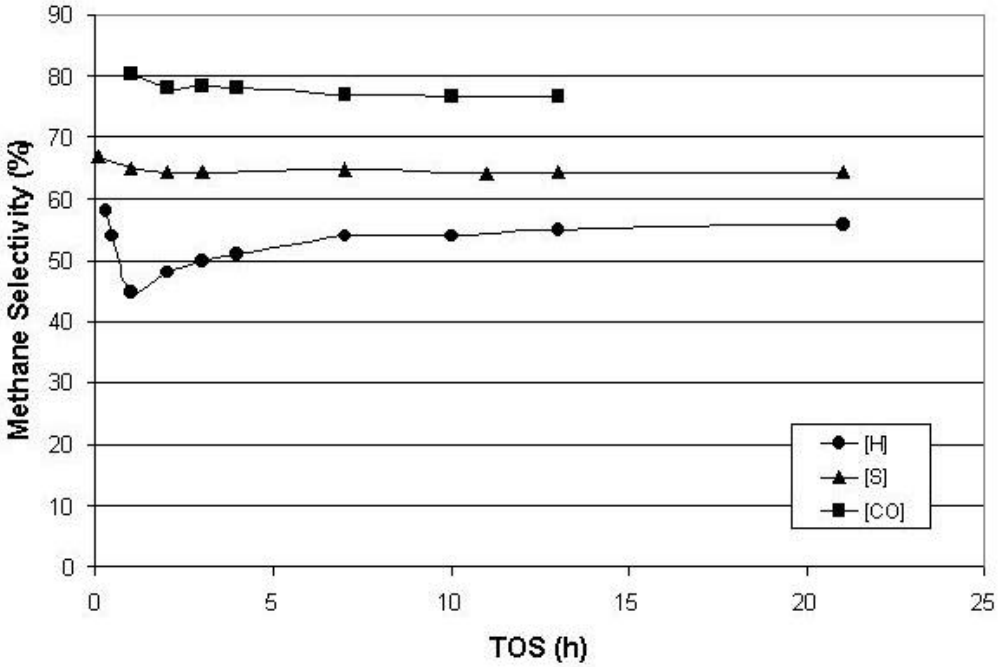

Figure 8.3 Methane Selectivity vs. TOS on the Differently Pretreated Samples.

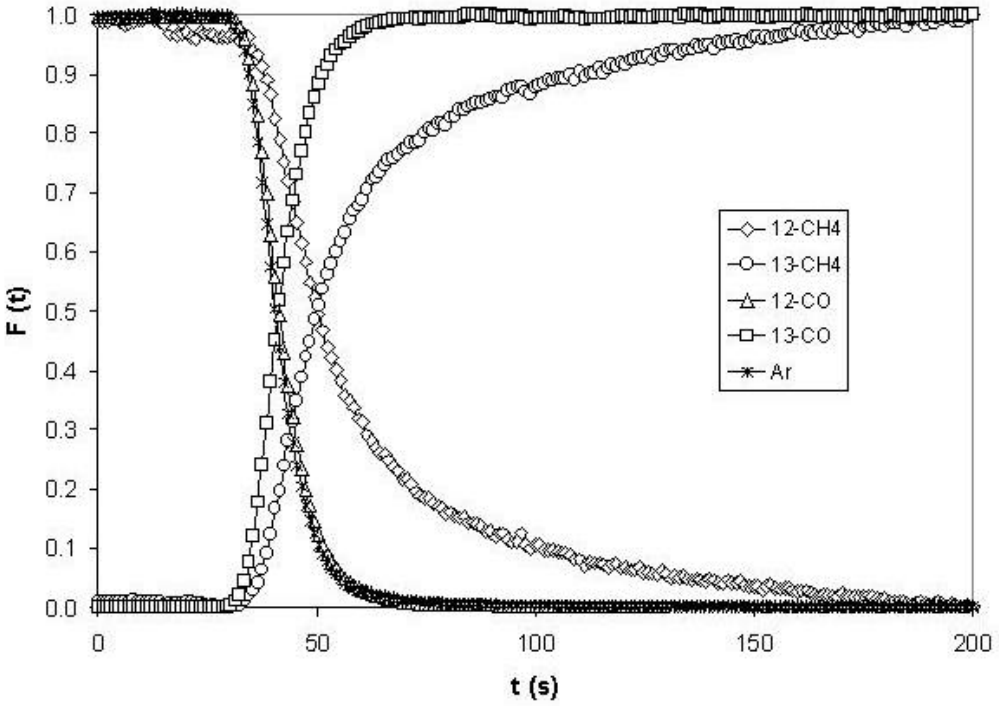

Figure 8.4 Typical Normalized Transient for the [H]-Pretreated Fe Catalyst during CO Hydrogenation.

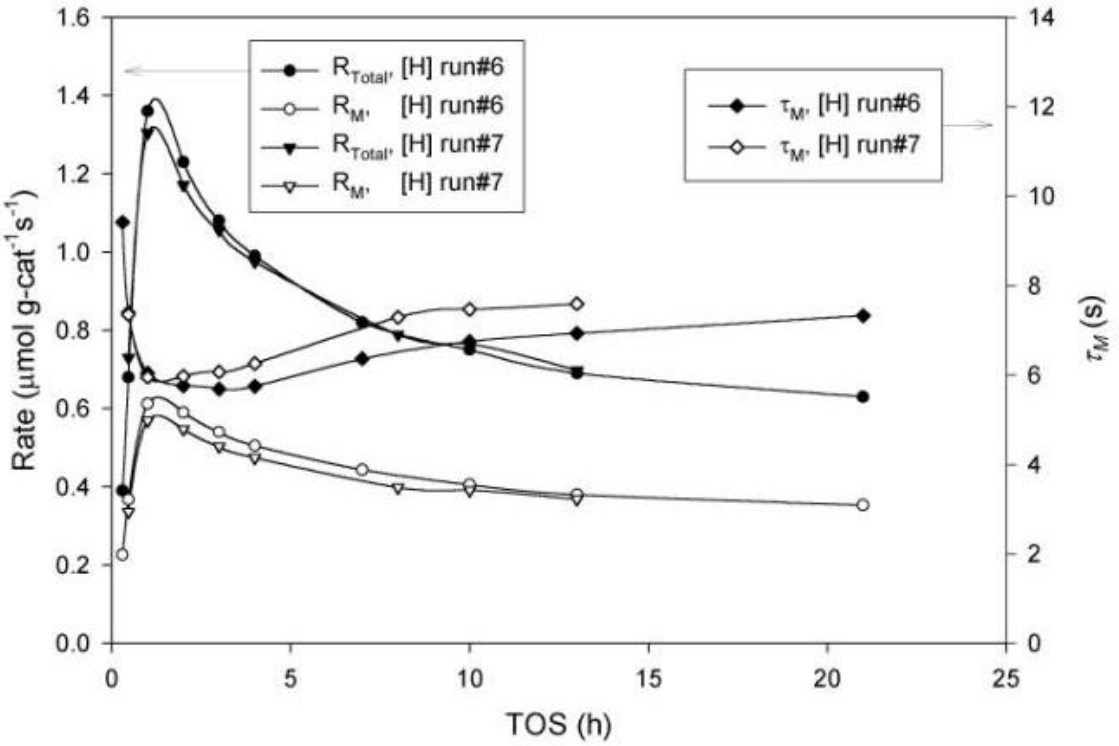

Figure 8.5 The Reproducibility of Rate and *t* Measurements for the Selected [H]-Pretreated Samples.

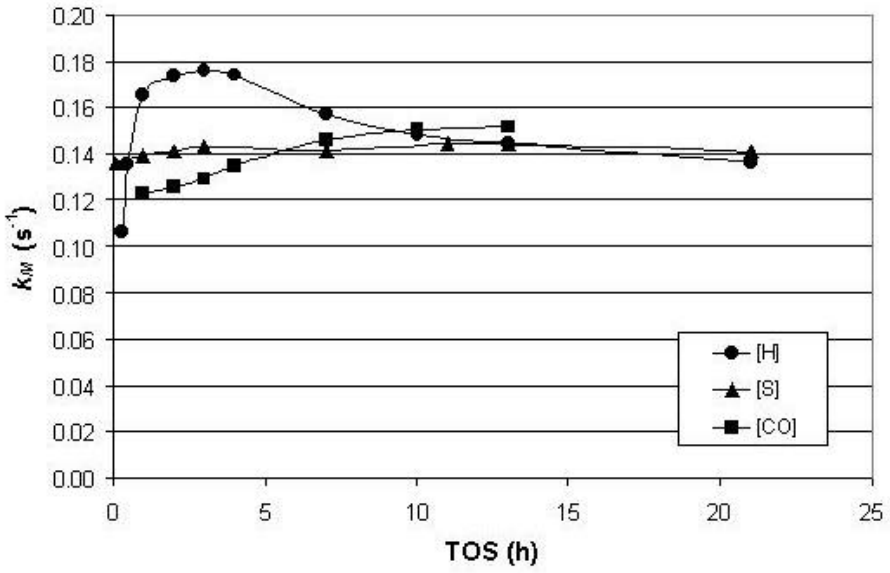

Figure 8.6 Effect of Pretreatments on the Development of Intrinsic Site Activity with TOS.

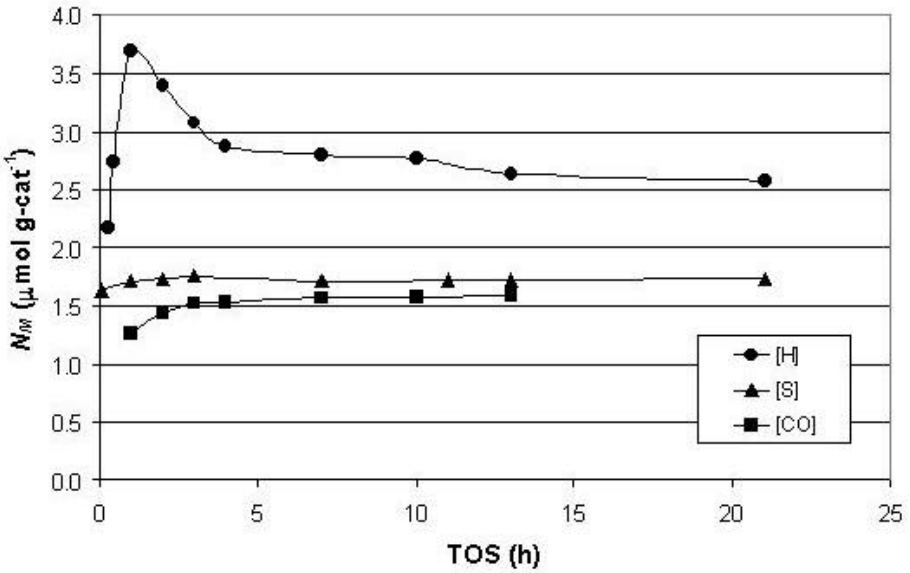

Figure 8.7 Effect of Pretreatments on the Development of Concentration of Methane Intermediates with TOS.

9.0 SUMMARY

The use of iron-based catalysts in coal-based Fischer-Tropsch synthesis still remain a major route for converting synthesis gas to more valuable fuels and chemicals, especially transportation fuel. Continued research on developing Fe Fischer-Tropsch catalysts has been inspired partly by their relatively low cost and abundance in nature that make production on a commercial scale highly feasible. However, application of Fe catalysts has suffered because of their low attrition resistances. Catalyst attrition causes not only a loss of catalyst from the reactor but also plugging of reactor filters, consequently leading to product contamination and difficulty in product separation. Therefore, the development of robust Fe catalysts is critical.

Previous studies have succeeded in preparing a high attrition-resistant Fe catalysts using spray-drying, but only when prepared with certain types (precipitated, binder, or a combination) and amounts of SiO_2. This hinted at a possible dependency of catalyst attrition on SiO_2, which later was found to directly determine the particle density – the only particle property that seems to strongly relate to attrition resistance. However, the general role played by SiO_2 on catalyst attrition has not been able to clearly delineate without investigating the effect of precipitated SiO_2.

This research investigated the attrition properties of a catalyst series prepared with only precipitated SiO_2 at low concentration. It was found that precipitated SiO_2 could be used to prepare robust catalysts when added in a small concentration (0-12 wt%). At these low concentrations, the amount of precipitated SiO_2 added inversely related to particle density as well as attiriton resistance. The importance of particle density in determining catalyst attrition was

reemphasized. In combining these results with the previous findings, it was found that the use of low SiO_2 concentrations does not always result in high catalyst particle density or high attrition resistance (since low binder SiO_2 concentrations resulted in poor attrition resistant catalysts). The type of SiO_2 and proper preparation is important in determining the resulting physical strength of catalysts. However, high particle density does not always result in a good catalyst. A good SBCR catalyst should have a proper density for good suspension in the slurry and in addition possess high surface for a high catalytic performance during F-T reactions. An optimum amount of precipitated SiO_2 that provides high catalyst performance was suggested to be 10-12 wt%.

An increase in metal-support interactions during pretreatment in the presence of water vapor hinted at a possibility of improving attrition resistance of Fe catalysts by inducing interactions between Fe and SiO_2. A low attrition resistance catalyst was selected and pretreated with H_2, CO, H_2 + water vapor, or CO + water vapor. It was found that pretreatments with either H_2 or CO resulted in the highest attrition resistances, due mainly to sintering of the Fe structure that significantly increased particle densities. Addition of water vapor to either H_2 or CO pretreatment was found to increase attrition resistance significantly as well but surprisingly lower than those treatments without water vapor. There was no trace of any increased Fe-SiO_2 interaction in any pretreated samples and no Fe-Si compound species was detected. It was therefore concluded that with an absence of such interaction that would help strengthen catalyst integrities, particle density remained the only key in determining attrition resistance. The presence of water vapor was found to decrease significantly the degree of Fe sintering and resulted in lower particle densities and lower attiriton resistance but preserved better the catalyst surface area. As mentioned previously, both surface area and attrition resistance should be

optimized. For this, the pretreatment with CO without water vapor addition was found to optimize these properties.

Different pretreatments result in different Fe phases in Fe catalysts. Fe is well known to undergo extensive phase change during activation and Fischer-Tropsch reaction. The catalytically active phase of Fe in a working catalyst has been a controversy among researchers due mainly to the lack of high spatial resolution technique to follow *in situ* such rapid phase change under actual reaction conditions. This study, although not focused on identifying the active Fe phase, was able to obtain kinetic information on surface reaction of these phases during CO hydrogenation. By using SSITKA, without involving in any high spatial resolution limitation, intrinsic site activities and concentrations of surface reaction intermediates with TOS of Fe pretreated in different ways were revealed for the first time. A high attrition resistant Fe catalyst was selected for this study since it was known to perform well during FTS with no physical degradation as an additional factor. This catalyst was pretreated with either H_2, CO, or syngas to result in different Fe phases. It was found that these differently pretreated Fe samples exhibited similar intrinsic site activities, although, there was some variation on the H_2 pretreated sample. In other words, the nature of active site for on Fe surface was the same, indicating that there was only one active form of surface Fe for CO hydrogenation. Considering the phases formed, the results are consistent with the active sites being on a (partially?) carburized Fe surface.

APPENDIX

Appendix A: Attrition Index Calculations

Weight percentage of fines lost

"Weight percentage of fines lost" was basically the percentage ratio of the weight of fines (W_f) collected by thimble, installed at the jet cup exit, and the weight of the total particles recovered (W_r) in the jet cup at the end of an attrition test:

$$W_r = \text{weight of fines generated } (W_f) + \text{weight of particles remaining at the bottom } (W_b) \quad \text{(A-1)}$$

$$\text{Weight percentage of fines lost (\%)} = \frac{W_f}{W_r} \times 100 \quad \text{(A-2)}$$

Net change in volume moment

"Net change in volume moment" was the percentage ratio of the difference of volume moments (X_{VM}) before and after attrition test and the volume moment before attrition test:

$$\textit{Net change in volume moment (\%)} = \frac{\left(X_{VM,\,\textit{before attrition}} - X_{VM,\,\textit{after attrition}}\right)}{X_{VM,\,\textit{before attrition}}} \times 100 \quad \text{(A-3)}$$

$$\textit{Volume moment } (X_{VM}) = \frac{\sum X^4 dN}{\sum X^3 dN} \quad \text{(A-4)}$$

where N is the number of particles of size X

Appendix B: Fe Reducibility Calculation

The Fe reducibility by H_2 TPR was calculated based on the following assumptions:

Assumptions: 1) all Fe in a calcined Fe catalyst is in form of Fe_2O_3.

2) all Cu and K in the catalyst are in the form of CuO and K_2O, respectively.

3) Fe_2O_3 reacts with H_2 as: $Fe_2O_3 + 3\ H_2 = 2\ Fe + 3\ H_2O$. (B-1)

Example: Calculation of Fe reducibility for 100Fe/5Cu/4.2K/21SiO_2

100 g or (100/55.8 = 1.8 mol) of Fe comes from (1.8/2 mol or 143.6 g of Fe_2O_3)

5 g or (5/63.5 = 0.08 mol) of Cu comes from (0.08 mol or 6.4 g of CuO)

4.2 g or (4.2/39.1 =0.11 mol) of K comes from (0.08/2 mol or 10.4 g of K_2O)

The weight of these components added to 21 g of SiO_2 gives the total catalyst weight of:

total catalyst wt. = 143.6+6.4+10.4+21 = 181.4 g.

Therefore, 1 g total calcined catalyst weight contains:

100/(55.8 * 181.4) = 0.01 mol of Fe or 143.6/(159.6*181.4) = 0.005 mol of Fe_2O_3

$5/(63.5 * 181.4) = 4.3 * 10^{-4}$ mol of Cu

$4.2/(39.1 * 181.4) = 5.9 * 10^{-4}$ mol of K and

$21/(60.1 * 181.4) = 5.5 * 10^{-3}$ mol of SiO_2.

From equation (B-1) 0.005 mol Fe_2O_3 consumes 3*0.005 = 0.015 mol H_2/g-cat.

This amount of H_2 consumed represents 100% of Fe reducibility. The Fe reducibilities reported are the percentages of this amount.

Appendix C: Calculations of t_P and N_P

At steady state rate, r_{ss}, during the isotopic transient:

Define: $r^p(t)$ = the rate of the unlabeled product (P), $^{12}CH_4$.

$r^{*p}(t)$ = the rate of the labeled product (*P), $^{13}CH_4$.

$F^p(t)$ = the normalized step-decay transient response.

$$F^p(t) = r^p(t) / r_{ss} \qquad \text{(C-1)}$$

$F^{*p}(t)$ = the normalized step-input transient response

$$F^{*P}(t) = r^{*p}(t) / r_{ss} \qquad \text{(C-2)}$$

Figure 7.4 shows a normalized transient step decay of unlabeled product (P), $^{12}CH_4$, and a normalized transient step input of labeled product ($^*P$), $^{13}CH_4$. The mean surface residence time (t^P_{avg}) is calculated based on the area between the normalized transients of the product $F^{P*}(t)$ and of the inert tracer Ar, $F^I(t)$:

$$t^P_{avg} = \int_0^\infty [F^p(t) - F^I(t)]dt \,. \qquad \text{(C-3)}$$

The concentration of surface reaction intermediates can be calculated as:

$$N^p = \int_0^\infty r^p(t)dt \qquad = \qquad t^P \times Rate_{SS} \qquad \text{(C-4)}$$

BIBLIOGRAPHY

BIBLIOGRAPHY

Chapter 1

1. Schulz, H., *Appl. Catal. A.* **186,** 3 (1999).
2. Jothimurugesan, K., Spivey, J.J., Gangwal, S.K., and Goodwin, J.G., Jr. in *"Natural Gas Conversion V"*, Studies in Surface Science and Catalysis, **Vol. 119**, Parmaliana, A., et al. (editors), Elsevier Science, NY, 1998, p.215.
3. Jothimurugesan, K., Goodwin, J.G, Jr., Spivey, J.J., and Gangwal, S.K., in *"Proceedings of 217th National Meeting of ACS, Symposium on Syngas Conversion to Fuels and Chemicals"*, American Chemical Society, Anaheim, California, March 21-25, 1999.
4. Jothimurugesan, K., Goodwin, J.G., Jr., Santosh, S.K., and Spivey, J.J., *Catal. Today* **58**, 335 (2000).
5. Zhao, R., Goodwin, J.G., Jr., Jothimurugesan, K., Spivey, J.J., and S.K. Gangwal, *Ind. Eng. Chem. Res.* **40,** 1065 (2001).
6. Zielinski, J., *Catal. Lett*. **12 (4)**, 389 (1992).
7. Zielinski, J., *J. Chem. Soc., Faraday Trans.* **93(19)**, 3577 (1997).
8. Kogelbauer, A., Weber, J.C., and Goodwin, J.G., Jr., *Catal. Lett.* **34 (3-4),** 259 (1995).
9. Biloen, P., Helle, J.N., van der Berg, F.G.A., and Sachtler, W.M.H., *J. Catal.* **81**, 450 (1983).
10. Stockwell, D.M., and Bennett, C.O., *J. Catal.* **110**, 154 (1988).
11. Winslow, P., and Bell, A.T., *J. Catal.* **158**, 86 (1984).

Chapter 2

1. Storch, H.H., Golumbic, N., and Anderson, R.B., *The Fischer-Tropsch and Related Syntheses*, John Wiley: New York, 1951.
2. Anderson, R.B., *The Fischer-Tropsch Synthesis*, Academic Press: New York, 1984.
3. Schulz, H., and Weitkamp, J., *IEC, Prod. Res. Dev*., **11**, 46 (1972).
4. Iglesia, E., *Stud. Surf. Sci. Catal.*, **107**, 153 (1997).
5. Satterfield, C.N., *"Heterogeneous Catalysis in Industrial Practice"* 2nd Ed., McGraw Hill Inc. (1996).
6. Fischer, F., and Tropsch, H., *Brennstoff-Chem.*, **7**, 97 (1926).
7. Fischer, F., and Tropsch, H., *Brennstoff-Chem.*, **11**, 489 (1930).
8. Roelen, O., *DRP*: **849**, 548, (1938).
9. Roginski, S.Z., in: *Proc. 3 rd Congress on Catalysis*, Amsterdam, 939 (1965).
10. Sternberg, A.W., and Wender, I., in: Proc. *Intern. Conf. On Coordin. Chem*., London, 1959, the Chem. Soc. London, 53 (1959).
11. Pichler, H., and Schulz, H., *CIT* **42**, 1162 (1970).
12. Schulz, H., *Appl. Catal. A*. **186**, 3 (1999).
13. Geerlings, J.J.C., Wilson, J.H., Kramer, G.J., Kuipers, H.P.C.E., Hoek, A., and Huisman, H.M., *Appl. Catal. A*. **186**, 27 (1999).
14. Iglesia, E., *Appl. Catal. A*. **161**, 59 (1997).
15. Kuipers, E.W., Scheper, C., Wilson, J.H., Vinkenburg, I.H., and Oosterbeek, H., *J. Catal*., **158**, 288 (1996).
16. Biloen, P., Helle, J.N., and Sachtler, W.M.H., *J. Catal*. **58**, 58 (1979).

17. Brady, R.C., and Pettit, R., J. *Am. Chem. Soc*. **103**, 1287 (1981).

18. Biloen, P., and Sachtler, W.M.H., *Adv. Catal*. **30**, 165 (1981).

19. Bell, A.T., *Catal. Rev. Sci. Eng*. **23**, 203 (1981).

20. Gormley, R.J., Zarochak, M.F., Defenbaugh, P.W., and Rao, K.R.P.M, *Appl. Catal. A.* **161**, 263 (1997).

21. Patzlaff, J., Liu, Y., Graffmann, C., and Gaube, J., *Appl. Catal. A.* **186** (1999).

22. Dry, M.E., in *Catalysis-Science and Technology*; Anderson, J.R., Boudart, M., Eds.; Springer-Verlag: New York 1981; Vol. 1, p. 159.

23. Espinoza, R.L., Steynberg, A.P., Jager, B., and Vosloo, A.C., *Appl. Catal. A*. 13 (1999).

24. Fischer, F., and Pichler, H., *Brennstoff-Chemie* **20**, 41 (1939).

25. Sie, S.T., *Rev. Chem. Eng*. **94**, 109 (1998).

26. Jager, B., Kelfkens, R.C., and Steynberg, A.P., *Natural Gas Conv. II*, Elsevier Sci. B.V. 419 (1994).

27. Jager B. and Espinoza R., *Catal. Today* 23 (1995).

28. Jager B., *Stud. in Surf. Sci and Catal*., Vol. **107**, 219 (1997).

29. Steynberg, A.P., Espinoza, R.L., Jager, B., and Vosloo, A.C., *Appl. Catal. A*. **186**, 41 (1999).

30. Satterfield, C.N., Heterogeneous Catalysis in Industrial Practice, 2nd ed., Krieger Publishing Company, (1991).

31. Schulz, H., Claeys, M., and Harms, S., *Stud. in Surf. Sci. and Catal*., Vol **107**, 193 (1997).

32. Storch, H.H., Golumbic, N., and Anderson, R.B., *"The Fischer-Tropsch and Related Syntheses"*, Wiley, New York (1951)

33. Zhang, Y., Wei, D., Hammache, S., Goodwin, J.G., Jr., *J. Catal.*, **188**, 281 (1999).

34. Iglesia, E., *Appl. Catal. A*. **161**, 59 (1997).

35. Reuel, R.C., and Bartholomew, C.H., *J. Catal.* **85**, 63 (1984).

36. Adachi, M., Yoshii, K., Han, Y.Z., and Fujimoto, K., *Bull. Chem. Soc. Jpn.* **69**, 1509 (1996).

37. Kogelbauer, A., Goodwin, J.G. Jr., and Oukaci, R., J. *Catal*. **160**, 125 (1996).

38. Schanke, D., Hilmen, A.M., Bergene, E., Kinnari, K., Rytter, E., Ådnanes, E., and Holmen, A., *Eng and Fuel* **10(4)**, 867 (1996).

39. Van de Loosdrechet J., Van der Haar M., Van der Kraan A.M., Van Dillen A.J., and Geus J.W., Appl. Catal. 150, 365 (1997).

40. Nimelä, M.K., Krause, A.O.I., Vaara, T., Kiviaho J.J., and Reinikainen, *Appl. Catal. A*: Gen. **147**, 325 (1996).

41. Nimelä, M.K., Krause, A.O.I., Vaara, T., and Laathinen J., *Top. Catal.* **2**, 45 (1995).

42. Matsuzaki, T., Takeuchi, K., Hanaoka, T., Arakawa, H., Sugi, Y., Wei, K.M., Dong, T.L, and Reinikainen M., Catal. Today **36(3)**, 311 (1997).

43. Zhang, Y.L, Sun, Q., Deng, J.F., Wu, D., and Chen, S.Y., *Appl. Catal.* A. **158**, 105 (1997).

44. Ho, S.W. and Su, Y.S., *J. Catal*. **175**, 139 (1998).

45. Iglesia, E., Soled, S.L., Fiato, R.A., and Via, G.H., *Stud. Surf. Sci. Catal.* **81**, 433 (1994).

46. Van't Blik, H.F.J., and Prins, R., *J. Catal*. **97**, 188 (1985).

47. Vada, S., Hoff, A., Adnanes, E., Schanke, D., and Holmen, A., *Top. Catal.* **2**, 155 (1995).

48. Iglesia, E., Soled, S.L., Fiato, R.A., and Via, G.H., *J. Catal.* **143,** 345 (1993).

49. Anderson, R.B, Kölbel, and Ralek, M., *The Fischer-Tropsch Synthesis*, Academic Press, Inc. (1984).

50. Pichler, H., Schulz, H,. and Kühne , *Brennst.-Chem*. **49**, 344 (1968).

51. Schulz, J.F., Hall, W.K., Dubs, T.A, and Anderson, R.B. *J. Am. Chem. Soc.* **78**, 282 (1956).

52. Anderson, R.B, Kolbel, H., and Ralek, M., *The Fischer-Tropsch Synthesis*, Academic Press, Inc. (1984).

53. Fischer, F., *Brennst.-Chem*. **16**, 1 (1935).

54. Kogelbauer, A., Goodwin, J.G., Jr., and Oukaci, R., *J. Catal.* **160**, 125 (1996).

55. Schanke, D., Hilmen, A.M., Bergene, E. Kinnari, K., Rytter, E., Ådnanes, E., and Holmen, A., *Catal. Lett* **34**, 269 (1995).

56. Jothimurugesan, K., Goodwin, J.G., Jr., Spivey, J.J., and Gangwal, S.K., in "*Proceedings of 217th National Meeting of ACS, Symposium on Syngas Conversion to Fuels and Chemicals*", American Chemical Society, Anaheim, California, March 21-25, (1999).

57. Bukur, D.B., Norwicki, L., and Patel, S.A., *Can. J. Chem. Eng.* **74**, 399 (1996).

58. Jothimurugesan, K., Goodwin, J.G., Jr., Santosh, S.K., and Spivey, J.J., *Catal. Today*, **58**, 335 (2000).

59. Pham, H., and Datye, A.K., *Catal. Today*, **58**, 233 (2000).

60. Zhao, R., Goodwin, J.G., Jr., Jothimurugesan, K., Spivey. J.J., and Gangwal, S.K., *Ind. Eng. Chem. Res.* **40**, 1065 (2001).

61. Anderson, R.B., in *"Catalysis"* (P.H. Emmett, Ed.), Vol. IV, 29-255, Van Nostrand-Reinhold, New York (1956).

62. O'Brien, R.J., Xu, L., Spicer, R.L., and Davis, B.H., *Eng and Fuels* **10,** 921 (1996).

63. Huang, C.-S., Xu, L., and Davis, B.H., *Fuel Sci. and Tech. Intl.* **11,** 639 (1993).

64. Huang, C.-S., Ganguly, B., Huffman, G.P., Huggins, F.E., and Davis, B.H., *Fuel Sci. and Tech. Intl.* **11,** 1289 (1993).

65. Wang, Y., and Davis, B.H., *Appl. Catal. A* **180**, 277 (1999).

66. Jung, H., and Thomson, W.J., *J. Catal*. **134**, 654 (1992).

67. Jung, H., and Thomson, W.J., *J. Catal.* **139**, 375 (1993).

68. LeCaer, G., Dubois, J.M., Pijolat, M., Perrichon, V., and Bussiere, P., *J. Phys. Chem.* **86**, 4799 (1982).

69. Niemantsverdriet, J.W., van der Kraan, A.M., van Dijk, W.L., and van der Baan, H.S., *J. Phys. Chem.* **84**, 3363 (1980).

70. Shroff, M.D., Kalakkad, D.S., Coulter, K.E., Köhler, S.D., Harrington, M.S., Jackson, N.B., Sault, A.G., and Datye, A.K., *J. Catal.* **156**, 185 (1995).

71. Blanchard, F., Reymond, J.P., Pommier, B., and Teichner, S.J., *J.Mol. Catal*. **17**, 171 (1982).

72. Reymond, J.P., Meriaudeau, P., and Teichner, S.J., *J. Catal.* **75**, 39 (1982).

73. Kuivila, C.S., Stair, P.C., and Butt, J.B., *J. Catal*. **118**, 299 (1989).

74. Butt, J.B., *Catal. Lett*. **7**, 61 (1990).

75. Butt, J.B., *Catal. Lett*. **7**, 83 (1990).

76. Dictor, R.A., and Bell, A.T., *J. Catal.* **97**, 121 (1986).

77. Huang, C.-S., Xu, L., and Davis, B.H., *Fuel Sci. Technol. Int.* **11**, 639 (1993).

78. Raupp, G.B. and Delgass, W.N., *J. Catal.* **58**, 361 (1979).

79. Happel, J., *Chem. Eng. Sci*. **33**, 1567 (1978).

80. Bennett, C.O. in *Catalysis under Transient Conditions*, Bell, A.T., and Hegedus, L.L., Eds.; ACS Symposium Series; Am. Chem.. Soc., Washington D.C. 178, 1 (1982).

81. Biloen, P., *J. Mol. Catal.* **21**, 17 (1983).

82. Hammache, S., Shannon, S.L., Kim, S.Y., and Goodwin, J.G., Jr., submitted for publication.

83. Shannon, S.L., and Goodwin, J.G., Jr., *Chem. Rev.* **95**, 677 (1995).

Chapter 4

1. Zhao, R., Goodwin, J.G., Jr., Oukaci, R., *Appl. Catal. A* **189** (1999) 99.

Chapter 5

1. Jothimurugesan, K., Goodwin, J.G., Jr., Santosh, S.K., and Spivey, J.J., *Catal. Today* **58,** 335 (2000).
2. Dry, M.E., *The Fischer-Tropsch synthesis.* In *Catalysis-Science and Technology*, Anderson, J.R., and Boudart, M., Eds.; Springer-Verlag: New York, 1981; Vol. 1.
3. Anderson, R.B. *The Fischer-Tropsch Synthesis*; Academic Press, Inc.: New York, 1984.
4. Huang, C-S., Xu, L., and Davis, B.H., *Fuel Sci. Tech. Int'l.* **11**, 639 (1993).
5. Srinivasan, R., Xu, L., Spicer, R., Tungate, F.L., and Davis, B.H., *Fuel Sci. Tech Int'l.* **14**, 1337 (1996).
6. Bhatt, B.L., Heydorn, E.C., and Tijm, P.J.A., in *"Proceedings of the 1997 Coal Liquefaction & Solid Fuels Contractors Review Conference"*, U.S. Department of Energy, Federal Energy Technology Center, Pittsburgh, Pennsylvania, September 3-4, 1997, p. 41.
7. Bhatt, B.L., *Liquid Phase Fischer-Tropsch (II) Demonstration* in *"The LaPorte Alternative Fuels Development Unit, Performer: Air Products and Chemicals"*, Allentown, PA, PR: PC A07/MF A02.
8. Wei, D.G., Goodwin, J.G., Oukaci, R., and Singleton, A.H., *Appl. Catal. A* **210**, 137 (2001).
9. O'Brien, R.J., Xu, L., Bao, S., Raje, A., and Davis, B.H., *Appl. Catal. A* **196**, 173 (2000).
10. Bukur, D.B., and Mukesh, D., Patel, S.A., *Ind. Eng. Chem. Res.* **29**, 194 (1990).
11. Bukur D.B., Lang, X., Mukesh, D., Zimmerman, W.H., Rosynek, M.P., and Li, C., *Ind. Eng. Chem. Res.* **29**, 1588 (1990).

12. Zhao R., Goodwin, J.G., Jr., Jothimurugesan, K., Spivey, J.J., and Gangwal, S.K., *Ind. Eng. Chem. Res.* **40**, 1065 (2001).
13. Zhao R., Goodwin, J.G., Jr., Jothimurugesan, K., Spivey, J.J., and Gangwal, S.K., *Ind. Eng. Chem. Res.* **40**, 1320 (2001).
14. Zhao R., Sudsakorn, K., Goodwin, J.G., Jr., Jothimurugesan, K., Gangwal, S.K., and Spivey, J.J., *Catal. Today* **71 (3-4),** 319 (2002).
15. Jothimurugesan, K., Spivey, J.J., Gangwal, S.K., and Goodwin, J.G., Jr., in *"Natural Gas Conversion V"*, Studies in Surface Science and Catalysis, Vol. 119, Parmaliana, A., et al. (editors), Elsevier Science, NY, 1998, p.215.
16. Pham, H.N., and Datye, A.K., *Catal. Today*, **58**, 233 (2000).
17. Jothimurugesan, K., Goodwin, J.G., Jr., Spivey J.J., and Gangwal, S.K., in *"Proceedings of 217th National Meeting of ACS, Symposium on Syngas Conversion to Fuels and Chemicals"*, American Chemical Society, Anaheim, California, March 21-25, 1999.
18. Jager, B., and Espinoza, R. *Catal. Today*, **23**, 17 (1995).
19. Bergna, H.E., in "*Characterization and Catalyst Development: an interactive approach*", Bradley, S.A., Gattuso, M.J., and Bertolacini, R.J. (editors), American Chemical Society, Washington, D.C., 1989, p.55.
20. Zhao, R., Goodwin, J.G., Jr., and Oukaci, R., *Appl. Catal. A* **189**, 99 (1999).
21. Zhao, R., Goodwin, J.G., Jr., Jothimurugesan, K., Spivey, J.J., and Gangwal, S.K., *Ind. Eng. Chem. Res.* **39**, 1155 (2000).

Chapter 6

1. Huang, C-S., Xu, L., and Davis, B.H., *Fuel Sci. Tech. Int'l.* **11**, 639 (1993).
2. Bhatt, B.L., *Liquid Phase Fischer-Tropsch (II) Demonstration* in *"The LaPorte Alternative Fuels Development Unit, Performer: Air Products and Chemicals"*, Allentown, PA, PR: PC A07/MF A02.
3. Srinivasan, R., Xu, L., Spicer, R., Tungate, F.L., and Davis, B.H., *Fuel Sci. Tech Int'l.* **14**, 1337 (1996).
4. Bhatt, B.L., Heydorn, E.C., and Tijm, P.J.A., in *"Proceedings of the 1997 Coal Liquefaction & Solid Fuels Contractors Review Conference"*, U.S. Department of Energy, Federal Energy Technology Center, Pittsburgh, Pennsylvania, September 3-4, 1997, p. 41.
5. Mansker, L.D., Jin, Y., Burkur, D.B., and Datye, A.K., *Appl. Catal. A.*, **186** 277 (1999).
6. Eliason, S.A., and Bartholomew, C.H., in *"Catalyst Deactivation 1997", Studies in Surface Science and Catalysis,* Vol. 11, Bartholomew, C.H., and Fuentes, G.A. (editors), Elsevier, New York, 1997, p. 517.
7. Dry, M.E., in *Catalysis-Science and Technology*; Anderson, J.R., and M., Boudart, Eds.; Springer-Verlag: New York 1981; Vol. 1, p. 159.
8. Bukur, D.B., Koranne, M., Lang, X., Rao, K.R.P.M., and Huffman, G.P., *Appl. Catal.* **126,** 85 (1995).
9. O'Brien, R.J., Xu, L., Milburn, D.R., Li, Y.-X., Klabunde, K.J., and Davis, B.H., *Top. Catal*. **2** (1995) 1.
10. Bukur, D.B., Lang, X., Rossin, J.A., Zimmerman, W.H., Rosynek, M.P., Yeh, E.B., and Li, C., *Ind. Eng. Chem. Res*. **28,** 1130 (1989).
11. Kolbel, H., and Ralek, M., *Catal. Rev.-Sci . Eng*. **21,** 225 (1980).

12. Kuo, J.C.W., *Slurry Fischer-Tropsch/Mobil Two-Stage Process of Converting Syngas to High Octane Gasoline*; DOE/PC/30022-10, Final Report, June 1983.
13. Kuo, J.C.W., *Two-Stage Process for Conversion of Synthesis Gas to High Quality Transportation Fuels*; DOE/PC/60019-9, Final Report, Oct 1985.
14. Bukur, D.B., Nowicki, L., and Lang, X., *Eng. & Fuels* **9,** 620 (1995).
15. Bukur, D.B., Lang, X., and Ding, Y., *Appl. Catal. A* **186,** 255 (1999).
16. Bukur, D.B., Okabe, K., Rosynek, M.P., Li, C., Wang, D., Rao, K.R.P.M., and Huffman, G.P., *J. Catal.* **155,** 353 (1995).
17. Bukur, D.B., Nowicki, L., Manne, R.K., and Lang, X., *J. Catal.* **155**, 366 (1995).
18. Rao, K.R.P.M., Huggins, F.E., Huffman, G.P., Gormley, R.J., O'Brien, R.J., and Davis, B.H., *Eng. & Fuels* **10,** 546 (1996).
19. O'Brien, R.J., Xu, L., Spicer, R.L., and Davis, B.H., *Eng. & Fuels* **10,** 921 (1996).
20. Kalakkad, D.S., Shroff, M.D., Kohler, S., Jackson, N., and Datye, A.K., *Appl. Catal. A*. **133,** 335 (1995).
21. Zhao, R., Goodwin, J.G., Jr., Jothimurugesan, K., Spivey, J.J., and Gangwal, S.K., *Ind. Eng. Chem. Res.* **40**, 1320 (2001).
22. Zhao, R., Sudsakorn, K., Goodwin, J.G., Jr., Jothimurugesan, K., Gangwal, S.K., and Spivey, J.J., *Catal. Today* **71 (3-4),** 319 (2002).
23. Pham, H.N., and Datye, A.K., *Catal. Today* **58,** 233 (2000).
24. Pham, H.N., Veiergutz, A., Gormley, R.J., and Datye, A.K., *Powder Tech.* **110**196, (2000).
25. Jothimurugesan, K., Goodwin, J.G.., Jr., Santosh, S.K., and Spivey, J.J, *Catal. Today* **58**, 335 (2000).
26. Zhao, R., Goodwin, J.G., Jr., and Oukaci, R., *Appl. Catal. A* **189**, 99 (1999).

27. Zhao, R., Goodwin, J.G., Jr., Jothimurugesan, K., Spivey, J.J., and Gangwal, S.K., *Ind. Eng. Chem. Res.* **40,** 1065 (2001).

28. Sudsakorn, K., Goodwin, J.G., Jr., Jothimurugesan, K., and Adeyiga, A.A, *Ind. Eng. Chem. Res.* **40,** 4778 (2001).

29. Zielinski, J., *Catal. Lett.* **12 (4),** 389 (1992).

30. Zielinski, J., *J. Chem. Soc., Faraday Trans*. **93(19),** 3577 (1997).

31. Menacherry, P.V., and Haller, G.L., *Catal. Lett*. **44 (3-4),** 135 (1997).

32. Zhang, Y., Wei, D., Hammache, S., and Goodwin, J.G., Jr., *J. Catal.* **188,** 281 (1999).

33. Hilmen, A.M., Schanke, D., Hanssen, K.F., and Holmen, A., *Appl. Catal. A.* **186**, 169 (1999).

34. Bernal, S., Calvino, J.J., Lopez-Cartes, C., Pintado, J.M., Perez-Omil, J.A., Rodriguez-Izquierdo, J.M., Hayek, K., and Rupprechter, G., *Catal. Today* **52 (1),** 29 (1999).

35. Pereira, M.M., Pereira, E.B., Lau, L.Y., and Schmal, M., *Catal. Today* **57 (3-4)**, 291 (2000).

36. Jongsomjit, B., Panpranot, J., and Goodwin, J.G., Jr., *J. Catal.* **204,** 98 (2001).

37. Kogelbauer, A, Weber, J.C., and Goodwin, J.G., Jr., *Catal. Lett.* **34 (3-4),** 259 (1995).

38. Shirai, H., Kobayashi, M., and Nunokawa, M., *Kagaku Kogaku Ronbunshu* **25 (5),** 714 (1999).

39. Smirnov, V.M., Voronkov, G.P., Semenov, V.G., Povarov, V.G., and Murin, I.V., *Surf. Rev. Lett.* **7 (1-2),** 1 (2000).

40. Jothimurugesan, K., Spivey, J.J., Gangwal, S.K., and Goodwin, J.G., Jr., in *"Natural Gas Conversion V", Studies in Surface Science and Catalysis*, Vol. 119, Parmaliana, A., et al. (editors), Elsevier Science, NY, 1998, p.215.

41. Jothimurugesan. K., Goodwin. J.G., Jr., Spivey. J.J., and Gangwal. S.K., *Symposium on Syngas Conversion to Fuels and Chemicals, Proceedings of 217th National Meeting of the American Chemical Society,* Anaheim, CA, March 21-25, 1999.
42. Shroff, M.D., Kalakkad, D.S., Coulter, K.E., Kohler, S.D., Harrington, M.S., Janckson, N.B., Sault, A.G., and Datye, A.K. *J. Catal.* **156** 185 (1995).
43. See Figure 7.1.
44. Zhao, R., Attrition Resistance Study of Spray-Dried Fe Fischer-Tropsch Catalysts, Ph.D. dissertation, University of Pittsburgh, 2000.
45. Reed, T.B., *Free Energy of Formation of Binary Compounds: An Atlas of Charts for High-Temperature Chemical Calculations*; MIT Press: Cambridge, MA, 1971.
46. Anderson, R.B., *The Fischer-Tropsch Synthesis,* Academic Press, Orlando, FL, 1984.

Chapter 7

1. Huang, C-S., Xu, L., and Davis, B.H., *Fuel Sci. Tech. Int'l.* **11**, 639 (1993).
2. Bhatt, B.L., *Liquid Phase Fischer-Tropsch (II) Demonstration in "The LaPorte Alternative Fuels Development Unit,* Final Topical Report PC A07/MF A02; National energy Technology Laboratory, U.S. Department of Energy: Washington, D.C., 1995.
3. Srinivasan, R., Xu, L., Spicer, R., Tungate, F.L., and Davis, B.H., *Fuel Sci. Tech Int'l.* **14**, 1337 (1996).
4. Bhatt, B.L., Heydorn, E.C., and Tijm, P.J.A., in *"Proceedings of the 1997 Coal Liquefaction & Solid Fuels Contractors Review Conference",* U.S. Department of Energy, Federal Energy Technology Center, Pittsburgh, Pennsylvania, September 3-4, 1997, p. 41.

5. Zhao, R., Goodwin, J.G., Jr., Jothimurugesan, K., Spivey, J.J., and Gangwal, S.K., *Ind. Eng. Chem. Res.* **40,** 1065 (2001).
6. Sudsakorn, K., Goodwin, J.G., Jr., Jothimurugesan, K., and Adeyiga, A.A, *Ind. Eng. Chem. Res.* **40,** 4778 (2001).
7. Jothimurugesan, K., Goodwin, J.G., Jr., Santosh, S.K., and Spivey, J.J., *Catal. Today* **58,** 335 (2000).
8. Dry, M.E., in *Catalysis-Science and Technology*; Anderson, J.R., and Boudart M., Eds.; Springer-Verlag: New York 1981; Vol. 1 pp 159-255.
9. Bukur, D.B., Koranne, M., Lang, X., Rao, K.R.P.M., and Huffman, G.P., *Appl. Catal.* **126,** 85 (1995).
10. O'Brien R.J., L. Xu, D.R. Milburn, Y.-X. Li, K.J. Klabunde and B.H. Davis, Top. Caltal. 2 (1995) 1.
11. Bukur, D.B., Lang, X., Rossin, J.A., Zimmerman, W.H., Rosynek, M.P., Yeh, E.B., and Li, C., *Ind. Eng. Chem. Res.* **28,** 1130 (1989).
12. Kolbel, H. and Ralek, M. *Catal. Rev.-Sci . Eng.* **21,** 225 (1980).
13. Kuo, J.C.W., *Slurry Fischer-Tropsch/Mobil Two-Stage Process of Converting Syngas to High Octane Gasoline*; DOE/PC/30022-10, Final Report, June 1983.
14. Kuo, J.C.W., *Two-Stage Process for Conversion of Synthesis Gas to High Quality Transportation Fuels*; DOE/PC/60019-9, Final Report, Oct 1985.
15. Zhao R.; Sudsakorn, K.; Goodwin, J.G., Jr.; Jothimurugesan, K.; Gangwal, S.K.; and Spivey, J.J. *Catal. Today* **71 (3-4),** 319 (2002).

16. Jothimurugesan, K., Goodwin, J.G., Jr., Spivey, J.J., and Gangwal, S.K., *Symposium on Syngas Conversion to Fuels and Chemicals. Proceedings of 217th National Meeting of the American Chemical Society,* Anaheim, CA, March 21-25, 1999.
17. Jothimurugesan, K., Spivey, J.J., Gangwal, S.K., and Goodwin, J.G., Jr., in *"Natural Gas Conversion V"*, Studies in Surface Science and Catalysis, Vol. 119, Parmaliana, A., et al. (editors), Elsevier Science, NY, 1998, p.215.
18. Jager, B., and Espinoza, R., *Catal. Today* **23**, 17 (1995).
19. Zhao, R., Goodwin, J.G., Jr., Jothimurugesan, K., Spivey, J.J., and Gangwal, S.K., *Ind. Eng. Chem. Res.* **40**, 1320 (2001).

Chapter 8

1. Jung, H., and Thomson, W.J., *J. Catal*. **134**, 654 (1992).
2. Jung, H., and Thomson, W.J., *J. Catal.* **139**, 375 (1993).
3. LeCaer, G., Dubois, J.M., Pijolat, M., Perrichon, V., and Bussiere, P., *J. Phys. Chem.* **86**, 4799 (1982).
4. Niemantsverdriet, J.W., van der Kraan, A.M., van Dijk, W.L., and van der Baan, H.S., *J. Phys. Chem.* **84**, 3363 (1980).
5. Shroff, M.D., Kalakkad, D.S., Coulter, K.E., Köhler, S.D., Harrington, M.S., Jackson, N.B., Sault, A.G., and Datye, A.K., *J. Catal.* **156**, 185 (1995).
6. Blanchard, F., Reymond, J.P., Pommier, B, and Teichner, S.J., *J.Mol. Catal.* **17**, 171 (1982).
7. Reymond, J.P., Meriaudeau, P., and Teichner, S.J., *J. Catal*. **75**, 39 (1982).
8. Kuivila, C.S., Stair, P.C., and Butt, J.B., *J. Catal.* **118**, 299 (1989).
9. Butt, J.B., *Catal. Lett*. **7**, 61 (1990).

10. Butt, J.B., *Catal. Lett*. **7**, 83 (1990).

11. Amelse, J.A., Butt, J.B., and Schwartz, L.J., *J. Phys. Chem*. **82**, 58, (1979).

12. Dictor, R.A., and Bell, A.T., *J. Catal*. **97**, 121 (1986).

13. Raupp, G.B., and Delgass, W.N., *J. Catal.* **58**, 348 (1979).

14. Raupp, G.B., and Delgass, W.N., *J. Catal.* **58**, 361 (1979).

15. Huang, C.-S., Xu, L., and Davis, B.H., *Fuel Sci. Technol. Int.* **11**, 639 (1993).

16. Anderson, R.B., *The Fischer-Tropsch Synthesis*, Academic Press: Orlando, FL, 1984.

17. Dry, M.D., in *Catalysis-Science and Technology*, Anderson, J.R., and Boudart, M., Eds., Springer-Verlag, New York 1981, Vol. 1, p 159.

18. O'Brien, R.J., Xu, L., Milburn, D.R., Li, Y.-X., Klabunde, K.J., and Davis, B.H., *Top. Catal*. **2**, 1 (1995).

19. Happel, J., *Chem. Eng. Sci*. **33**, 1567 (1978).

20. Bennett, C.O., in *Catalysis under Transient Conditions,* A.T. Bell and L.L. Hegedus, Eds., ACS Symposium Series; Am. Chem. Soc., Washington D.C. **178**, 1 (1982).

21. Biloen, P., *J. Mol. Catal.* **21**, 17 (1983).

22. Mims, C.A., and McCandlish, L.E., *J. Am. Chem. Soc*. **107**, 696 (1985).

23. Mims, C.A. and McCandlish, L.E., *J. Phys. Chem*. **91**, 292 (1987).

24. Stockwell, D.M., Bianchi, D., and Bennett, C.O., *J. Catal.* **113**, 13 (1988).

25. Jothimurugesan, K., Goodwin, J.G., Jr., Santosh, S.K., and Spivey, J.J, *Catal. Today* **58**, 335 (2000).

26. Jothimurugesan, K., Goodwin, J.G., Jr., Spivey, J.J., and Gangwal, S.K., *Symposium on Syngas Conversion to Fuels and Chemicals, Proceedings of 217th National Meeting of the American Chemical Society,* Anaheim, CA, March 21-25, 1999.

27. Jothimurugesan, K., Spivey, J.J., Gangwal, S.K., and Goodwin, J.G., Jr. in *"Natural Gas Conversion V"*, Studies in Surface Science and Catalysis, Vol. 119, Parmaliana, A., et al. (editors), Elsevier Science, NY, 1998, p.215.
28. Hwang, J.S., Jun, K.-W., and Lee, K.-W., *Appl. Catal. A* **208**, 217 (2001).
29. Emmett, P.H., and Brunauer, S., *J. Am. Chem. Soc*. **59**, 1553 (1937).
30. Chen, B., and Goodwin, J. G., Jr., *J. Catal.* **154**, 1 (1995).
31. Sudsakorn, K., Goodwin, J.G., Jr., and Adeyiga, A.A., submitted for publication (2002).
32. Kalakkad, D.S., Shroff, M.D., Kohler, S., Jackson, N., and Datye, A.K., *Appl. Catal. A.* **133,** 335 (1995).
33. Bukur, D.B., Lang, X., and Ding, Y., *Appl. Catal. A.* **186**, 255 (1999).
34. Bukur, D.B., Okabe, K., Rosynek, M.P., Li, C., Wang, D., Rao, K.R.P.M., and Huffman, G.P., *J. Catal.* **155**, 353 (1995).
35. Shannon, S.L., and Goodwin, J.G., Jr., *Chem. Rev*. **95**, 677 (1995).